NASA CR-66615

DESIGN, DEVELOPMENT AND TESTING OF BI-EXPLOSIVE SHAPED CHARGE METEORITIC SIMULATORS

Prepared under Contract No. NAS1-6886 by
THE FIRESTONE TIRE AND RUBBER COMPANY
Defense Research Division
Akron, Ohio
44317

for

NATIONAL AERONAUTICS AND SPACE ADMINISTRATION

NASA CR-66615

DESIGN, DEVELOPMENT AND TESTING OF BI-EXPLOSIVE SHAPED CHARGE METEORITIC SIMULATORS

April, 1968

Prepared under Contract No. NAS1-6886 by
THE FIRESTONE TIRE AND RUBBER COMPANY
Defense Research Division
Akron, Ohio 44317

for

NATIONAL AERONAUTICS AND SPACE ADMINISTRATION

ABSTRACT

The results of a contract to develop meteoritic simulators using shaped charge techniques are presented. Explosive wave shaping theory is discussed and radiographs of firing tests are shown. The effect of material properties such as purity and grain size on shaped charge jet formation and integrity is explored. It is concluded that the acceleration of single pellets of two grams mass to velocities of about 12 km/sec is feasible.

TABLE OF CONTENTS

TABLES

FIGURES

SECTION 1

SECTION 2

DESIGN, DEVELOPMENT AND TESTING OF BI-EXPLOSIVE SHAPED CHARGE METEORITIC SIMULATORS

SUMMARY

A research and development program was conducted under contract NAS1-6886 for the purpose of developing meteoritic simulators using shaped charge techniques. The meteoritic simulators were to have a mass of 2 grams and a velocity in excess of 12 km/sec.

Work conducted previously on contracts NAS1-4187 and NAS1-5212 had lead to the conclusions that for a given shaped charge liner cone angle, the jet integrity was related to the jet velocity and to the liner material. Furthermore, there was evidence that the velocity, at which jet degradation began, increased as the liner cone angle was increased.

Based on the above observations it was proposed for contract NAS1-6886 to form the meteoritic simulator jets using large angle liners (50° to 70°) and to study the effects of material properties on jet integrity. In order to achieve the required jet velocities from large angle liners, it was proposed to develop a bi-explosive charge which could deliver more energy to the liner.

The project was conducted in two major phases. First, the bi-explosive shaped charge development was completed. Then a program was conducted to develop a shaped charge liner which could produce an integral jet. Concurrently, studies were made of the effects of shaped charge liner material and explosive charge configuration on jet integrity using a mono-explosive charge, referred to as the hyperbolic charge (developed on contract NAS1-5212), as the test vehicle.

The approach to the bi-explosive design was to surround the inner explosive, which contained the shaped charge liner, with an outer explosive that had a greater detonation rate. The design incorporated an inert unit called a waveshaper that was to prevent the inner explosive from being initiated anywhere except at the bi-explosive interface. An analysis of this approach using Huygens' wavefront construction techniques showed that a convergent conical detonation wave would be formed. The conical detonation wave would intercept the liner wall so as to give a high effective detonation rate. Furthermore, the small angle between the wave front and the liner wall would result in a more efficient transfer of energy from explosive to liner.

Tests with this design showed that the initial waveshaper design and waveshaper material (Lucite) were allowing the inner explosive to be initiated at the waveshaper-inner explosive interface. Tests were then conducted with lead waveshapers whereupon radiographs of the detonation wavefronts showed the wave configuration to be just as predicted. Since the weight limitation imposed by NASA would not allow the use of lead waveshapers, an investigation was made of rigid polyurethane foam as a possible substitute. It was found that although polyurethane was not as effective as lead, with the proper design of waveshaper it would be acceptable. Tests were also conducted where various explosive combinations were evaluated in terms of the velocity produced by shaped charge liners in the bi-explosive assembly. It was concluded that the inherent energy of the explosives was a dominant factor, i.e., pentolite/octol would be less effective than comp.B/octol where octol is the outer explosive and pentolite is less energetic than comp.B.

Shaped charge liner development began after the explosive charge had been evaluated. The majority of the tests during this phase of the project were conducted with lead waveshapers because the polyurethane waveshaper development was not completed until later. The first tests were conducted with conical liners which would not produce integral jets (an integral jet is both radially and axially stable). This was done for the sake of both economy and expediency. Using conical liners, it was possible to determine the velocities possible from large angle liners in the bi-explosive charge and to determine the relative degree of jet integrity which would exist, without waiting for the development of a liner design which could produce an integral jet. It was found that cohesive jets (radially stable) with velocities as high as 12.47 km/sec were produced. These tests showed that the 70° liners were more prone to forming cohesive jets than 50° liners. They also showed that it was possible to obtain high velocity jets from large angle liners, using the bi-explosive charge.

The next phase of the liner development program was to develop a shaped charge liner design which would produce an integral jet. The approach was to control the liner cross-sectional area so that the C/M ratio (the ratio of explosive-charge-mass to liner-mass, measured in a plane perpendicular to the charge-liner axis) could be controlled. The majority of the work was done with iron liners because NASA considered this to be the most important material. This made the problem more difficult because the purity and grain size of the iron which was available affected the results. The first tests with controlled liner cross-sectional areas were done with 70° liners. This approach was taken because it had been demonstrated during conical liner tests that the best chance of producing cohesive jets was with 70° liners. All of the liners tested had hyperbolic inside sur-

faces. The liner cross-sectional area was varied by modifying the conical exterior surface of the liner. Two types of modifications were evaluated: one produced a non-linear increase in the liner cross-sectional area from liner base to liner apex; the second produced a linear increase in the liner cross-section area from liner base to liner apex. Tests indicated the non-linear variation to be the most promising. Tests were then conducted with the 50°, 60° and 70° liners machined to the non-linear area variation. This was done to evaluate the effect of cone angle on jet integrity; i.e., it appeared that it would be difficult to obtain 12 km/sec with the 70° liner (using the existing bi-explosive design)therefore, it was desired to see whether 60° or 50° liners could be used. The liners for this test were made from electron beam melted iron which was the best iron available at the time, but which unfortunately possessed a grain structure composed of large and mixed grain sizes. None of the liners tested formed a cohesive jet. The results showed the same trend that had been exhibited by the conical liners, i.e., the 50° liners gave the highest velocities, but the resultant jets showed the largest degree of degradation. On the basis of this test and others being conducted concurrently on a material properties study, it was concluded that any further development of an iron shaped charge liner should be done with a pure fine-grained iron.

At this point of the project the funds available did not allow the further effort that would have been required to obtain and test liners made from pure fine-grained iron. It was therefore decided to expend the remaining effort on the development of a nickel shaped charge liner. Previous tests with conical liners had shown that a 50° liner angle was borderline in terms of jet integrity; however, since there was not time for an extended development program and since a jet velocity in excess of 12 km/sec was desired, it was decided that a 50° liner with the proper cross-sectional area variation offered the best chance that an integral jet of the desired velocity would be produced. Tests were conducted with comp.B/octol and octol/HMX bi-explosive charges where variations in both liner area and adaptor material were tried. Jets with velocities above 12 km/sec were obtained; however, they were not cohesive. One integral nickel jet with a velocity of 11.25 km/sec was produced. The charge design which produced it was borderline because a second test with the same design produced a fragmented jet. The development ended at this point because of lack of funds. It was concluded from the test results that any further development should begin with 60° liners where the loss in velocity due to increasing the cone angle should be compensated for by a reduction in liner wall thickness.

Concurrent to the major developments discussed above, tests were conducted to evaluate the effects of liner material properties on jet integrity.

Also tests were conducted to evaluate the effects of variation in charge configuration on jet character. Both programs were conducted using the mono-explosive charge previously described. The results of these programs were fed into the main development program as the data was obtained. The material property study, in particular, provided valuable information. Based on these tests it was concluded that purity and grain size were important in the formation of cohesive iron jets.

Although the main objective of the project was not reached, all of the key developments leading to the desired goal were successful. The results which were achieved indicate that the goal, of a 2 gram nickel or iron jet with a velocity in excess of 12 km/sec, can be obtained with further development of the bi-explosive charge design.

INTRODUCTION

The objective of this project was to develop a shaped charge meteoritic simulator which would accelerate a minimum of 2 grams of the materials nickel and iron to velocities in excess of 12 km/sec. The meteoritic simulators with known mass, density, velocity and material composition are needed to evaluate key coefficients in the physical theory of natural meteors. The artificial meteors are to be carried above the earth in a rocket and then be projected downward through the atmosphere. The light intensity which is recorded by photographic equipment is used to determine a value for luminous efficiency. The latter value can then be used to determine the masses of natural meteors which are observed.

Firestone in collaboration with Ballistic Research Laboratories, Aberdeen Proving Ground, had conducted meteoritic simulator development work on two previous contracts. On contract NAS1-4187 (Ref. 1) an attempt was made to develop a 15 km/sec jet pellet using a bi-metallic cylindrical liner. The bi-metal cylinder was composed of an inner cylinder of the material to be jetted and an outer cylinder of beryllium which was intended to effect a cohesive jet by modifying the jet formation process. Jet material with a velocity near 15 km/sec was produced; however, it was not cohesive.

A second attempt was made to produce 15 km/sec jet pellets on contract NAS1-5212 (Ref. 2). In this case the approach was to begin the development with small angle shaped charge liners (20° - 30°) which would produce jet velocities of 10 to 11 km/sec. These designs would then be modified to increase the jet velocity. Using this approach it was not possible to form cohesive jet

material at velocities beyond 11 km/sec for nickel and 8.5 km/sec for 1020 steel. During the course of the work on contract NAS1-5212 a new shaped charge (called the hyperbolic design) was developed and observations regarding the jet formation process were made which led to the approach taken on the present contract. Also, both the hyperbolic shaped charge and a slightly modified version of a BRL shaped charge design were calibrated for mass and velocity of the jet pellets (Ref. 3). Three of the hyperbolic designs, assembled with nickel liners, and three of the BRL designs, assembled with iron liners, were delivered to NASA for rocket reentry tests.

The basis of the hyperbolic charge design was the control of the cross-sectional area of both the explosive charge and the liner in order to obtain an axially integral jet. The whole jet (neglecting some non-steady state material) produced by this design was utilized for the meteoritic simulator; whereas, for a conventional conical design only the jet tip which is a small fraction of the total jet could be utilized. It is believed that the importance of the design, in regard to the work conducted on the present contract, was the demonstration of the degree to which the jet formation process could be controlled by charge geometry.

The following observations made during work on contract NAS1-5212 were considered significant:

1. For a given shaped charge liner cone angle and liner material there appeared to be an upper limit to the jet velocity beyond which the jet material became progressively less cohesive (radially unstable) as the jet velocity was increased.

2. There was evidence that as the cone angle was increased the velocity at which jet degradation began increased. An analysis was made (see Appendix A) using steady-state shaped charge theory and it was found that this observation was predictable if the sound velocity of the liner material was assumed to be a critical parameter.

3. For a given cone angle, the velocity at which jets from iron liners began to degrade was lower than that for the jets from nickel liners.

4. Tests with ingot iron and 1020 steel liners indicated that both material purity and grain size might be important in forming cohesive jets.

As a result of the above observations it was proposed to meet the goals of this project by working with large angle liners (in the range 50° to 70°). Once this approach was taken, it became necessary to design an explosive charge which could deliver additional energy to the large angle liners because, in general,

the jet velocity produced by a shaped charge liner decreases as the cone angle is increased. It was proposed to do this by developing a bi-explosive charge which would produce a convergent conical detonation wave. This detonation wave configuration would deliver more energy to the liner by increasing the effective detonation rate and by a more efficient energy coupling between the liner and the detonation wave.

The project was subdivided into three major programs as follows:

1. The largest and most extensive program was the development of the bi-explosive charge design and the subsequent evaluation of liner designs and liner materials in an attempt to produce an integral jet.

2. A program was conducted to test various types of nickel and iron to evaluate the effect of liner material chemical and physical properties on jet integrity. The majority of the tests were conducted with the hyperbolic charge developed on contract NAS 1-5212. This charge design was used because it allowed testing to begin prior to the development of the bi-explosive charge. This was also reasonable from the point of view that it was planned to use a hyperbolic type liner in the bi-explosive charge.

3. A program was conducted to evaluate the effects of changes in charge configuration (which change the C/M ratio) on the jets from hyperbolic liners. Again, this was done with the existing hyperbolic charge design so that testing could commence prior to the development of the bi-explosive charge. It was important to do this because very little of this kind of work had been done on the hyperbolic charge under Contract NAS1-5212 and it was important to determine how sensitive the hyperbolic charge was to variations in C/M ratios.

The above programs were carried on concurrently; and as soon as important information was developed on the latter two programs, it was used in designing charges for future bi-explosive charge tests.

In the following main body of this report the Bi-Explosive Charge Development and Shaped Charge Liner Development sections are presented first because they represent the main effort. The Nickel and Iron Material Properties Study and the Charge Configuration Program follow in that order.

There were many people and organizations contributing to the research and development work described in this report. In appreciation of this The Firestone Tire and Rubber Company expresses its gratitude to the following:

Messrs. A. R. Wineman and Moses Long of the Langley Research Center, NASA, for their technical guidance and unreserved cooperation.

To Ballistic Research Laboratories, Aberdeen Proving Ground for providing technical guidance and for providing machined explosives when they were critically needed and specifically, to Dr. C. M. Glass, S. K. Golaski and S. Kronman who gave valuable technical counsel and who recognized the need for the special explosive, and to J. Cole who pressed and machined the explosive.

To Battelle Memorial Institute and Dr. George W. P. Rengstorff for counsel on the properties of pure iron and for the fabrication of a sample of very pure iron which was used on the project.

To the American Iron and Steel Institute and Dr. D. J. Blickwede for donating the very high purity iron which was fabricated at Battelle.

To the ARMCO Steel Corporation and S. W. Zeller for donating their technical counsel and services in the preparation of pure iron samples, using their unique decarburization process.

TEST FACILITY

All design testing was done at the Defense Research Division test facility at the Ravenna Army Ammunition Plant.

Two test sites were used to study the experimental shaped charge designs. These are referred to as the Open Test Site and the NASA Test Site. The Open Test Site shown schematically in Fig. 1 was used to examine detonation wave formation, jet formation, and jet integrity at distances up to 30-inches from the base of the test charge. All Open Test Site testing was done in air (i.e. atmospheric pressure). The NASA Test Site, shown schematically in Fig. 2, was used to examine the jet character under vacuum conditions and most of the tests were conducted with the air pressure in the vacuum tube being in the range of 1 to 40 microns. The jets were radiographed after relatively long travel times at the NASA Test Site which resulted in a more accurate velocity determination than was possible at the Open Test Site.

At the Open Test Site the charges were placed 8 to 12-inches in front of blast-resistant cassettes (protective film holders used to cushion film from the shock of the explosive detonation). The upper cassette was used to radiograph the detonation wave configuration or to radiograph the collapse process of the liner and the resultant jet. It was also used to radiograph the jet at distances

of about 2 to 4-inches from the base of the test charge. A second "window" in the upper cassette permitted a radiograph of the jet pellet at approximately 10-inches of travel. The second cassette (below the first one) was used during the latter half of the testing program to radiograph the pellet at 25 to 30-inches of travel. Velocities were measured over the interval from the top window of the upper cassette to the lower cassette unless otherwise noted. Field Emission Corporation Model 233 X-ray pulsers (maximum voltage 300 Kv) were used for the radiography. Times used to determine the velocity were recorded using a Polaroid camera attached to a Tektronix model 545 single trace oscilloscope.

At the NASA Test Site rounds are fired through an evacuated 6-inch diameter aluminum tube 9-feet in length, passing two orthogonal radiographic stations centered approximately 35 and 95-inches from the base of the round. Using the data supplied by the orthogonal views and a computer program written to perform a three dimensional analysis, the jet pellet position and attitude in space were calculated. The mass and velocity of the jet could then be obtained directly from an IBM 1620 or an IBM 360 computer output (the jet mass was determined by this method only if the jet was integral). Field Emission Corporation Model 231 X-ray pulsers (maximum voltage 105 Kv) were used for the radiography. Times were measured by two independent methods. Two Beckman Model 7270 digital readout counters (triggered to start during the initiation of the tetryl booster and to stop by current viewing resistors mounted on the face of the X-ray pulser) were used in one method with a second back-up method using a Tektronix Model 545 oscilloscope similar to the test set-up at the Open Test Site. The pressure level was measured with a Kinney model KT93 Thermocouple Vacuum Gage.

The vacuum system used under contracts NAS1-4187 and NAS1-5212 was capable of reaching 40 microns in a pumping time of 60 to 90 minutes. For the work on contract NAS1-6886, NASA requested improvements on the system so that a 1 micron vacuum level could be reached. The system was re-designed to include a Kinney Model KDP-6, 6-inch diameter diffusion pump coupled to the existing Kinney Model KC-15 mechanical pump. Plumbing from the pumps to the vacuum tank was shortened and opened to a 4-inch inside diameter. A remotely operated 4-inch diameter ball valve was built into the system to protect the pumps during firing. Warm-up time for the diffusion pump was found to be about 15-minutes. The new system is presently capable of reaching less than one micron and has a pump-down time (starting with a cold diffusion pump) of 20 to 30 minutes.

RESULTS AND DISCUSSION

Bi-Explosive Charge Development

The development of an explosive charge which would produce a conical detonation wave was the first objective of the meteoritic simulator program. A conical detonation wave was required because the general approach to the problem included the use of large angle liners (50° to 70°) and the principal way known to obtain high jet velocities from the large angle liners was to increase the effective detonation rate of the explosive. It was decided to do this by waveshaping and specifically, to form a conical wave so that the effective detonation rate would be constant.

The waveshaping was accomplished by the use of bi-explosive charges. The functioning of these charges depended upon the use of two explosives with different detonation rates and an inert waveshaper. An analysis was made to determine the effect of various charge parameters on the bi-explosive charge design. Based on this study, two charge configurations were designed which would allow the evaluation of shaped charges with cone angles in the range 50° to 70°.

The first tests consisted of radiographing the wave fronts for various explosive combinations. A study was then made of the effect of both waveshaper material and waveshaper design on the detonation wave configuration. Finally, preliminary tests were conducted to determine the effectiveness of various explosive combinations in producing nickel and iron jet velocities in the neighborhood of 12 km/sec. A detailed discussion of the bi-explosive charge development follows.

Design studies. - An analysis of the bi-explosive system was made using the assumption that any point in the explosive which is initiated will act as a center from which a spherical detonation wave will emanate. Experience indicates that this is a reasonable assumption. The spherical wave front will expand into the undetonated explosive at a constant rate equal to the explosive detonation rate.

Consider the schematic drawing in Fig. 3 where a two-dimensional bi-explosive system is shown. Assume that explosive 2 has a greater detonation rate than explosive 1 and assume that a detonation originates at point A. The detonation will progress into explosive 2 as an expanding circular wave front and will initiate explosive 1 along the interface line , AB. As each point of explosive 1 is initiated along the line AB it acts as the center of an expanding circular wave. Fig. 3 was constructed by assuming that the detonation rate of explosive 2 (u_2) is 25 per

cent greater than the detonation rate of explosive 1 (u_1). It is seen that as the detonation front moves from A to B in explosive 2, the detonation front in explosive 1 moves from A to C. Also, as the detonation front in explosive 2 moves from E to B, the front in explosive 1 moves from E to J, etc.

It is seen that the envelope of the circular wave fronts is a straight line, BC, at the instant the detonation front in explosive 2 is at point B. Note that the straight line BC ends at point C and that for points to the right of C, the detonation front in explosive 1 is circular.

Since line BC is tangent to the circular front of radius AC at point C, it follows that angle ACB is a right angle. It follows then that the angle between the linear wave front BC in explosive 1 and the bi-explosive interface BA can be determined from the ratio of the detonation rates. Let angle ABC equal ϕ then

$$\sin \phi = \frac{AC}{AB} \qquad (1)$$

but $AC = u_1 t$ where t is time

and $AB = u_2 t$

therefore $$\sin \phi = \frac{u_1 t}{u_2 t}$$

$$\text{or } \sin \phi = \frac{u_1}{u_2} \qquad (2)$$

This result is analogous to that which occurs when a supersonic projectile moves through the air and produces a shock wave where u_2 would be the projectile velocity and u_1 would be the velocity of sound in air. Watson et. al. (Ref. 4) have conducted experiments with bi-explosive charges and have found that measured values of ϕ (from radiographs) correlated very well with those calculated from equation 2.

Design of bi-explosive shaped charge. - The purpose of the bi-explosive concept is to generate a conical detonation front which will have an included angle that is as close to the liner cone angle as possible. For a given explosive in contact with the liner, the greatest jet velocity should occur for this condition. An analysis was made to determine what values of conical detonation front cone angle could be obtained with available explosives and within the restrictions of the charge dimensions allowed by NASA.

The analysis was approached in the manner shown in Fig. 4. The line P_2P_4 represents the interface between explosive 1 and explosive 2 (where $u_2 > u_1$).

The line BCD represents the wave front in explosive 1 at some time after the initiation has started at point P_4. The initiation at point P_4 will be effected by a detonation wave starting at the rear of the charge and traveling around an inert barrier referred to as a waveshaper. The straight segment of the wave front is line BC while the line segment CD is a circular arc. It is desired that the geometry of the system be such that the linear portion of the wave front BC will intersect the liner wall as shown by the line B'C' (where C' and P_5 are coincident). The angle between the detonation front and the charge axis is $(\alpha+\theta)$ where α is the shaped charge liner half-angle.

For purposes of discussion it is convenient to consider the angle θ, which is the angle between the detonation front and the shaped charge liner wall. In general the optimum condition will occur when θ is zero. An examination of Fig. 4 shows that, for a given pair of explosives (which fixes the angle θ), the angle θ is a function of the liner radius, P_1P_2, the liner height, P_1P_5, and angle $P_4P_2P_3$ which is the angle that the bi-explosive interface makes with the horizontal. Angle $P_4P_2P_3$ is controlled primarily by the charge radius P_1P_7.

That is, the radius of the waveshaper, P_6P_4 (equals length of P_1P_3) is made to be about 1/8-inch less than the charge radius, therefore, the radial position of point P_4 depends on the radius P_1P_7. If there were no limitation on charge radius, then the line P_2P_4 could be rotated about P_2 until the detonation front BC was parallel to the liner wall P_2P_5, making θ equal to zero. However, the charge radius is fixed, which fixes the maximum radial positions of P_4 and allows only a vertical movement of point P_4. Thus, for a given shaped charge liner configuration there is an optimum vertical position of P_4. If P_4 is too far above the line P_1P_7, the line P_4P_5 will intersect the charge axis $P_1P_5P_6$ above the liner apex, adding unnecessary explosive to the charge. If P_4 is too low, the line P_4P_5 will intersect $P_1P_5P_6$ below the liner apex causing a portion of the curved detonation front, CD, to strike the liner wall, which is not desirable.

A general solution to the problem of determining the position of P_4 for a given liner angle (2α), liner diameter, and explosive combination was obtained. The mathematical development is described in Appendix B. Values for the position of P_4 and for θ were determined for the following parameters:

Liner Angle (2α)	-	50°, 70°
Explosive 1	-	octol, comp. B, pentolite, TNT, baratol
Explosive 2	-	octol, HMX

where octol and HMX were paired with each of the other explosives to form the bi-explosive system. The results are listed in Table I. It is seen that for a given outer explosive, the Y position of P_4 and θ both decrease as the detonation rate of the inner explosive decreases. Also, note that the value of θ is smaller for a given inner explosive when HMX rather than octol is the outer explosive. The values of θ obtained for the cases where baratol is the inner explosive are seen to be negative. This means that the conical detonation wave is tilted sufficiently such that it will strike the base of the liner first, instead of the apex. This result occurs because of baratol's low detonation rate and because the radial position of P_4 was held constant. The value of θ could be made zero by reducing the radial coordinate of P_4. This would be comparable to rotating the line P_2P_4 in Fig. 4 counterclockwise.

A value u_E is listed in the table which gives the effective detonation rate of the bi-explosive charge as though it were a single explosive. The effective detonation rate is obtained from the expression

$$u_E = \frac{u_1 \cos \alpha}{\sin \theta} \tag{3}$$

where, u_1 is the detonation rate of the inner explosive of the bi-explosive system, θ is the angle between the detonation front and the liner wall, and α is the liner half angle. The expression is obtained by equating the time it would take a conical detonation front to sweep a given length of liner wall to the time it would take a plane detonation wave (traveling parallel to the liner axis) to sweep the same length. The relationship is derived in Appendix B.

The values of u_E listed in Table I are probably the best measure of the relative effectiveness of various explosive combinations. The values u_E are generally very large relative to

the detonation rate of single explosives. In fact, when θ is zero, u_E becomes infinite. This would be the case for baratol if the design were adjusted to cause θ to be zero (the negative value of u_E for baratol simply means the detonation wave would sweep the liner from liner base to liner apex). The bi-explosive design can be thought of as a way of making a higher detonation rate explosive from two ordinary explosives. There is a limitation to the concept, however, in that the jet velocity depends on the energy inherent in the inner explosive, as well as on the effective detonation rate. Thus, even though the data in Table I would seem to indicate that baratol is the best inner explosive, this was not the case, because it is the least energetic of the explosives considered.

In order to limit the number of loading fixtures which would have to be made, it was decided to try one design (one value of P_4) for the 50° liner and one for the 70° liner. A value of P_4 was chosen from Table I for each of the two designs, one that lies between the optimum values for octol/comp.B and octol/pentolite. The decision to choose a value of P_4 below the comp.B optimum was made to insure sufficient explosive above the waveshaper.

All explosive combinations were tested in these two designs. Since the point P_4 was arbitrarily chosen for the latter two designs, the values of θ listed in Table I were not valid. A set of values for θ was calculated for the chosen values of P_4 and is presented in Table II. The method of calculation is included in Appendix B. Note that for the case of an octol/baratol charge and a 50° liner, the angle θ is positive and almost zero; for the 70° liner θ is negative. It should be pointed out that because the values for P_4 were chosen below the optimum value for comp.B, a small portion of curved detonation front would be expected to strike the apex of the liner for the octol/comp.B combination.

Two bi-explosive charges were designed using the values of P_4 given in Table II. Assembly drawings of them are shown in Figs. 5 and 6. The method of assembling the charges is shown in Fig. 7.

Bi-explosive charge waveshaper tests. - The purpose of the initial bi-explosive charge studies was to radiograph the detonation wavefront for various explosive combinations in order to observe the wave forms produced and to measure the angle θ between the wavefront and the liner wall. These tests revealed that waveshaping was occurring and that the straight portion of the wavefront formed approximately the predicted angle θ. However, the portion of the curve near the charge axis was different than expected; it formed a smooth curve through the center of the charge, convex upward (toward the waveshaper). This result showed that the Lucite waveshaper had not completely performed its function; it had allowed the inner charge (of the bi-explosive system) to be initiated at the waveshaper-inner charge interface.

Tests were then conducted with lead waveshapers. It was known that lead had the property of transmitting shocks at low velocity and would, therefore, perform the required waveshaping. Tests conducted with the lead waveshapers showed that the detonation wavefronts were remarkably close to those predicted by Huygens' construction methods.

A third series of tests was then conducted using rigid polyurethane foam as the waveshaper material. It was necessary to find a lighter waveshaper material as a substitute for lead because the weight of a lead waveshaper could not be tolerated in the final design. Polyurethane waveshapers of various angles were tested. It was found that while the rigid polyurethane foam did not work as well as lead, it would be acceptable with the proper waveshaper configuration.

Details of the tests summarized above are given in the following sections.

Lucite waveshaper tests: The first bi-explosive charges tested were not assembled with shaped charge liners. A 40° liner with a 2-inch diameter base and a 0.25-inch flat apex was used to mold a conical cavity inside the inner charge. (This liner configuration was used simply because it was available at the time.) The bi-explosive charges incorporated a Lucite waveshaper with a 90° apex angle (shown as item 7 in Fig. 8). Lucite was chosen as a waveshaper material because it had been previously used for this purpose in shaped charge designs. The particular configuration shown in Fig. 8 had been used in a test conducted on Contract NAS1-4187.

The test results are summarized in Table III. Discussion of the results follows:

1. (Tests 923-1, 923-2, 923-4, 923-6) - These charges were the first ones tested to determine the degree of waveshaping achieved with the bi-explosive charge design. The explosive combinations comp.B/octol, pentolite/octol and baratol/octol were evaluated. It was found that a waveshaping effect was occurring. The detonation wave in the outer explosive (octol) was observed to lead the detonation front, while the detonation wave in the inner explosive started at the octol front and swept back toward the base (initiation point) of the charge. For the two inner explosives, comp.B and pentolite, the detonation wave had a straight line portion near the bi-explosive interface, then became curved near the charge axis. The curve was convex upward (toward the initiator). The detonation front in baratol was not observed because of the high X-ray absorption of the gaseous explosive products.

2. (Tests 923-9 through 923-14) - This group of charges was fired in an attempt to obtain better resolution of the detonation front and to obtain radiographs of the detonation front at various positions between the waveshaper and the apex of the conical cavity in the inner explosive.

It was found that a smaller X-ray source-to-film distance improved the resolution of the detonation front in the radiographs. Radiographs of the detonation front taken between the waveshaper and the apex of the conical cavity confirmed that the Lucite waveshaper transmitted a shock wave of sufficient pressure and velocity to initiate the inner explosive (at the waveshaper-explosive interface) before it could be initiated by the detonation wave originating at the bi-explosive interface. A comparison is made between predicted wave fronts and radiographs of the wave fronts in Fig. 9 for various charge designs. It can be seen that the detonation front for the Lucite waveshaper(Tests 923-13) spans the whole inner explosive. It should be pointed out that the modification of the wavefront due to shock initiation by the Lucite waveshaper was most severe in the region between the waveshaper and the liner apex. As the detonation wave proceeded toward the bottom of the charge, the effect of initiation at the bi-explosive interface became dominant. (This is due to the higher detonation rate of the outer charge of the bi-explosive system.) In fact, the wave (for Lucite waveshapers) was observed to be approaching a conical form by the time it reached the apex of the charge cavity.

Lead waveshaper tests: As a result of the tests just discussed, it was concluded that the shock velocity in Lucite was too high to be used in the existing bi-explosive charge design. In order to study the waveshaping phenomena with the waveshaper performing its intended function, a new waveshaper was designed (Fig. 8 - item 5) where the angle β was changed from 90° to 80°. Lead was chosen as the waveshaper material because of its known low shock velocity. As stated previously, lead was used strictly for purposes of the experiment; its high density would prohibit its use in the final design.

The test data for the first lead waveshaper tests are included in Table III(Tests 923-15, 923-16, and 923-17) and radiographs of the detonation waves are included in Fig. 9. Notice the excellent correspondence between the predicted waveshape (by Huygens' construction) and the actual waveshape. This indicates that detonation waves formed with bi-explosive designs can be described quite well using the relatively simple Huygens' construction approach.

Table IV compares the predicted angle θ, between the wave front and the conical cavity wall, with the average measured value. The two values are seen to compare very well for the case of the

lead waveshaper. This further indicates the usefulness of the technique used for analyzing bi-explosive charge designs.

There is a phenomenon involved in the waveshaping process which should be mentioned. Experimental studies have been conducted (Ref. 5) which show that when detonation waves intersect, another wave called a Mach wave (Mach bridge or Mach stem) can be formed. The Mach wave travels in a direction along the axis of symmetry between the intersecting waves. It has been found that Mach waves form when the included angle between the intersecting waves is in the neighborhood of 100°. The question arose as to whether the intersecting detonation waves produced by the bi-explosive system would give rise to Mach waves. Radiographs of the detonation such as shown in Fig. 9,Test 923-17, showed no evidence of Mach waves; however, this may have been due to the small angle of intersection. As the wave approaches the conical shape, the angle of intersection will increase to the point that a Mach wave may form. However, at this point the detonation wave will begin to intersect the shaped charge liner, thereby preventing the formation of a Mach wave.

It was concluded that the bi-explosive system would generate the desired conical wave when the waveshaper functioned properly.

Polyurethane foam waveshaper tests: Rigid polyurethane foam was evaluated in four configurations. Three of the designs incorporated 60°, 70°, and 80° angles, shown as items 1, 3, and 5 in Fig. 8. The fourth design, shown in Fig. 10, had an included angle of 43° and was truncated.

The test data are summarized in Table V and radiographs of the resultant wave are included in Fig. 9.

The test with the 80° waveshaper (Fig. 9,Test 923-21) shows that this design was a great improvement over Lucite. It is seen that there is some curving of the wave near the charge axis; however, the basic waveshape desired was produced. Radiographs for the 70° and 60° designs (Fig. 9,Tests 923-32, 923-33) were taken at an earlier time than that for Test 923-21 in order to observe conditions at the waveshaper-explosive interface. Examination of the radiographs revealed that some initiation might be occurring for both the 70° and 60° designs.

During a review of these results it was recommended by Ballistic Research Laboratories that a truncated waveshaper design be tried. It was agreed that the design shown in Fig. 10 be tried. A radiograph taken during one test with this design (Fig. 9,Test 923-35) shows a wave with about the same shape as that from a lead waveshaper (Fig. 9, Test 923-15).

It was concluded that, although the above results did not definitely prove that the 43° truncated design is as good as a lead waveshaper, it would be acceptable. It was reasoned that even though there might be a small modification to the center of the wave in the region between the waveshaper and the liner apex, the wave would be conical by the time it reached the liner apex. A photograph of an inert sectioned model, which incorporates the 43° polyurethane waveshaper, is shown in Fig. 12.

Bi-explosive charge jet velocity tests. - The initial tests, to determine the velocities which could be obtained from bi-explosive charges, were conducted with 40° hyperbolic liners, Fig. 11. These liners, discussed later in this report, were used because it was convenient to do so at the time of the test. The 40° liners were assembled in the 50° loading fixture (Fig. 7). Since the 40° liners were taller than the 50° liners, their apexes would be intercepted by a curved portion of the detonation front. This would tend to produce a velocity gradient in the jet because the rate at which the detonation wave swept the liner wall would vary.

Tests were conducted with comp.B/octol, pentolite/octol, and baratol/octol bi-explosive charges. The first charges tested were assembled with Lucite waveshapers, the later ones were assembled with lead waveshapers. Both nickel and iron liners were evaluated.

Most of the tests were conducted in air where the jets were radiographed after only six to ten inches travel. This was done because the velocities which would be produced by the various explosive combinations were unknown and more error can be tolerated in estimated radiograhic times when jet travel is short.

The data are summarized in Table VI where it is seen that velocities in the range 10.1 km/sec to 11.9 km/sec were achieved and that the jets produced were not cohesive. The latter condition was attributed primarily to the fact that the cone angle was too small to permit cohesive jet formation at the velocities achieved.

The first three charges listed in Table VI(Tests 923-3, 923-5, 923-7) show that the comp.B/octol and pentolite/octol charges produced approximately the same jet velocities, while the baratol/octol charge produced the lowest velocity (10.1 km/sec). The latter result provides two important insights into the bi-explosive charge designs. First, the fact that a shaped charge liner cast with baratol produced a jet velocity as high as 10.1 km/sec shows the effectiveness of the waveshaping process. This follows from the fact that baratol is a very low energy explosive and that even a cylindrical shaped charge liner, cast in a cylindrical baratol charge and initiated in the conventional way, would be expected to produce a jet velocity no greater than 8.2 km/sec (twice baratol's detonation rate). The other important

observation is that while waveshaping enhances the effectivenss of a given inner explosive, the inherent energy of the inner explosive is very important. That is, it can be determined from Table II (taking into consideration that a 40° liner was tested) that the effective detonation rate was about 38.7 km/sec for the baratol/octol charge, yet the jet velocities for the comp.B/octol and pentolite/octol charges were greater even though their effective detonation rates were much lower. Based on these results, it was decided to employ bi-explosive charges with the highest energy explosive combination available. At first this was comp.B/octol; later it was octol/PBX 9404 or octol/HMX.

The data for Rds. 923-19, 923-23 in Table VI show the results of a first attempt to eliminate the jet velocity gradient by modifying the liner design. This technique is discussed in detail later in the report. It is seen that the velocity difference between jet tip and jet tail was reduced from 0.6 km/sec to 0.3 km/sec by the modification. This encouraging result was the basis for using this approach in later designs aimed at eliminating the jet velocity gradient.

Conclusions. - The results of the bi-explosive charge development allow the following conclusion to be made:

1. The bi-explosive method of forming a conical detonation wave was successful.

2. The Huygens' construction method adequately described the bi-explosive detonation wave formation for purposes of charge design.

3. Waveshaping can produce a significant increase in jet velocity for a given inner explosive.

4. The selection of a pair of explosives for a bi-explosive charge should be made such that the highest energy explosive possible is used as the inner charge, for a given outer charge. For example, octol/HMX is preferable to comp.B/octol because octol as the inner charge will deliver more energy to the liner than comp.B as the inner charge.

Shaped Charge Liner Development

The liner development studies were conducted in two major phases. First, conical liners were evaluated in the bi-explosive charge and then hyperbolic liners, designed to reduce the jet velocity gradient, were tested.

The conical liners were tested knowing that a jet with a large velocity gradient would be produced. The reason for testing them was that the range of jet velocities and the degree of jet integrity obtainable from bi-explosive charges could be determined for a range of cone angles with relatively low cost liners. Cone angles of 50°, 60° and 70° were evaluated with wall thicknesses varying in the range .030 to .050-inch. The liners were tested in both comp.B/octol and octol/PBX 9404 bi-explosive charges.

The various hyperbolic liner designs tested were aimed at producing an integral jet (a jet exhibiting no axial or radial dispersion). The tests with the conical liners had shown that it was possible to form cohesive jet material with a nominal jet velocity of 12 km/sec. The hyperbolic liners were designed to control the charge-to-mass (C/M) ratio in a manner to reduce or eliminate the jet velocity gradient, thereby producing an integral jet.

Detailed discussions of the liner designs and test results are presented in the following sections.

Conical liner tests. - The conical liners tests, as was stated earlier, were intended to determine the velocities obtainable from the bi-explosive charge system as well as the character of the jet material for a series of liner cone angles. The majority of the tests were conducted with 50° and 70° nickel and iron liners with wall thicknesses of .030 and .050-inch. A few tests were also conducted with 70° nickel liners that had wall thicknesses of .015 and .020-inch and with a 60° iron liner that had a .040-inch wall.

The conical liners were tested in either of two bi-explosive charge configurations; the 50° design or the 70° as shown in Figures 5 and 6. As was stated earlier in the section on bi-explosive charge development, the 50° and 70° charges were designed such that the 50° and 70° liners would be swept by conical detonation waves except for a very slight curvature at the liner apex for most explosive combinations. Thus, for the case of the 50° charge, all 2-inch diameter liners with cone angles greater than 50° will be swept by a conical detonation wave. Any liner with a cone angle less than 50° will have its apex region swept by a curved front (due to the greater height of the smaller angle liner). The same reasoning follows for the 70° charges.

The shapes of the detonation fronts (at one microsecond time intervals) for the 50° and 70° charges are shown in Fig. 13 for the two explosive combinations comp.B/octol and octol/PBX 9404. It is seen that for all cases the liner apex experienced a very slight curved detonation front.

All of the bi-explosive charges, for the conical liner program, were assembled with lead waveshapers because the polyurethane waveshaper had not yet been developed.

The results of the conical liner tests are summarized in Table VII. Note that except for a few cases each liner design was tested in both air and vacuum. The velocities determined under vacuum conditions are considered more accurate because of a more accurate time interval measurement. In the following discussions, wherever possible, the velocities referred to are those determined in vacuum.

50 Degree conical liner tests: Fifty degree conical liners made from nickel 200 and Forma iron were tested in the 50° comp.B/octol bi-explosive charge. Liner wall thicknesses of .030-inch and .050-inch were tested. A drawing of the 50° conical liner is shown in Fig. 14.

The data in Table VII shows that the .030-inch wall thickness liners produced jets with tip velocities of 11.3 km/sec and > 11.6 km/sec for the materials nickel 200 and Forma iron respectively. However, liners from both materials failed to produce cohesive jets as shown by the radiographs in Fig. 15(Tests 923-45, 923-30).

The .050-inch wall thickness liners produced jet velocites of 10.23 km/sec and 10.7 km/sec for nickel and iron respectively. The radiograph in Fig. 15(Tests 923-44, 923-29) show that the nickel jet was cohesive and that all but the tip of the Forma iron jet was cohesive.

It was concluded that for 50° conical liners, a jet velocity of 11.34 km/sec is borderline in regard to nickel jet integrity while a velocity of 10.7 km/sec is borderline for Forma iron. Further evaluation of 50° liners in an attempt to produce an integral 12 km/sec jet was not ruled out however, for two reasons. First, purer forms of both nickel and iron were available for subsequent tests and it is shown in other sections of this report that jet integrity is related to the chemical and physical properties of the liner material. Secondly, there was the possibility that changing the liner configuration could improve the jet integrity.

60 Degree ingot iron liners: Two tests were conducted with .040-inch wall ingot iron liners in the comp.B/octol bi-explosive charge. The liners were made from ingot iron because they could be easily modified from some existing 60° liners in stock. It is seen in Table VII that a nominal jet velocity of 10.6 km/sec was obtained. The jets appeared to be cohesive after about 36-inches of travel in air.

70 Degree conical liner tests: The majority of the 70° liners were made from Forma iron and nickel 200 and were tested with wall thicknesses of .030-inch and .050-inch. A few additional tests were conducted with nickel liners where wall thicknesses of .015-inch and .020-inch were tried. A drawing of the 70° liner is shown in Fig. 16. The 70° liners were tested in both the 70° and 50° bi-explosive charge designs. The latter charge configuration was used for the 70° liners when PBX 9404 was used as the outer explosive. This was necessary because loading fixtures to assemble bi-explosive charges with PBX 9404 or HMX were fabricated only in the 50° design.

The .030-inch wall thickness liners were tested with comp.B/octol, comp.B/PBX 9404 and octol/PBX 9404 bi-explosive charges.

The PBX 9404 referred to above is a plastic bonded explosive containing 94% HMX which is described in more detail in a following section of the report. The outer charges composed of this explosive were fabricated by Ballistic Research Laboratories. When tests with this material showed it to be desirable for achieving higher jet velocities, a press loading fixture (Fig. 17) was designed which made it possible to press load HMX outer charges at the Ravenna explosive loading facility. These charges consisted of 98% HMX. Tests with both units indicated that their performance was such that they could be interchanged in the bi-explosive charge. Thus, in the following discussion no effort is made to separate the results for the two types of outer charges, other than to show which one was used for a given test.

The other 70° liners with .015-inch, .020-inch and .050-inch wall thicknesses were tested in comp.B/octol charges except for one .050-inch wall liner where the inner and outer explosives were both octol (which produced a peripherally initiated charge). The test data are included in Table VII and the results are described in the following sections:

1. 70 Degree nickel liners with comp.B/octol bi-explosive charge: a jet tip velocity of 10.3 km/sec was obtained for the conical nickel liner with the .030-inch wall thickness (Test 924-4) and a velocity of 9.2 km/sec was observed for the .050-inch wall thickness liner(Test 924-2). A velocity difference of about 1.2 km/sec existed between the jet tip and jet tail for these charges. The jet material was cohesive in that there was no radial dispersion as shown in Fig. 15(Tests 924-4, 924-3)

Two additional nickel liners were tested, one with .020-inch wall thickness and the other with .015-inch wall thickness. The .020-inch wall liner(Test 946-7) gave a jet velocity of 12.49 km/sec. The jet material tended to be radially unstable although the jet tip was composed of cohesive segments. The .015-

inch wall liner(Test946-8) produced a jet tip so badly dispersed that it was not recorded on the radiograph. The velocity of 10.81 km/sec which is listed in Table VII was for the slower elements of the jet.

These tests showed that it is possible to achieve high jet velocities from 70° nickel liners by employing comp.B/octol bi-explosive charges and relatively thin wall liners.

2. 70 Degree nickel liners with octol/PBX 9404 bi-explosive charge: The 70° nickel liners with .030-inch wall thicknesses were also tested in octol/PBX 9404 charges. This charge with octol as the inner explosive is capable of delivering more energy to the shaped charge liner than the comp.B/octol charge.

The PBX 9404 explosive used for the outer charges for these tests is composed of 94% HMX, 3% Nitrocellulose, and 3% CEF (tris β-chloroethylphosphate). The outer charges were fabricated at the Ballistic Research Laboratories by first pressing the powdered explosive into 6-inch diameter billets then machining them to the required configuration. When the outer charges were assembled to the inner charges (which were cast at Firestone's test facility) it was found that there was a slight mismatching. The thick end of the outer charge extended beyond the liner base. The units were then removed and machined in a remote control drilling fixture. Because the drilling fixture had been designed for other purposes it was difficult to machine the explosive to close tolerances. The result of the face-off operation was to make the units shorter than desired. One of the units in particular was faced-off too short; as a result when it was assembled to the charge there was a .105-inch gap between the adaptor plate and the PBX 9404 explosive as shown in Fig. 18. This is mentioned because it is thought that the air gap may have had some effect on the shape of the jet. The other outer charges also failed to contact the adaptor plate, however, the gap was only a nominal .038-inch. Cohesive jets with velocities of 11.87 km/sec were produced. A radiograph of the jet for Test 939-5 is shown in Fig. 19. Thus, it is seen that the octol/PBX 9404 bi-explosive charge increased the jet tip velocity from 10.3 km/sec (for comp.B/octol) to 11.87 km/sec. It must be emphasized that this was only the jet tip velocity and that the greatest part of the jet was moving at lower velocities.

3. 70 Degree Forma iron liners with comp.B/octol bi-explosive charge: Cohesive iron jets were produced by the .030-inch and .050-inch wall thickness liners with jet tip velocities of 11.1 km/sec(Test 924-8) and 9.5 km/sec(Test 924-9) respectively. This was the first time a cohesive iron jet had been observed at such high velocities. This provided a positive demonstration that liner cone angle was important in producing cohesive jet material since 50° Forma iron liners with jet velocities of 10.7 km/sec and 11.7 km/sec were not cohesive.

4. 70 Degree Forma iron liners with comp.B/PBX 9404 and octol/PBX 9404 bi-explosive charges: Three tests were conducted with the .030-inch wall thickness liners. One was tested with the comp.B/PBX 9404 charge and two with the octol/PBX 9404 charge; cohesive jets with tip velocities of 12.2 km/sec (Rd. 939-1) and 12.47 km/sec (Rd. 939-4) respectively were obtained from the two types of bi-explosive charges. A radiograph of the latter jet is included in Fig. 19 (Rd. 939-4).

It is interesting to compare the effective detonation rates and energy coupling angle for the comp.B/PBX 9404 and the octol/PBX 9404 charges as follows:

Bi-Explosive Charge	Effective (1) Detonation Rate (km/sec)	Energy (2) Coupling Angle θ (degrees)
comp.B/PBX 9404	15.7	24.4
octol/PBX 9404	13.2	31.3

(1) Rate at which a plane wave would have to move to sweep the liner wall in the same time as a conical wave.

(2) Angle between conical wave front and liner wall.

It is seen that even though the comp.B/PBX 9404 charge had a higher effective detonation rate and more favorable angle, the octol/PBX 9404 jet velocity was greater. This shows that the energy of the inner explosive is a dominant factor (since octol is more energetic than comp.B).

The jets from bi-explosive charges with PBX 9404 outer charges appeared to be composed of two sections; a small diameter high velocity section followed by a larger diameter lower velocity section. This effect was especially evident for Rd. 939-1 as seen in Fig. 20. Since Rd. 939-1 had a .105-inch air gap between the outer charge and adaptor it is possible that the somewhat unusual jet configuration is related to the air gap. One effect that the air gap would produce would be to allow an ambient pressure rarefaction wave to move into the high pressure gaseous explosion products as soon as the detonation wave reached the bottom of the charge. This would tend to reduce the impulse given to the lower end of the liner and reduce the velocity of the jet elements coming from the bottom of the liner. Consideration of this effect later lead to the use of iron adaptors instead of aluminum adaptors for certain charge designs.

Two significant results were observed from these tests. First, it was shown that cohesive iron jet material could be produced at velocities as high as 12.47 km/sec. Secondly, it was

shown that high jet velocities could be achieved from large angle liners by the employment of waveshaping.

5. Peripheral initiation tests with 70 degree Forma iron liner: The charge configuration for this test was that of the 70° bi-explosive charge except that the inner charge and outer charge were both octol; thus, no conical detonation wave would be expected to form. Because the explosive below the waveshaper would be initiated from a point (considering a cross-section of the charge) at the outer radius of the waveshaper, the liner would be swept by a spherically expanding wave. The sweep rate would be greatestat the liner apex, then it would decrease as it moved down the liner.

It is seen in Table VII (Rd. 924-7) that the jet tip velocity was equal to that obtained with the comp.B/octol bi-explosive charge. At first sight this might appear to be a good approach to the problem of achieving high meteoritic simulator velocities (historically, this technique was used many years ago in shaped charge warhead studies). There are two reasons why the peripheral initiation method is not considered as good as the bi-explosive charge approach:

1. The rate at which the detonation wave would sweep the liner wall would not be constant, thereby introducing a velocity gradient into the jet.

2. Since the comp.B/octol bi-explosive charge produced a jet tip velocity equal to that from peripherally initiated octol, it is possible to obtain a greater velocity by utilizing an octol/HMX charge where octol is the inner explosive.

Conclusions - conical liner tests: It was found that jet tip velocities as high as 12.47 km/sec could be achieved (with 70° iron liners) by use of bi-explosive charges. This demonstrated the effectiveness of waveshaping in producing high jet velocities with large cone angle liners. A more important result was that the jet material from 70° liners was cohesive. There was no evidence of radial dispersion of the jet material. Prior to these tests iron had not been observed in a cohesive form above 9.4 km/sec and even the latter velocity level was achieved only by using a special electron beam melted iron. This demonstrated the effectiveness of employing large angle liners to achieve jet integrity.

Hyperbolic liner tests. - The conical liner tests had established that liners with cone angles in the range 50° to 70° were capable of producing cohesive jet material with velocities as high as 12.5 km/sec. The problem now was to produce an integral jet, one exhibiting no radial or axial dispersion.

Work done on Contract NAS1-5212 had shown that an integral jet could be produced from a conical liner by keeping C/M nearly constant along the charge-liner axis. (The C/M is defined as the ratio of the explosive charge mass to the metal mass propelled by the explosive. In this application the ratio of the charge cross-sectional areas, measured in a plane perpendicular to the charge-liner axis, is multiplied by the ratio of the explosive to liner material densities to obtain the C/M ratio.) Both the explosive charge area and the liner area were controlled for the design developed on contract NAS1-5212. It was required that C/M remain constant. This meant that both the charge and liner wall cross-sectional areas were required to remain constant at all points along the liner axis (so that their ratio would be constant). It was found that when a liner with a conical exterior is required to have a constant cross-sectional area, the inside surface of the liner had to be hyperboloid. That is, it is generated by revolving a hyperbola about its axis of symmetry. Liners designed on this principle were referred to as hyperbolic liners. The charge designs under discussion also required that the external charge surface be generated by a hyperbola in order to produce a constant cross-sectional charge area. In practice, the hyperbolic surface for the explosive was approximated by a conic surface which caused a relatively small variation in C/M. The resultant shaped charge design produced an integral jet. Thus, it was shown that an integral jet could be produced by controlling C/M.

It was not practical to modify the external charge configuration for the bi-explosive charge. The C/M ratio had to be controlled by varying only the liner wall cross-sectional area. If it is required that the ratio of explosive charge cross-sectional area (between the charge's cylindrical exterior surface and its conical interior surface) to the liner wall cross-sectional area remain constant, then it is found that, again, a hyperbolic interior surface is required for the liner. However, in this case the shape of the hyperbola (which generates the interior liner surface) is such that the cross-sectional area of the liner increases from liner base to liner internal apex.

The fact that it was possible to achieve a constant C/M by employing a hyperbolic liner did not constitute a solution to the problem of forming an integral jet. Experience on contract NAS1-5212 and further studies of the hyperbolic charge conducted on this project (discussed later in this report) showed that a constant C/M condition does not always assure an integral jet. The shaped charge jetting process is a very complex one and the constant C/M criterion, while effecting a very good first approximation to the required design, is not a sufficient condition for assuring the formation of an integral jet. Realizing this, it was decided to approach the problem by starting with constant

cross-sectional area hyperbolic liners, then making various modifications to the liners so that their cross-sectional areas would vary, thereby varying C/M.

A discussion of the liner design and results of tests with 50°, 60° and 70° liners are given in the following sections.

Hyperbolic liner design: A study was made of the liner wall cross-sectional area variations and the resultant C/M variation which could be achieved by modifying constant cross-sectional area liners. The reason for taking this approach was that it minimized the templates needed to study a number of C/M variations. This reduced the cost, but more important, it eliminated the time required to obtain the templates.

Two ways of modifying a constant cross-sectional area liner are shown in Fig. 21. If material is removed from the outer surface of the liner by making a tapered cut from liner apex to liner base as shown in Fig. 21a, the liner cross-sectional area varies as shown in Fig. 22a where the base wall thicknesses shown are those which exist after the cut is made. The explosive charge cross-sectional area variation is shown in Fig. 23. The resultant C/M obtained by dividing the explosive charge area in Fig. 23 by the liner areas shown in Fig. 22a is shown in Fig. 24a for type (a) liner area variation. The C/M curves shown in Fig. 24a do not take into account the fact that there are two explosives; it assumes a homogeneous explosive. (The effect of introducing weighting factors to account for the two explosives was investigated and found to produce a minor effect on the C/M curve.) It is seen in Fig. 24a that various degrees of C/M variation can be achieved depending on the amount of material removed from the outer surface of the liner. This includes one modification which produces a constant C/M condition. Thus, it is seen that a range of C/M variations can be studied for the same hyperbolic interior surface.

The second way of modifying constant cross-sectional area liners is to cut material off the outer surface parallel to the outer surface as shown in Fig. 21b. This causes the cross-sectional area of the liner to increase linearly from base to apex as shown in Fig. 22b. The C/M ratio produced by this modification is shown in Fig. 24b. It is seen that some of the C/M curves have maximum values between the apex and base of the liner. The latter feature might have been cause for rejection of this modification were it not for the fact that the original hyperbolic liner design discussed in detail later exhibited this general type of C/M curve and it formed an integral jet.

Liner designs of both modification were tested. In discussing tests with these designs in following sections of this report, the first type (Figs. 21a, 22a, 24a) is referred to as

the Non-Linear Wall Area Design and the second type (Figs. 21b, 22b, 24b) as the Linear Wall Area Design. That is, the liner type is described in terms of its liner wall cross-sectional area variation. The degree of liner wall cross-sectional area variation is given in either of two ways. One is in terms of the ratio of cross-sectional area at the internal apex to the cross-sectional area at the base (where the area is measured in a plane perpendicular to the liner axis). Another measure of the degree of cross-sectional area variation is the wall thickness at the base (measured in a direction perpendicular to the liner axis). Most of the liners studied were modified from constant cross-sectional area designs which had .030-inch wall thicknesses at the base. Thus, if for example the modified design had a .020-inch wall thickness at the base, this would represent a greater degree of variation than a modified design which had a .025-inch wall thickness at the base.

Iron hyperbolic liner tests: The major effort to produce a 12 km/sec integral jet pellet was made with iron. There were two reasons for this. First, an iron meteoritic simulator was considered to be of greater importance than a nickel one. Secondly, nickel is more prone to form a cohesive jet than iron and it was assumed that if an integral iron jet could be obtained, then the subsequent development of an integral nickel jet would be relatively simple.

The sequence of liner designs tested was dependent on the availability of various types of iron. In a later section of this report the results of a liner material study are presented. This work was carried on concurrently with liner development and was almost exclusively devoted to obtaining a form of iron which would form an integral jet. In the latter work it was found that the purity and grain size of the iron were important to cohesive jet formation. When plans were made to begin the testing of iron hyperbolic liners, the best form of iron (electron beam melted iron) as determined by the materials study was not yet available. Therefore, it was decided to conduct the initial tests only with 70° liners, since tests with conical liners had demonstrated that the greatest chance of achieving a cohesive jet would be with the large cone angle liners. Later, when the EBM iron became available, a liner cone angle study was made where 50°, 60° and 70° liners were tested. A type of iron comparable in purity to EBM iron and another exceptionally pure (99.995% pure) form of iron were also tested in 70° liner designs. Details of the tests are presented in the following sections.

1. Liner wall area variation studies with 70° liners: The liner material used for these tests was Forma iron, the same type of iron as used for the conical liner tests previously discussed. However, the Forma iron used for these liners was from

a different lot of material (Appendix C, lot 73) than that used for the conical liners. Its grain size was generally larger and not as uniform as the first lot.

Both non-linear and linear cross-sectional area variations were tried, each with two degrees of variation, as shown in Figs. 25, 26, 27, and 28.

The liners were cast in comp.B/octol bi-explosive charges which were assembled with lead waveshapers and aluminum adaptors. The test results are summarized in Table VIII.

It was found that the attempt to reduce the velocity gradient was successful,but that none of the liners produced a cohesive jet. A study of the radiographs showed that the non-linear wall area liners produced a jet with some residual positive velocity gradient and that the linear wall area liners tended to produce a slight reverse velocity gradient. Jets from both liner types tested in air (rather than vacuum) are shown in Fig. 29. Vacuum radiographs of the other non-linear area variation liners (Rds. 946-5, 946-6) showed the jets to be severely fragmented.

Two additional tests were conducted with the linear design liner where the liner wall thickness at the base was .020-inch. The ratio of the liner cross-sectional area at the internal apex to that at the base was made to be 1.75-inches and 2.00-inches by use of special templates. The main difference between these two liners and the other linear designs tested was that wall thickness was generally greater due to the use of the special templates. The results are shown in Table IX where it is seen that both liner variations failed to produce cohesive jets. The condition of the jets was much worse than for those described in Table VIII.

It was concluded that the non-linear area variation design was superior to the linear area variation because the latter design tended to produce a reverse velocity gradient, which experience has shown, will cause jet fragmentation. It is believed that the fragmented jets formed by the non-linear area variation liners were due to the Forma iron liner material. That is, tests conducted on the Nickel and Iron Material Properties Study phase of the project show that Forma iron with a carbon content of .04% and a grain size of ASTM4 to ASTM1 did not form cohesive jets as readily as EBM iron with a carbon content of .01% and a grain size of ASTM6 to ASTM8. Thus, it is seen that both the purity and grain size of this lot of Forma iron were not conducive to cohesive jet formation.

2. Test of constant C/M, 70° liners: The liners for this test were designed with a hyperbolic interior that would produce a constant C/M. A drawing of the liner is shown in Fig. 30.

The liners were made from Ferrovac Iron (Appendix C, lot 79B), which is comparable in purity to EBM iron. They were tested in both comp.B/octol and octol/HMX bi-explosive charges. Polyurethane waveshapers, as shown in Fig. 10, were used in these charges.

The results are shown in Table X where it is seen that a velocity of 11.3 km/sec was achieved with the octol/HMX bi-explosive charge (Rd. 974-3). None of the jets formed were cohesive. A radiograph of the jet from the comp.B/octol charge which was tested in air (Fig. 31, Rd. 974-1) shows that the jet definitely had a reverse velocity gradient since it is seen to be shorter in the second view relative to the first view. Radiographs of the jets from the octol/HMX charges tested in vacuum show the jets to be severely fragmented and dispersing radially.

It was concluded that the 70° constant C/M liner design will not form a cohesive jet in the existing bi-explosive charge design. In fact, the results just presented along with those presented in the previous section (tests of non-linear and linear liner area variations) show that a liner design which produces a C/M that increases from liner base to liner apex is required. Furthermore, it appears that the shape of the C/M curve is important since the non-linear area variation tended to produce a better jet than the linear area variation.

3. Tests of 50°, 60° and 70° EBM iron hyperbolic liners: The purpose of these tests was to determine the best cone angle for achieving a cohesive iron jet with a velocity of 12 km/sec or better, using electron beam melted iron. Tests already conducted with conical liners had indicated that it might be difficult to obtain a cohesive jet with a 50° liner. Furthermore, tests with hyperbolic 70° iron liners had failed to produce a cohesive jet It was believed that the chance of producing cohesive jets in these tests was much greater because EBM iron would be used as the liner material.

The liner design chosen for these tests was the non-linear wall area modification with the 1.48 area ratio. The C/M for this design is shown as the .020-inch base wall thickness curve in Fig. 24a. This design was chosen because previous tests showed that it tended to produce an integral jet, although the jet exhibited some velocity gradient. It was reasoned that it would be better to produce a jet with a slight positive velocity gradient than to choose another design and risk getting a reverse velocity gradient. Liner drawings are shown in Figs. 32, 33, and 25.

The EBM iron used for the liner material was of the same general chemical purity as the original piece tested in the materials study phase of this project. However, the grain size of the material was extremely large and variable in size. The EBM

iron had been received in the form of two billets 5-inches in diameter by 10-inches long (Appendix C, lot 74A). All but a 3-inch length of the material was hot forged to 2-1/2 inch diameter bars and annealed. The forging was done by people who were specialists in working with pure iron. Unfortunately, the resultant grain structure varied greatly in size, having a nominal value of ASTM1 (Appendix C, lot 74B). Although there was no specific data available at the time to prove it, it was felt the large grain size would be detrimental to cohesive jet formation (later tests strongly indicated the small grain size is an important factor in cohesive jet formation). Since it was not possible to obtain small grain size EBM iron in a reasonable time, it was decided to use the existing material (lot 74B), because it was the best available when the liners were machined.

The liners were tested in both comp.B/octol and octol/PBX 9404 bi-explosive charges assembled with lead waveshapers and aluminum adaptors. (The PBX 9404 outer charges were supplied by Ballistic Research Laboratories, Aberdeen Proving Ground.)

The test results are summarized in Table XI. Velocities in the range 10.54 km/sec to 11.88 km/sec were achieved, however, none of the jets formed were cohesive. A trend was observed (in keeping with previous results) where the jets from the 70° liners showed the greatest degree of stability and the jets from the 50° liners showed the least, as shown in Fig. 34. Furthermore, for each cone angle the jets from the comp.B/octol charge tended to be more stable than the jet from the octol/PBX 9404 charge. This is shown in Fig. 35 for jets from 60° angle liners. The latter effect is attributed to the greater jet velocity produced by the octol/PBX 9404 charge. This corroborates previous observations that for a given liner angle, the jet integrity is related to the jet velocity, or more precisely, the jet integrity is related to the condition required to produce a higher velocity.

The results as presented in Fig. 34 show that the 70° liner came very close to producing an integral jet. It is believed that there is a good probability of producing an integral jet if a fine grained pure iron is used for the liner material.

4. Effect of pure iron on 70° liner jet: During the course of the liner material study, a source of extremely pure iron in machinable bar form was located. It was found that Battelle Memorial Institute, Columbus, Ohio, prepares the pure iron by electron beam melting electolytic iron under vacuum conditions, then achieving further refinement by a floating-zone-melting technique. The iron produced by this technique is very expensive because of the time it takes to purify it and the detailed analysis needed to determine its purity. One bar of this iron was supplied, free of charge, for use on this project by the

American Iron and Steel Institute. The bar was 1-3/4 inches in diameter by 6-3/4 inches long. It was identified as Bar 102. A detailed analysis of its impurities (supplied by Battelle Memorial Institute) is given in Appendix C, lot 81.

The purpose of testing this iron was to determine whether extreme purity would produce a cohesive jet. Tests already conducted on the Nickel and Iron Material Properties Study had shown that the purity of the iron was important. However, there was also strong evidence that the material grain size and uniformity was a significant factor in cohesive jet formation. The Battelle iron, while extremely pure, had a very large grain structure evidently related to its purity. For example, one grain observed in a macro-etched sample of the material was approximately .20-inch by .60-inch in cross-section. It was reasoned that if a cohesive jet were formed from this material it could be concluded that the effects of purity are of prime importance. If a cohesive jet were not formed, then the effects of grain size must be considered equal in importance to material purity.

Tests were conducted using 70° liners with the same non-linear wall area variation used in the tests described in the previous section. (See Fig. 24a, .020-inch wall). Since the iron bar was only 1-3/4 inches in diameter (while the liner diameter for the bi-explosive charge was 2-inches) it was necessary to fabricate the liners as a two-piece unit. As shown in Fig. 36 the lower 1/4-inch of the liner was made of EBM iron from the same lot of material used for the cone angle tests (lot 74B), as described in the previous section. There was no reason to believe that the jet integrity (in regard to radial stability) would be effected by the cemented joint. Four liners were manufactured, two with the Battelle iron/EBM iron material combination and two with EBM iron being used for both top and bottom sections of the liners, where the latter liners were used as controls.

The liners were cast in octol/HMX bi-explosive charges assembled with polyurethane foam waveshapers and aluminum adaptors. One of each type was radiographed just after the jet formation process was completed (in order to see whether anything unusual occurred due to the two-piece design) and one of each was tested in vacuum.

The results are given in Table XII where it is seen that the average velocity obtained was over 11 km/sec. Radiographs of the jets (Fig. 37) show that the Battelle iron jets were not cohesive; however, they did exhibit a greater degree of stability than the EBM iron jets. This is a judgement based on the fact that there was less fine debris surrounding the major jet pieces for the Battelle iron.

It was concluded that the greater purity of the Battelle iron effected some improvement in jet material cohesiveness but that it was not significantly superior to EBM iron under the conditions of the test. It is believed that these results, along with those presented in the materials study section of the report reveal the importance of grain size on jet integrity.

5. Conclusions - Iron hyperbolic liner tests: None of the iron hyperbolic liners tested formed an integral jet. The 70° liner designs (as opposed to 50° and 60° designs) came closest to forming integral jets in that large cohesive fragments of jet material were formed. It is believed, based on the test results just presented and those obtained on the Nickel and Iron Material Properties Study, that integral jets can be formed if the proper iron is used. The iron should be as pure as the EBM iron used for some of the tests discussed above and its grain size should be uniform and in the size range ASTM6 to ASTM8. It is believed that, using the proper iron, integral jets can be formed with either 60° or 70° liner designs.

Nickel hyperbolic liner tests: The development of a liner for producing a nickel jet was not emphasized during the major portion of the project because iron was considered to be of prime importance, and because it was felt that once an iron jet was developed, the nickel liner development would be relatively simple. About four weeks before it became necessary to terminate work on the project it became clear that further development of an iron liner would require the use of a fine grained pure iron (comparable in purity to EBM iron). Since it was not possible to obtain this material and machine liners from it in the short time remaining, it was decided to concentrate on the development of a nickel liner.

Due to the short time available the test program had to be an abreviated one where the liner designs to be tested were finalized at the beginning of the program.

All of the liners tested were of the 50° hyperbolic type. The decision to test 50° liners represented somewhat of a gamble in that there would be less chance of forming a cohesive jet with a 50° rather than a 60° or 70° liner. However, the best chance of achieving a jet velocity of 12 km/sec was with the 50° liner; therefore, it was decided to evaluate liners with this angle. The test results are described in the following sections.

1. Initial 50° hyperbolic liner tests: Only three liners were fired for this test series. The tests showed the effect of modifying the liner design and the effect of changing the explosives. The data for these liners are given in Table XIII.

It is seen that the first shot (Rd. 950-1) tested the constant cross-sectional area hyperbolic liner (Fig. 38) in the comp.B/octol bi-explosive charge. The jet radiograph from this charge is included in Fig. 39, where it is seen that the jet is segmented but cohesive. The second shot of this series (Rd. 950-2) was made with a hyperbolic liner modified to reduce the velocity gradient (See Fig. 24a, curve for .020-inch wall liner). This is the same liner design as shown in Fig. 32. The resultant radiograph, included in Fig. 39, shows that a reduction in velocity gradient was accomplished and that the jet material was cohesive. The charge for the third shot in the series (Rd. 950-3) incorporated the same liner modification as did the charge for Rd. 950-2, however, the bi-explosive charge was octol/HMX. The resultant jet exhibited about the same degree of jet segmentation as the previous shot (Rd. 950-2); however, it is seen in Fig. 40, where the jets for Rd. 950-2 and Rd. 950-3 are compared, that the jet material is not as stable. A close examination of the radiograph reveals that the jet produced by the octol/HMX bi-explosive charge is beginning to fragment.

It was concluded that the hyperbolic liner with the .020-inch base wall thickness was very close to the design which would produce an integral jet. It was also concluded that the jet from the octol/HMX charge, although about 1/2 km/sec faster than that from the comp.B/octol charge, was borderline in terms of jet cohesiveness.

2. Effect of wall area variation and adaptor materials on nickel jets: The data presented in this and the following section are the result of the abbreviated attempt to finalize a nickel jet during the last month of the project. As was stated earlier, it was decided to employ the 50° design for the final tests even though the jets from these liners tended to exhibit borderline integrity at velocities near 12 km/sec.

Liners with base wall thicknesses of .020-inch, .018-inch and .016-inch were evaluated. The resultant C/M variations for these designs are shown in Fig. 24a, where it is seen that the .016-inch base wall thickness modification represented a constant C/M condition (it was decided to test the constant C/M conditions for the 50° nickel liner even though the 70° constant C/M iron liner had failed, since the liner angle and liner material were different).

Both steel and aluminum adaptors were evaluated in this test series. All previous charges had been assembled with aluminum adaptors. The reason for trying steel adaptors was as follows. Shaped charge experience has shown the explosive confinement has a significant effect on the liner collapse in that the total impulse given to the liners (by the explosive) is enhanced by confinement.

Confinement produces this effect by delaying the arrival of the rarefaction wave (in the gaseous explosive products) at the liner wall, thereby, allowing a greater impulse to be delivered to the liner. In the present case the hyperbolic liner is subcaliber in the sense that explosive surrounds the liner at its base. The impulse given to the lower part of the hyperbolic liner depends on how long the adaptor delays the entrance of a rarefaction wave into the gaseous explosive products. It was reasoned that since the 50° hyperbolic liner with the .020-inch base wall thickness exhibited only a small velocity gradient (see previous section), a change in end confinement might provide just enough additional impuse to the base of the liner to eliminate the velocity gradient. Iron was chosen because it possesses a much higher shock impedance than aluminum.

The test data for this group of rounds are summarized in Table XIV. It was found that the use of the iron adaptor produced an integral pellet for one test but not for a second identical test. The integral jet formed with the use of the iron adaptor is compared with a segmented jet produced by a charge with an aluminum adaptor in Fig. 39 (Rd. 973-2 and Rd. 950-2). Radiographs comparing the jets from two identical charges with iron adaptors are shown in Fig. 41. It is seen that by using the iron adaptor the velocity gradient was eliminated; unfortunately the jet integrity was borderline.

The data in Table XIV shows that the .018-inch base wall thickness liners (Rds. 976-1, 976-2) were tested with aluminum and with iron adaptors as were the .016-inch wall liners (Rds. 976-3, 976-4). Velocities in the range 11.8 km/sec to 12.1 km/sec were obtained with these four charges, however, none of the resultant jets were cohesive.

It was concluded that it is possible to form a cohesive nickel jet in the velocity range 11 km/sec to 12 km/sec; however, the jet integrity is borderline for the designs tested. It is believed that the shape of the C/M curve is important. That is, the failure of the charges to form cohesive jets may be due to a slight reverse velocity gradient, causing the jet to be axially compressed and thereby fragmented.

3. Evaluation of inhibited 50° hyperbolic liners: The final tests were conducted with inhibited liners. The purpose of the inhibitor was to isolate the jet from the non-steady state debris following it. It was demonstrated on contract NAS1-5212 that thickening the base of the hyperbolic liner was a possible method of inhibiting. Two degrees of inhibiting were tried as shown in the liner drawings in Figs. 42 and 43. It should be noted that this method of inhibiting the jet differed from that tried before because the metal for the previously tested liners had been added to the outside of the liner. This was not possible

for the present design because the resultant liner could not have been assembled to the bi-explosive charge (the outer charge configuration could not easily be changed).

Two liner wall area variations were tried with each of the two inhibitor types. They were the .016-inch and .020-inch base wall thickness modifications (the C/M variations shown in Fig. 24a hold for these designs except in the inhibitor sections of the liners). The .016-inch base wall thickness liners were assembled with aluminum adaptors and the .020-inch designs were assembled with steel adaptors. The aluminum adaptors were used for the .016-inch design liners because the results of the tests described in the previous section indicated that the steel adaptor may have induced a reverse velocity gradient in the jet. The steel adaptor was used for the .020-inch design because, in at least one instance, the integral jet had been produced with this combination.

There was reason for expecting that the inhibiting process might improve the jet integrity. This is based on results of tests conducted with 30° conical iron liners on contract NAS1-5212 where the use of a Lucite inhibitor improved the jet pellet integrity. The latter type of inhibiting technique differs in detail from that being discussed; however, generally the effect on the jet would be expected to be similar.

The results of the tests are given in Table XV. Velocities in the range 11.7 km/sec to 12.33 km/sec were observed; however, none of the jets were cohesive. Radiographs of jets from each design are shown in Fig. 44 where it is seen that each jet fragmented into a few large pieces surrounded by a cloud of fine debris.

4. Conclusions - 50° nickel hyperbolic liner tests: The test results show that 50° nickel hyperbolic liners assembled in bi-explosive charges are capable of forming jet material with a velocity in excess of 12 km/sec. The jet material, except for one case, was in a fragmented form. The fragmented jets were composed of relatively large cohesive pieces surrounded by clouds of much smaller particles. This kind of jet degradation is considered to be borderline. A modification in the shape of the C/M curve might provide a condition where the jet would be integral. The use of a fine grain nickel should also improve the jet condition. However, it is believed that the best approach to forming a cohesive jet would be to increase the liner angle to 60°. There is ample evidence that jet integrity would be improved by a larger cone angle. There would be some loss in jet velocity; however, this could be overcome by reducing the liner wall thickness.

Conclusions - shaped charge liner development. - The results of the liner development tests show that it is possible to form cohesive jet material at velocities in the neighborhood of 12 km/sec with liner cone angles in the range 50° to 70°. However, the

task of forming an integral (radially and axially stable) jet requires further development work. The following is a summary of the results obtained, and observations made, during the liner development program:

1. Cohesive iron and nickel jet material was produced with velocities as high as 12.5 km/sec. This material was formed as cohesive segments and/or fragments, but not as an integral jet.

2. An integral nickel jet with a velocity of 11.25 km/sec was produced by a 50° hyperbolic liner. The jet integrity was apparently borderline because a second test of the same design produced a jet which was splitting into three pieces.

3. It was demonstrated that high velocity jets can be formed with cone angles as large as 70°. Jet tip velocities as high as 12.5 km/sec were achieved with 70° liners.

4. It was demonstrated that increasing the cone angle improves jet integrity. This was best demonstrated for iron liners where cohesive jet material was produced with velocities as high as 12.5 km/sec with 70° liners, whereas previously cohesive iron jets were not observed above 9.4 km/sec with 40° liners.

5. It was found that the production of an integral jet (radially and axially stable) with the bi-explosive charge will require fine adjustments in the existing shaped charge design. This was demonstrated by the fact that changing the adaptor material from aluminum to iron reduced the jet velocity gradient from about 0.2 km/sec to zero.

In conclusion, it is believed that the results were encouraging. It was demonstrated that it is possible to control the shaped charge jet in a bi-explosive charge and that it is possible to produce an integral jet at velocities near 12 km/sec.

Nickel and Iron Material Properties Study

The effects of liner material chemical and mechanical properties on jet integrity were studied because there were indications during the work on Contract NAS1-5212 that both material purity and grain size were important. Tests were conducted with both nickel and iron; however, the main effort was made with iron. This was because iron was considered more important than nickel as a meteoritic simulator and because iron has proven to be more

difficult to jet in cohesive form. All of the tests discussed in this section of the report were conducted with 40° hyperbolic liners (Fig. 11) assembled in the charge design shown in Fig. 45. This charge was chosen because a large amount of test data was available from tests with this design conducted on contract NAS1-5212. Octol was chosen as the explosive rather than comp.B because it produced the most severe effects on the jet, i.e., previous tests showed that 1020 steel and ingot iron would not form a cohesive jet when this explosive was used with 40° hyperbolic liners. Thus, it was assumed that if one of the iron types to be evaluated was superior to those previously tested, the jet integrity would be improved.

The nickel liner material was evaluated for two hardness conditions only. A total of six iron types were evaluated, where some iron types were tested in two different hardness and grain size conditions. The metallurgical data for all of the materials tested are given in Appendix C where each set of data is presented sequentially in terms of its Firestone lot number.

Nickel liner material tests. - The purpose of this test was to evaluate the effect of material hardness on jet integrity. Nickel 270 had been purchased for use on the meteoritic simulator program. It was the purest nickel commercially available.

Liners were made from the nickel 270 in both the as-received and annealed condition. It had been hoped that a difference in grain size would be obtained. However, the grain size of the as-received material was very large and subsequent annealing changed it very little. The annealing process changed the hardness from Rockwell B52 to Rockwell B23 (Appendix C, lot 62, lot 62B).

Two liners were tested with the nickel 270 in the as-received condition and two with the nickel 270 in the annealed condition. The test results are included in Table XVI along with those from other liner material properties tests. Radiographs of the jets for both nickel hardnesses are included in Fig. 46. It is seen that the harder liner material (as-received) produced an integral jet. Identical results were obtained from both liners for each of the two material conditions. Thus, it was demonstrated that the form of the shaped charge jet was dependent on the condition of the parent liner material.

The fact that the jets from the annealed nickel 270 liners segmented shows that there was a small velocity gradient inherent in the jets when they were formed. One might then infer that the reason the jets from the as-received liners did not segment was due to the greater strength of the parent liner material. This would imply that the jet material is acting plastically as it is segmented and that mechanical properties are important in jet formation.

It was decided, based on the foregoing results, to use the nickel 270 in the as-received condition since it was conducive to forming an integral jet when the shaped charge liner is a hyperbolic type. This decision was based on the fact that hyperbolic type liners were being used in the Shaped Charge Liner Development Program. It should be recognized that the decision to use the as-received nickel 270 was made only in regard to the production of an integral jet. If one were attempting to form a long segmented jet the annealed nickel 270 might be a better choice.

Iron liner material tests. - The main effort in the liner material study was the evaluation of various irons. The results of previous tests with 1020 steel and ingot iron had shown that chemistry might be an important factor. Also, there had been some indication that the material grain size might be important. An effort was made to obtain types of iron which contained a minimum of impurities and possessed a small grain size.

The following is a list of the types of iron tested.

1. 1020 steel - commercial grade low carbon steel.

2. Ingot iron - this material as sold commercially has a nominal carbon content of .04 per cent. It also exhibits a mixed grain structure.

3. Forma iron - this is an imported iron with a carbon content comparable to that of ingot iron. Two lots of this material were purchased. The first lot had fine uniform grain structure. The second lot, while being chemically the same, had a mixed grain structure.

4. Electron beam melted iron - this material was also obtained in two lots. The first lot was a sample donated to the project by the ARMCO Steel Corporation. As received, it was an extremely fine grain 1010 steel, where carbon was the only significant impurity. Liners made from this material were first rough machined, then sent to ARMCO for decarburization by a special technique developed by that organization. After decarburization, the carbon content was .003 per cent.

The second lot of EBM iron was purchased from Airco Temescal (the fabricators of the 1010 steel obtained from ARMCO) in pure form with a carbon content nominally the same as that just described. However, for this lot of material the grain structure was unusually large; too large to classify in the ASTM system.

5. Ferrovac iron - this material, made by the Crucible Steel Corporation, had a carbon content comparable to that of EBM iron. Its grain structure was smaller than the second lot of EBM iron discussed above; however, it was still relatively large and mixed.

6. Battelle pure iron - this material was the purest form of iron obtained during this project. It was made by Battelle Memorial Institute by first electron beam melting electrolytic iron, then achieving further purification by a floating-zone process. The sample, which was donated to the project by the American Iron and Steel Institute, was 1.75-inches in diameter by 6.75-inches long, and was 99.995 per cent pure. The grain structure was extremely large, evidently due to the material purity. This iron was not tested in the materials study phase of the project because of it's limited availability and the limited diameter of the sample. It was tested directly in the bi-explosive shaped charge system and is discussed in the Shaped Charge Liner Development section of the report.

Metallurgical details of the various materials are given in Appendix C.

Effect of iron purity: The first series of tests were conducted to determine the effect of purity on iron jet cohesiveness. The materials evaluated were 1020 steel, ingot iron as received, ingot iron annealed, Forma iron and EBM iron. All materials were fabricated as 40° hyperbolic liners, Fig. 11, and cast in octol charges, Fig. 45. Test data are included in Table XVI (Rds. 922-7 through 922-18) and radiographs of the jets are shown in Fig. 46. A study of the radiographs reveals that the jet integrity improves in going from 1020 steel (Rd. 922-16) to EBM iron (Rd. 922-12). In fact, the EBM iron jet, although axially segmented, is seen to be radially stable. The jet segmentation is attributed to a small velocity gradient.

In order to demonstrate more conclusively that an integral EBM iron jet could be formed, a second EBM iron liner was cast in a modified charge. This charge, discussed in the next section of this report, eliminated a small velocity gradient which was inherent in the jets produced by the 40° hyperbolic liners (shown by the annealed nickel 270 jets discussed above). The EBM iron jet produced by the modified charge, shown in Fig. 46, Rd. 922-18, is seen to be integral except for a small segment preceding the main jet. This was the best iron jet produced during this study.

The results of these tests indicate that iron purity is a significant factor in jet integrity; however, in estimating the effect of purity, one must also consider the effect due to grain size. Since the EBM iron for these tests had the smallest grain size of any of the materials tested, there is a strong possibility that grain size affected the results.

Effect of iron grain size: The purpose of this test was to evaluate the effect of grain size on jet integrity using a pure iron as the test material.

Ideally it would have been desirable to have taken a given pure iron and modified it to produce a range of grain sizes in a set of test samples. This is difficult to do, however, because pure iron tends to form large grains. There are undoubtedly techniques which could be used to achieve various grain sizes with a given pure iron; however, doing this would have taken more time and effort than was available within the scope of the contract. In view of the above, tests were conducted with the following irons which were on hand:

1. EBM iron, as-received, lot 74A
2. EBM iron, forged and annealed, lot 74B
3. Ferrovac, as-received, lot 79.

The lot 74A iron, as-received, possessed a very large grain size because it was processed differently than the first-tested lot 64 EBM iron. As stated earlier, EBM iron and Ferrovac were of comparable purity. The grain sizes for the three items above were:

1. Too large to classify in the ASTM system
2. Mixed - ASTM1 to >>ASTM1
3. Mixed - ASTM3 to ASTM6

Thus, it is seen that although the test conditions were far from ideal, a range of grain sizes in iron samples of comparable purity was available for testing.

The test data are included in Table XVI and in Fig. 46 for Rds. 922-19 through Rd. 922-23. The radiographs show that the jet integrity correlates directly with the grain size, Ferrovac (ASTM3 to ASTM6) giving the most cohesive jet and EBM Iron with the largest grain sizes giving the poorest jet. If the result for Rd. 922-18 (EBM iron, ASTM6-8) is included in this group, the effect of grain size on jet integrity is seen to be even more positively demonstrated.

Conclusions: It is believed that the results presented above demonstrate the importance of both purity and grain size in forming a cohesive iron jet.

The effect of purity was demonstrated when 1020 steel and Forma iron, both of which possessed approximately the same grain structure as the fine grained EBM iron (lot 64), failed to produce cohesive jets while the EBM iron did produce them. The effect of grain size was demonstrated when two types of EBM iron and Ferrovac iron, all approximately equal in purity, yielded significantly more coherent pellets for the smaller grained samples.

It is felt that once a certain degree of purity has been introduced into the shaped charge liner, grain size is the dominant factor. This was demonstrated both in the test just described and the results obtained with Battelle pure iron, discussed in the Shaped Charge Liner Development section of this report. The latter test compared EBM iron - lot 74B with Battelle pure iron which had an extremely large grain structure. The results showed that while the very pure Battelle iron improved the jet integrity slightly, it was not much better than EBM iron. From these results it is inferred that the high purity of the Battelle iron could not compensate for its unusually large grain structure.

It was concluded that a fine grained iron of EBM purity would be the ideal material for further iron jet development.

Charge Configuration Program

The effect of variations in explosive charge configuration for hyperbolic type charges was investigated. The hyperbolic charge which was developed on Contract NAS1-5212 was designed to produce a steady-state jet, i.e., an integral jet pellet which would not segment due to a velocity gradient. The charge was referred to as a hyperbolic charge because both the interior liner surface and the exterior charge surfaces were generated by hyperbolic curves. The design criteria requires that the ratio of charge cross-sectional area to liner cross-sectional area, measured in a plane perpendicular to the charge axis, remain constant. It is shown in Appendix D that this gives rise to the hyperbolic forms.

The hyperbolic charge, developed on Contract NAS1-5212, did not incorporate a true hyperbolic configuration for the exterior charge surface; instead, the hyperbolic surface was approximated by a conical surface. This approach was taken on the first design tested for the sake of expediency and the charge produced integral jets. Later, tests were conducted where the charge surface was approximated by two conical surfaces. This was closer to the hyperbolic surface required by the design criteria. It was found that for the latter case, the jets segmented into two pieces. The maximum difference in charge radius between the charge which produced the integral jet and the charge which produced the segmented jet was only about .050-inch, or about a 4 per cent change in charge radius. This demonstrated the sensitivity of the hyperbolic design to variations in charge configuration.

Based on the foregoing results, it was decided to study the effect of charge configurations on jets produced by hyperbolic liners in order to determine the degree of sensitivity which existed. This was considered important because, although the goal of this project was to develop a bi-explosive charge with a cylindrical exterior, it was planned to incorporate hyperbolic type liners in the charge.

It was decided to evaluate both conical and hyperbolic charge configurations. The conical surfaces were generated by lines which formed angles, (ϕ), which were nominally 0°, 4°, 6°, 8°, 10°9', 11°, 12° and 13° with respect to a line representing a cylindrical charge as shown in Fig. 47b. Two loading fixtures were made for the 11° design. Upon inspection it was found that their actual measured angles were 10°57' and 11°16'. The 12° design also differed slightly from the design value; the actual measured value was 11°59'. The charge with ϕ of 10°9' was the one which had produced an integral jet.

The hyperbolic charge surfaces were generated by requiring that the explosive charge cross-sectional area vary linearly in going from liner base to liner apex. It is shown in Appendix E that this results in the requirement for surfaces generated by hyperbolic curves. It was decided to test configurations with the charge cross-sectional area increased by zero, 12.5 and 25.0 per cent in going from the liner base to liner internal apex. The case where a zero per cent change occurs is the constant cross-sectional area case and is approximated by the 10°9' conical charge discussed above. The hyperbolic curves are illustrated in Fig.47a.

The hyperbolic liner chosen for these tests is designated as the 40°, .020-inch design. This means that the liner wall thickness is .020-inch at the liner base (as measured in a plane perpendicular to the liner axis). This design had produced a segmented jet when tested with the 10°9' charge whereas the 40°, .030-inch hyperbolic liners had produced integral jets in the same charge configuration. It was reasoned that if there were an obvious best charge configuration, it would be recognized by observing an improvement in jet integrity of the more sensitive liner design.

A typical charge assembly is shown in Fig. 45. All of the charges were cast with octol. The C/M variations for the various charge configurations are shown in Fig. 48.

The test data are summarized in Table XVII and radiographs of the jets are shown in Fig. 49. It is seen that none of the hyperbolic charge configurations produced an integral jet, while two of the conical charge configurations did.

It is interesting to compare the velocity gradient in the jet by taking the difference in jet segment velocities for each round. These values are listed in Table XVII. There is no significant trend seen within either the conical group or the hyperbolic group; however, it is seen that the hyperbolic charges as a group display a greater velocity gradient than the conical charges as a group. It appears that the conical charge configuration is more prone to form a cohesive jet than the hyperbolic configuration.

Another interesting observation is the existence of a bulbous section in the jets. This was most pronounced for the case, ϕ equals 10°9', which had produced integral jets from 40°, .030-inch hyperbolic liners. There was no bulbous section observed for the jets from the latter liner design. This shows the effect of liner wall thickness on the jet formation process, since in both cases, the liner wall cross-section area was constant.

It is seen in Fig. 48 that the C/M curves for the two cases, ϕ equals 12° and ϕ equals 13° (which had produced integral jets) decrease significantly in going from liner apex to liner base. For the case of the 10°9' conical charge which did not produce an integral jet from 40°, .020-inch hyperbolic liners but which had produced integral jets from 40°, .030-inch hyperbolic liners, the C/M ratio is seen to increase then decrease rather uniformly along the liner axis. This shows that more than one C/M variation can produce an integral jet and that the success of the given variation is related to the hyperbolic liner wall thickness. It appears that there may be one C/M variation which may successfully form integral jets for a range of wall thicknesses; however, it is not believed that there is a single, theoretically optimum C/M variation which can work for all liner wall thicknesses. The latter opinion is based on the assumption that there are too many variables involved for this to be possible.

The charge design, ϕ equals 12°, was used in the materials study phase of the project to produce an integral iron jet. Initially, iron liners (40°, .030-inch hyperbolic type) were tested in the 10°9' conical charge configuration. The jets produced were found to be segmenting due to a velocity gradient. However, when tested in the 12° conical charge configuration, the jet was integral for one of the irons tested.

This result emphasizes the effect of charge geometry as well as material properties on the ability to produce an integral jet.

Conclusions. - It was concluded that the development of an integral jet could be accomplished by employing hyperbolic type liners in the bi-explosive charge. However, it would be necessary to do the development work in the bi-explosive charge itself because of the sensitivity of the jet formation process to charge configuration and liner design.

CONCLUSIONS

The ultimate goal of the project, an integral 2 gram jet pellet with a velocity in excess of 12 km/sec, was not achieved; however, all of the key developments leading to the final design were successful, and in one test an integral nickel jet with a

velocity of 11.25 km/sec was produced. There is strong evidence that a 60° liner angle and a further adjustment of the liner cross-sectional area would yield an integral jet with a velocity of 12 km/sec.

During the course of the development the following results were achieved:

1. A bi-explosive charge was developed which produced a convergent conical detonation wave. This explosive charge design produced jet velocities as high as 12.5 km/sec with liner cone angles in the range 50° to 70°. The high velocities obtained with this design apparently result from the high effective detonation rate and the more efficient transfer of energy from explosive to liner.

2. The concept of employing large angle liners to increase the velocity level at which the shaped charge jet becomes non-cohesive proved successful. Cohesive jet material was observed at velocities as high as 12.5 km/sec whereas previously (Contract NAS1-5212) cohesive jet material was not observed beyond 11 km/sec.

3. The concept of controlling the jet velocity gradient by controlling the shaped charge liner cross-sectional area proved to be a good approach for the bi-explosive charge. While the problem of forming an integral jet at 12 km/sec was not completely solved, substantial improvements were obtained by this method.

4. Studies with various types of pure iron showed that both the material purity and grain size were important in the formation of an integral jet. It had previously been found that low carbon steels (including ingot iron) were less prone to form a cohesive jet than nickel. The results of this study indicate that a pure iron (.01 per cent carbon) with a small grain size (ASTM6 - ASTM8) can form a cohesive jet as readily as nickel.

RECOMMENDATIONS

The results of this project indicate that it is possible to form an integral nickel or iron jet with a velocity of 12 km/sec. It is recommended that in any further development to achieve the stated goal the following approach be taken.

1. Continue the development using bi-explosive charges and large angle liners. Specifically, it is believed that a 60° cone angle liner can accomplish the goal.

2. Conduct tests where the shape of the C/M ratio curve is varied. This variation should be effected by changing the shape of the liner cross-section area variation curve.

3. Manufacture iron liners from a pure fine grained iron. Iron with the purity and grain size of that shown as lot 64 in Appendix C should be used.

4. Conduct further tests to develop an inhibiting technique which will prevent non-steady state jet debris from following the main jet. It is believed that modifying the base of the liner will provide the inhibiting effect, but more study of the approach is required.

APPENDIX A

ANALYSIS OF SHAPED CHARGE JETTING PROCESS USING THE STEADY-STATE THEORY

Results of tests conducted with various shaped charge designs have indicated that for a given shaped charge liner cone angle and liner material there is an upper limit to the jet velocity beyond which the jet material becomes progressively less cohesive as the jet velocity is increased (by using more energetic explosive, thinning the liner wall, etc.). This phenomenon can be explained by the existing steady-state shaped charge theory if it is accepted that the sound velocity of the liner material is an important limiting parameter.

Consider the steady-state shaped charge process as shown in Fig. A-1. The figure, based on the shaped charge theory developed by Birkhoff et. al.,(Ref. 6) shows the relationships between the shaped charge variables from the point of view of a laboratory coordinate system (Fig. A-1a) and from the point of view of a coordinate system moving with velocity V, (Fig. A-1b). The velocity of the liner wall V_2 flowing into the stagnation point, relative to the moving coordinate system, is the object of this analysis. This velocity has been considered by shaped charge investigators such as Eichelberger (Ref.7) and Walsh et.al., (Ref.8) to be critical in the sense that when it exceeds the sound velocity in the liner material, shock waves appear in the region of the stagnation point. Furthermore, if V_2 is sufficiently high, the shock waves occur right at the stagnation point and prevent a jet from being formed.

In order to find how V_2 varies as a function of other shaped charge parameters, consider the following set of relationships provided by the steady-state charge theory

$$V_J = V_o \frac{\cos(\alpha/2)}{\sin(\beta/2)} \tag{4}$$

where

V_J = Jet velocity

V_o = Collapse velocity of liner material

α = Half angle of conical liner (5)

β = Collapse angle of liner material

$$\beta = 2 \sin^{-1} \frac{V_o \cos \alpha}{2 U_d} + \alpha \tag{5}$$

where

U_d = Detonation rate of explosive

$$V_1 = V_o \frac{\cos 1/2 (\beta - \alpha)}{\sin \beta} \tag{6}$$

where

V_1 = Stagnation point velocity

$V_2 = V_J - V_1$ (7)

where

V_2 = Liner wall flow velocity relative to moving coordinate system

It can be shown that the above equations can be solved to give the following relationship

$$V_2 = \frac{V_J}{2} \left[1 - \frac{\tan \alpha/2}{\cot \alpha/2 - \frac{V_J}{U_d} \cot \alpha} \right] \tag{8}$$

where V_2 is the velocity under discussion and V_J, α and U_d are the jet velocity, cone half angle and explosive detonation rate, respectively. It is seen that in this form the jet velocity is treated as an independent variable. A plot of V_2 as a function of three parameters is shown in Fig. A-2. In studying this figure it must be kept in mind that some of the points on the curves shown may not be physically possible. All that is implied here is that if it is possible to obtain a given jet velocity (V_J) with a given cone angle (2α) and a given detonation rate (U_d), then the indicated liner wall flow velocity (V_2) must have existed.

The sound velocities for iron and nickel are shown as horizontal lines in Fig. A-2. It is seen that the constant jet velocity curves intersect the sound velocity lines. The important point to be seen is that the coordinate points (V_2, 2α) on the constant jet velocity curves, which lie above the sound velocity line, have a V_2 greater than the sound velocity in the given material and those that lie below have a value of V_2 less than the sound velocity in the material. Furthermore, the value of V_2 decreases as the cone angle (2α) increases.

Thus, if it is assumed that jet instability is related to the value of V_2 and that it is desirable to keep the value of V_2 less than the velocity of sound in the liner material, then it is expedient to form the jet with a liner that has as large a cone angle as possible.

LABORATORY COORDINATE SYSTEM

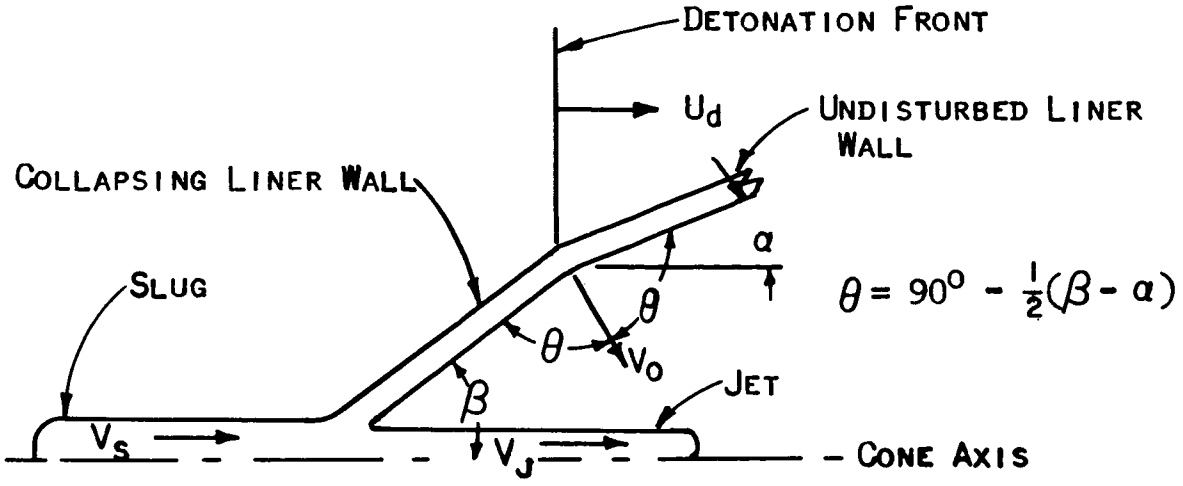

V_o - COLLAPSE VELOCITY

V_S - SLUG VELOCITY

V_J - JET VELOCITY

U_d - EXPLOSIVE DETONATION RATE

α - CONE HALF ANGLE

β - COLLAPSE ANGLE

MOVING COORDINATE SYSTEM

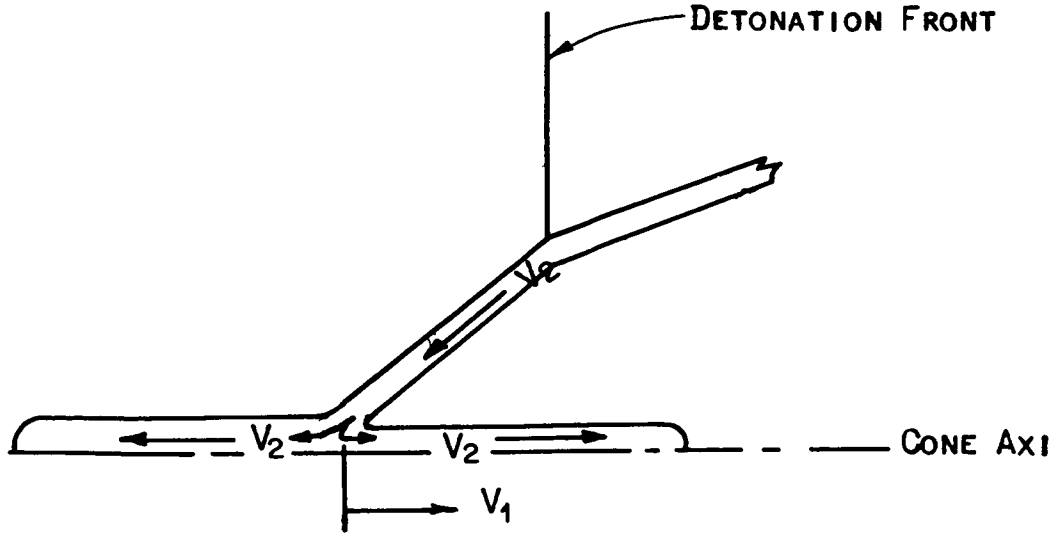

V_1 - VELOCITY OF JUNCTION OF COLLAPSING LINER WALL

V_2 - VELOCITY OF LINER WALL, JET AND SLUG RELATIVE TO MOVING JUNCTION

$V_J = V_1 + V_2$ $\qquad$ $V_S = V_1 - V_2$

Fig. A-1.

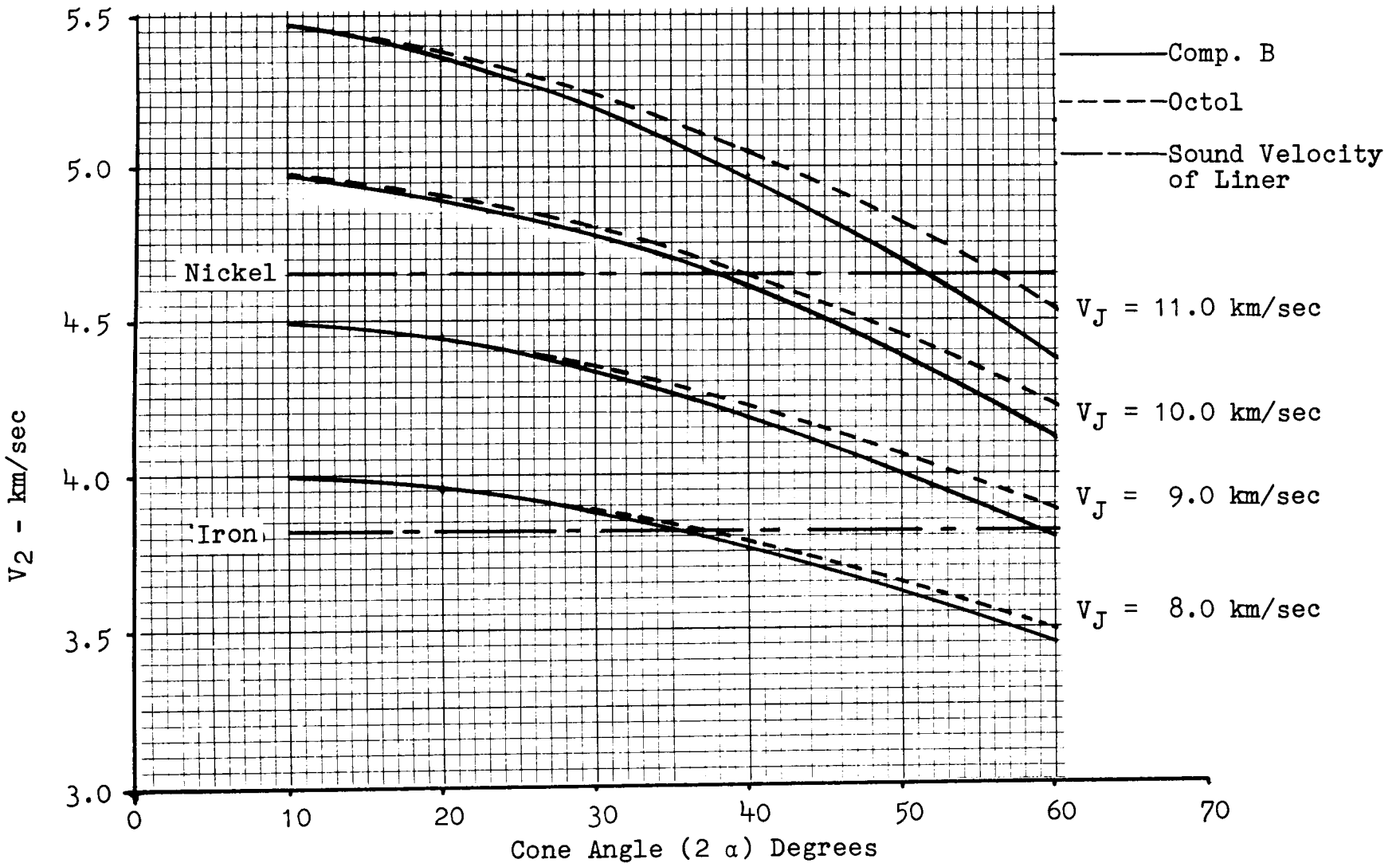
5.5
5.0
4.5
4.0
3.5
3.0
V_2 - km/sec
Nickel
Iron
0
10
20
30
40
50
60
70
Cone Angle (2 α) Degrees
Comp. B
Octol
Sound Velocity of Liner
V_J = 11.0 km/sec
V_J = 10.0 km/sec
V_J = 9.0 km/sec
V_J = 8.0 km/sec

Fig. A-2.

APPENDIX B

DEVELOPMENT OF DESIGN EQUATIONS FOR THE BI-EXPLOSIVE CHARGE CONFIGURATION

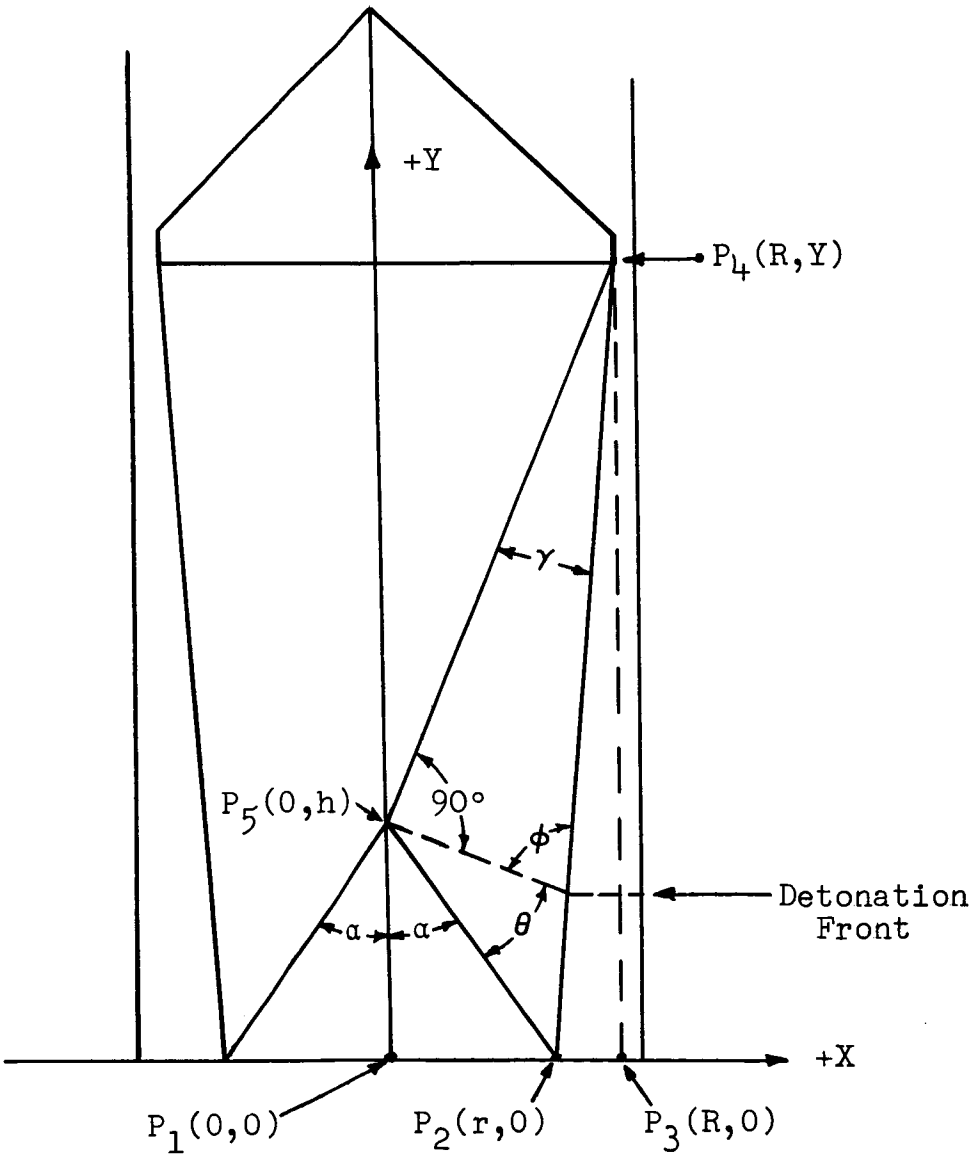

Fig. B-1. Cartesian co-ordinate system impressed on the bi-explosive design.

Fig. B-1 shows the lower portion of the bi-explosive charge configuration. The points P_1, P_2, P_3, and P_5 are fixed and P_4 is the variable. The following are designated as constants: R, r, and α. Since γ and h are defined by the following equations, Eqn. 9 and Eqn. 10, the only variable remaining is "Y".

Equation 9 relates the detonation rates to the angle γ.

$$\cos \gamma = u_1/u_2, \quad \text{where } u_1 \text{ is the detonation rate of the inner explosive and } u_2 \text{ is the detonation rate of the outer explosive.} \tag{9}$$

$$h = r \cot \alpha \tag{10}$$

Representing the points P_1, P_2, P_4, and P_5 as vectors, then Fig. B-2 corresponds to the associated portion of the charge configuration in Fig. B-1.

where $\vec{P}_1 = (0,0)$

$\vec{P}_2 = (r,0)$

$\vec{P}_4 = (R,Y)$

$\vec{P}_5 = (0,h)$

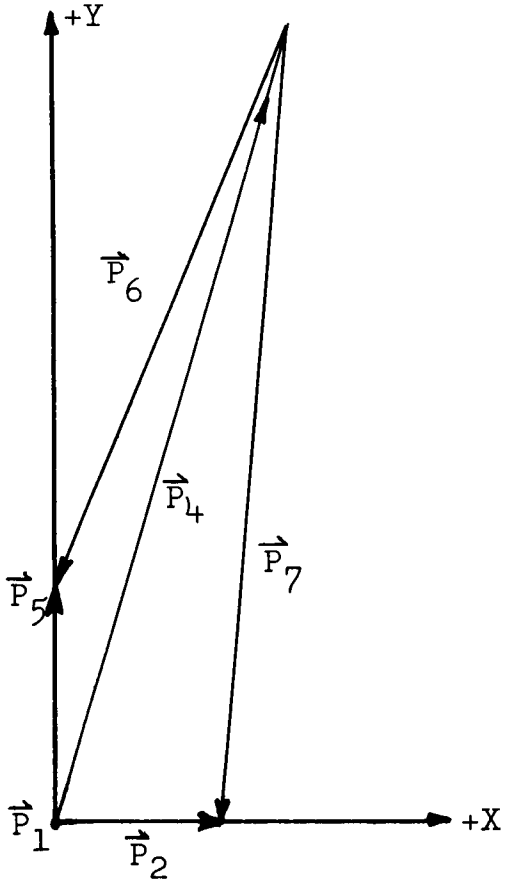

Fig. B-2. Vector system impressed on bi-explosive design.

From Fig. B-2:

$$\begin{aligned}\vec{P_6} &= \vec{P_5} - \vec{P_4} \\ &= (0 - R, h - Y) \\ &= (-R, h - Y)\end{aligned} \tag{11}$$

$$\begin{aligned}\vec{P_7} &= \vec{P_2} - \vec{P_4} \\ &= (r - R, 0 - Y) \\ &= (r - R, - Y)\end{aligned} \tag{12}$$

Then the dot product (inner product) of P_6 and P_7 could be written as:

$$|\vec{P_6}| \cdot \vec{P_7} = |\vec{P_6}| \; |\vec{P_7}| \cos \gamma \tag{13}$$

where $$|\vec{P_6}| = (R^2 + (h - Y)^2)^{1/2} \tag{14}$$

$$|\vec{P_7}| = ((r - R)^2 + Y^2)^{1/2} \tag{15}$$

Substituting $|\vec{P_6}|$ and $|\vec{P_7}|$ from Eqn. 14 and Eqn. 15 respectively into Eqn. 13:

$$-R(r - R) - Y(h - Y) = (R^2 + (h - Y)^2)^{1/2}((r - R)^2 + Y^2)^{1/2} \cos \gamma \tag{16}$$

or

$$-(R(r - R) + Y(h - Y)) = (R^2 + (h - Y)^2)^{1/2}((r - R)^2 + Y^2)^{1/2} \cos \gamma \tag{17}$$

Squaring both sides of Eqn. 17:

$$(R(r - R) + Y(h - Y))^2 = (R^2 + (h - Y)^2)((r - R)^2 + Y^2) \cos^2 \gamma \tag{18}$$

Expanding both sides of Eqn. 18:

$$R^2(r - R)^2 + 2RY(r - R)(h - Y) + Y^2(h - Y)^2 = (R^2(r - R)^2 + R^2Y^2 + (r - R)^2(h - Y)^2 + Y^2(h - Y)^2)\cos^2 \gamma \tag{19}$$

Regrouping the quantities in Eqn. 19:

$$(R^2(r - R)^2 + Y^2(h - Y)^2) + (2RY(r - R)(h - Y)) = \quad (20)$$
$$(R^2(r - R)^2 + Y^2(h - Y)^2)\cos^2\gamma + (R^2Y^2 + (r - R)^2(h - Y)^2)\cos^2\gamma$$

Adding $-(R^2(r - R)^2 + Y^2(h - Y)^2)\cos^2\gamma$ to both sides of Eqn. 20 and adding $-(\cos^2\gamma)(2RY(r - R)(h - Y))$ to both sides to complete the square:

$$(1 - \cos^2\gamma)(R^2(r - R)^2 + 2RY(r - R)(h - Y) + Y^2(h - Y)^2) =$$
$$(\cos^2\gamma)(R^2Y^2 - 2RY(r - R)(h - Y) + (r - R)^2(h - Y)^2) \quad (21)$$

Dividing both sides of Eqn. 21 by $(1 - \cos^2\gamma)$:

$$R^2(r - R)^2 + 2RY(r - R)(h - Y) + Y^2(h - Y)^2 = \quad (22)$$
$$((\cos^2\gamma)/(1 - \cos^2\gamma))(R^2Y^2 - 2RY(r - R)(h - Y) + (r - R)^2(h - Y)^2)$$

Taking the square root of both sides of Eqn. 22 and setting $((\cos^2\gamma)/(1 - \cos^2\gamma))^{1/2} = S$:

$$R(r - R) + Y(h - Y) = S(RY - (r - R)(h - Y)) \quad (23)$$

or considering the other sign possibility:

$$R(r - R) + Y(h - Y) = -S(RY - (r - R)(h - Y) \quad (24)$$

Expanding both sides of Eqn. 23:

$$R(r - R) + Yh - Y^2 = SRY - Sh(r - R) + SY(r - R) \quad (25)$$

Shifting all of the quantities in Eqn. 25 to the left side of the equality sign and regrouping the quantities:

$$-Y^2 + Y(h - SR - S(r - R)) + (R(r - R) + Sh(r - R)) = 0 \quad (26)$$

or

$$-Y^2 + Y(h - Sr) + (R + Sh)(r - R) = 0 \quad (27)$$

Similarly Eqn. 24 can be written as:

$$-Y^2 + Y(h + Sr) + (R - Sh)(r - R) = 0 \qquad (28)$$

Both Eqn. 27 and Eqn. 28 are in the quadratic form:

$$AX^2 + BX + C = 0 \qquad (29)$$

which has solutions,

$$X = \frac{-B \pm (B^2 - 4AC)^{1/2}}{2A} \qquad (30)$$

where in Eqn. 27,

$$A = -1 \qquad (31)$$

$$B = h - Sr \qquad (32)$$

$$C = (R + Sh)(r - R) \qquad (33)$$

and in Eqn. 28,

$$A = -1 \qquad (34)$$

$$B = h + Sr \qquad (35)$$

$$C = (R - Sh)(r - R) \qquad (36)$$

and in both Eqn. 27 and Eqn. 28,

$$S = ((\cos^2\gamma)/(1 - \cos^2\gamma))^{1/2} \qquad (37)$$

Therefore, there are four solutions for "Y". Two solutions are found from Eqn. 27 and two solutions from Eqn. 28. But, the solutions for "Y" obtained from Eqn. 27 yield imaginary values of "Y". Then the desired positive real value for "Y" must be found by one of the two solutions for "Y" obtained from Eqn. 28. The desired solution for "Y" is shown below, Eqn. 38. Equation 38 was arrived at by substituting Eqn. 34, Eqn. 35 and Eqn. 36 into Eqn.30 and using the negative (-) sign before the square root in the numerator.

$$Y = (-h - Sr - ((h + Sr)^2 + 4(R - Sh)(r - R))^{1/2}) / -2 \qquad (38)$$

Having solved for "Y", it would be of interest to find the angle between the detonation wave and the liner surface. Since the explosives used to form the bi-explosive charge could be varied for a given loading fixture with fixed "Y", the following development is based on a general detonation rate ratio and a fixed "Y".

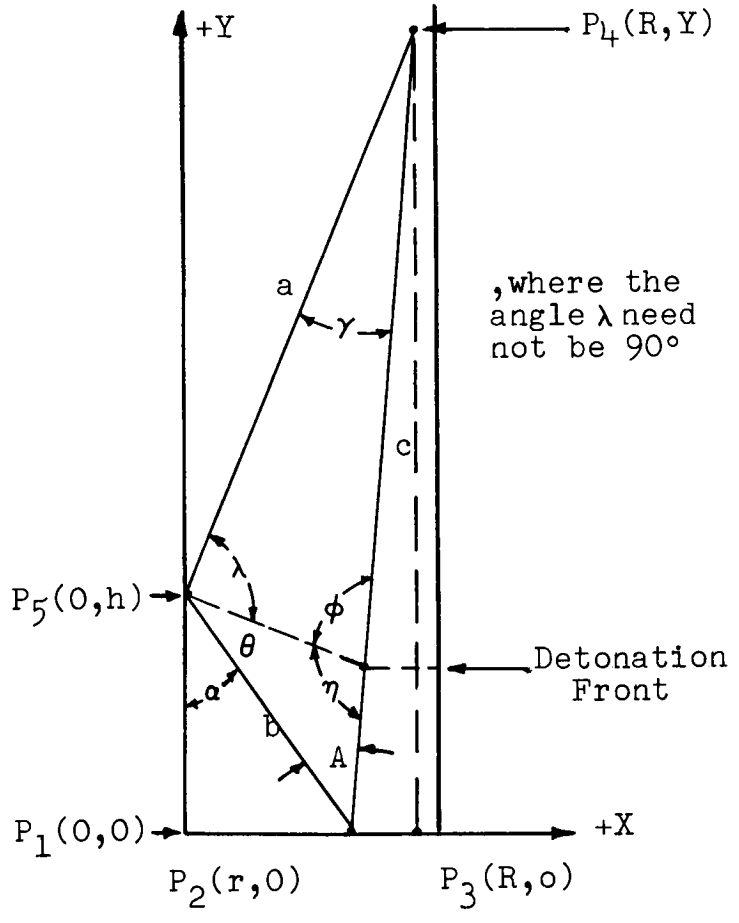

Fig. B-3. Cartesian co-ordinate system impressed on bi-explosive design which allows for changes in the explosives.

In Fig. B-3, the line between P_4 and P_5 is taken to be the line "a", the line between P_2 and P_5 is taken to be the line "b", and the line between P_2 and P_4 is taken to be line "c".

Equation 39 relates the detonation rates to the angle ϕ instead of the angle γ as in Eqn. 9.

$$\sin \phi = u_1'/u_2' \quad \text{, where } u_1' \text{ is the detonation rate of the new inner explosive and } u_2' \text{ is the detonation rate of the new outer explosive.} \tag{39}$$

Using the length formula for lengths of line segments:

$$a^2 = R^2 + (Y - h)^2 \tag{40}$$

$$b^2 = r^2 + h^2 \tag{41}$$

$$c^2 = (R - r)^2 + Y^2 \tag{42}$$

Applying the "Law of Cosines" to Fig. B-3:

$$\cos A = (b^2 + c^2 - a^2)/(2bc) \tag{43}$$

but,
$$\eta = 180° - \phi \tag{44}$$

and,
$$\theta + \eta + A = 180° \tag{45}$$

Substituting A and η from Eqn. 43 and Eqn. 44 respectively into Eqn. 45:

$$\theta + 180° - \text{arc sin}(u_1'/u_2') + \text{arc cos}((b^2 + c^2 - a^2)/(2bc)) = 180° \tag{46}$$

therefore,

$$\theta = \text{arc sin}(u_1'/u_2') - \text{arc cos}((b^2 + c^2 - a^2)/(2bc)) \tag{47}$$

Having solved for "θ" in terms of a fixed value of "Y" and designated detonation rates of the inner and outer explosives, it would be of interest to develop an effective detonation rate for the bi-explosive system. Conventional shaped charge designs assume the detonation front travels as a plane wave, which is normal to the liner central axis, moving down the liner central axis. Therefore, if the conic detonation front of the bi-explosive design sweeps the liner surface in a time interval Δt, the effective detonation rate could be defined as the rate at which a conventional plane detonation front would sweep the liner surface in the

same time interval Δt. The following development arrives at an equation for the effective detonation rate (u_E).

, where u_1' is the detonation rate of the inner explosive, u_α is the rate at which the conic detonation front sweeps the liner surface, u_E is the effective detonation rate.

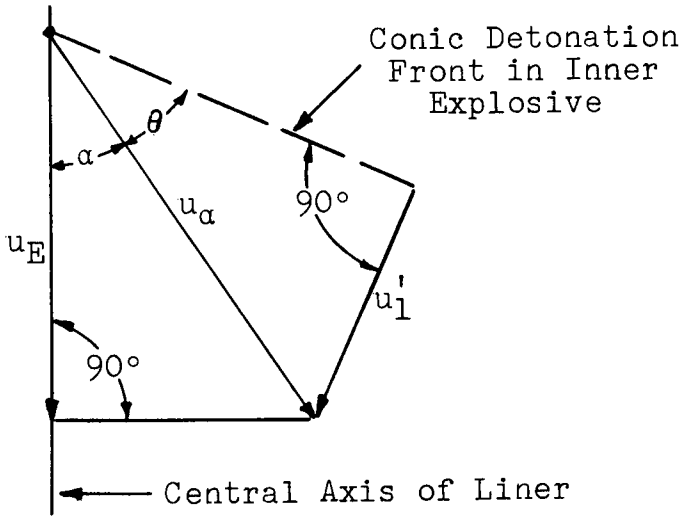

Fig. B-4. Sketch for bi-explosive charge configuration effective detonation rate development.

In Fig. B-4:

$$\sin \theta = u_1'/u_\alpha' \tag{48}$$

or,

$$u_\alpha = u_1'/\sin \theta \tag{49}$$

and,

$$\cos \alpha = u_E/u_\alpha \tag{50}$$

or,

$$u_E = u_\alpha \cos \alpha \tag{51}$$

Substituting u_α from Eqn. 49 into Eqn. 51:

$$u_E = (u_1' \cos \alpha)/\sin \theta \tag{52}$$

APPENDIX C

SUMMARY OF METALLURGICAL DATA FOR VARIOUS NICKEL AND IRON MATERIALS USED IN SHAPED CHARGE LINER TESTS

Material Record

Type Material: Type 200 Nickel, cold drawn, 3-inch diameter bars.

Firestone Lot No.: 50

Heat Treatment: None

Mechanical Properties:

Yield Strength	72,500 psi
Tensile Strength	77,000 psi
Elongation in 2-inches	30%
Reduction in Area	72%
Rockwell Hardness	B86

data obtained from material certifications.

Chemical Analysis:

Nickel	99.53%
Carbon	.07%
Manganese	.24%
Iron	.06%
Sulfur	.005%
Silicon	.06%
Copper	.01%

data obtained from material certifications.

(nickel includes small amount of cobalt)

Material Record

Type Material: C-1020 Steel, hot rolled special bar quality, 2-inch diameter bars.

Firestone Lot No.: 51

Heat Treatment: Rough machined pieces heated to 1300°F for 30 minutes and air cooled.

Mechanical Properties:

Rockwell Hardness	B65-67
Grain Size	ASTM7

Chemical Analysis:

Carbon	.18%
Manganese	.38%
Sulfur	.034%
Phosphorous	.009%

data obtained from material certifications

Material Record

Type Material: Type 200 Nickel, cold drawn, 2-1/8-inch diameter bars.

Firestone Lot No.: 57, 57A

Heat Treatment: Lot 57; rough machined pieces were heated to 1500°F for 30 minutes and air cooled.
Lot 57A; None

Mechanical Properties:	Lot 57	Lot 57A*
Yield Strength	26,500 psi	91,000 psi
Tensile Strength	73,000 psi	95,500 psi
Elongation in 2-inches	49%	18%
Reduction in Area	58%	73%
Rockwell Hardness	B51	B96
Grain Size	ASTM6	-

*data obtained from material certifications.

Chemical Analysis:

Nickel	99.52%
Carbon	.08%
Manganese	.28%
Iron	.04%
Sulfur	.005%
Silicon	.04%
Copper	.01%

data obtained from material certifications.

(nickel includes small amount of cobalt)

Spectrographic Analysis:

Nickel	Major
Carbon	.080%
Manganese	.15%
Iron	.04%
Sulfur	.004%
Silicon	.025%
Phosphorous	.0025%

Spectrographic Analysis showed no other trace metals greater than 0.01%.

Material Record

Type Material: Armco magnetic ingot iron, cold drawn, 2-1/4 inch diameter bars.

Firestone Lot No.: 59A (certified to be of the same heat number and composition as Lot 59)

Heat Treatment: Rough machine pieces heated to 1300°F for 1 hr. and slow cooled. This was later found to give an incomplete anneal, reducing the hardness to about Rockwell B58 with only partial recrystallization.

Microphotograph*:

Longitudinal View
Magnification X50

* Microphotograph taken from sectioned liner near the apex.

Material Record

Type Material: Armco Magnetic Ingot Iron, cold drawn, 3-1/2-inch diameter bars.

Firestone Lot No.: 60, also representative for Lot 59.

Heat Treatment: None

Mechanical Properties:

Yield Strength	48,600 psi
Tensile Strength	52,500 psi
Elongation in 2-inches	25%
Reduction in Area	65%
Rockwell Hardness	B69
Grain Size	Mixed

Chemical Analysis:

Carbon	.03%
Manganese	.04%
Sulfur	.023%
Silicon	.003%
Nickel	.02%
Copper	.10%
Phosphorous	.012%
Molybdenum	.02%
Chromium	.01%

Photomicrograph:

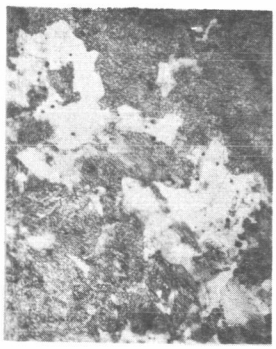

Transverse View
Magnification x50

Spectrographic Analysis:

Iron	Major
Carbon	.038%
Manganese	.021%
Sulfur	.014%
Phosphorous	.0065%
Chromium	.025%

Spectrographic Analysis showed no other trace metals greater than 0.01%.

Material Record

Type Material: Type 270 Nickel, hot finished, 2-1/4-inch diameter bars.

Firestone Lot No.: 62, 62B

Heat Treatment: Lot 62; None
Lot 62B; rough machined pieces were heated to 1500°F for 30 minutes and water quenched.

Mechanical Properties:	Lot 62	Lot 62B
Yield Strength	37,200 psi	10,600 psi
Tensile Strength	46,500 psi	46,900 psi
Elongation in 2-inches	56%	63%
Reduction in Area	81%	82%
Rockwell Hardness	B52	B23
Grain Size	ASTM1	ASTM1

Chemical Analysis:

Carbon	.01%
Manganese	.001%
Iron	.001%
Sulfur	.001%
Copper	.001%
Chromium	.0003%
Cobalt	.0004%
Selenium	.0001%

Photomicrograph:

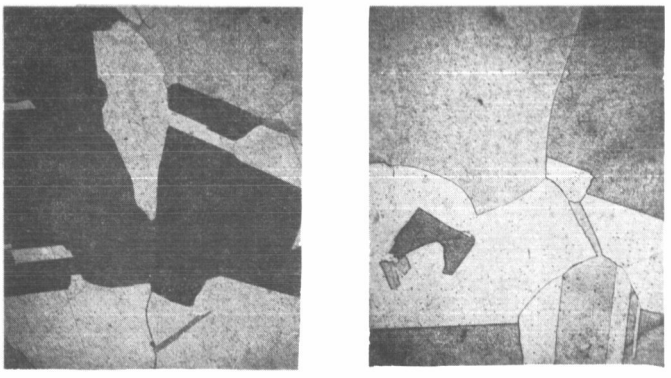

Lot 62 Lot 62B
Transverse View
Magnification x50

Lots 62 and 62B differ only by the stated difference in heat treatment.

Material Record

Type Material: Electron beam melted, forged, annealed, machined and extruded 1010 steel, 2.45-inches diameter bar 5-inches long.

Firestone Lot No.: 64

Heat Treatment: Material heated during decarburization process.

Material Processing: Decarburized after rough machining.

Mechanical Properties*:

Rockwell Hardness	H84
Grain Size	ASTM6 to 8

Chemical Analysis*:

Carbon	.003%
Manganese	.005%
Sulfur	.003%
Silicon	.005%
Copper	.005%
Phosphorous	.002%

Microphotograph*:

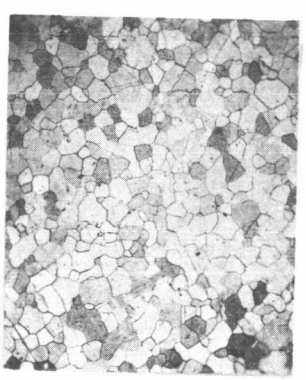

Transverse View
Magnification X50

* data taken after decarburization.

Material Record

Type Material: Forma Iron, hot rolled, 2-3/4-inch diameter bars.

Firestone Lot No.: 66

Heat Treatment: None

Mechanical Properties:

Yield Strength	24,750 psi
Ultimate Strength	42,200 psi
Elongation in 2-inches	55%
Reduction in Area	80.5%
Rockwell Hardness	B35
Grain Size	ASTM6

Chemical Analysis:

Carbon	.04%
Manganese	.21%
Sulfur	.020%
Silicon	.03%
Nickel	.05%
Copper	.05%
Phosphorous	.012%
Molybdenum	.01%
Chromium	.06%

Photomicrograph:

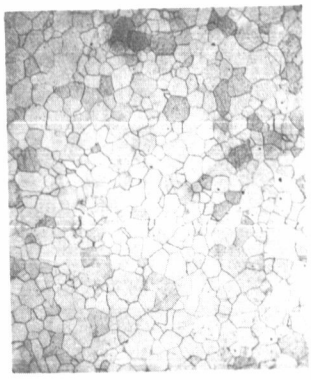

Transverse View
Magnification x50

Material Record

Type Material: Forma Iron, hot rolled, 4-inch diameter bars.

Firestone Lot No.: 73, 73B

Heat Treatment: Lot 73; None
Lot 73B; the rough machined pieces were heated to 1710°F for 15 minutes and air cooled.

Mechanical Properties:	Lot 73	Lot 73B
Yield Strength	28,500 psi	24,000 psi
Tensile Strength	43,800 psi	40,300 psi
Elongation in 2-inches	41%	50%
Reduction in Area	79%	80%
Rockwell Hardness	F81	F73
Grain Size	Mixed (ASTM4 to >1)	ASTM5

Chemical Analysis:

Carbon	.03%
Manganese	.24%
Sulfur	.017%
Silicon	.01%
Phosphorous	.001%

Photomicrograph:

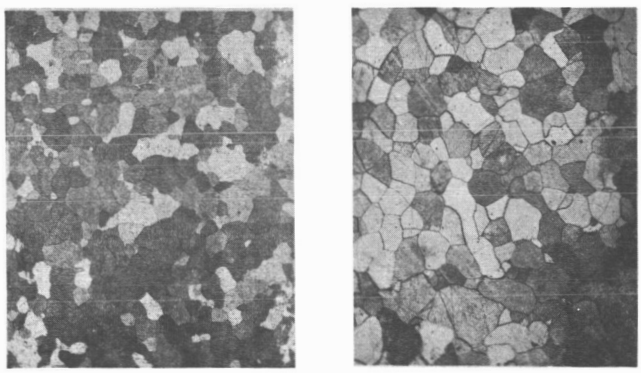

Lot 73 Lot 73B
Transverse View
Magnification x50

Lots 73 and 73B differ only by the stated difference in heat treatment.

Material Record

Type Material: Electron beam melted iron, 5-inches diameter bars.

Firestone Lot No.: 74A, 74B

Heat Treatment: Lot 74A; none
Lot 74B; the material was heated to 1600°F and forged to 2-1/2 inches diameter (finish temp. 1200°F) then heated to 1710°F for 1 hr. and air cooled, twice.

Mechanical Properties:	Lot 74A	Lot 74B	
		1st Anneal	2nd Anneal
Yield Strength	--	18,000 psi	17,000 psi
Tensile Strength	--	36,900 psi	38,000 psi
Elongation in 2-inches	--	46%	53%
Reduction in area	--	57%	85%
Rockwell Hardness	B21	F63-67	F63-67
Grain Size	Mixed-too large to classify	ASTM1	ASTM1

Chemical Analysis:

Carbon	.0015%
Manganese	.0020%
Sulfur	.008%
Phosphorous	.006%

Full Size Photograph:

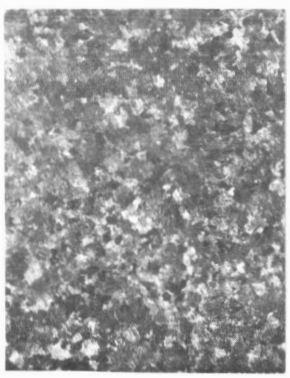

74A
Transverse View
Magnification Full Size

Photomicrograph:

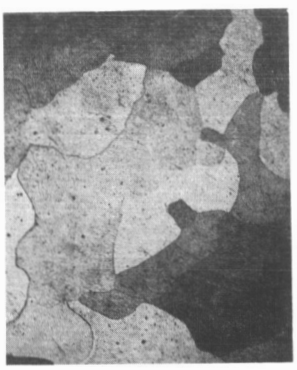

74B
Transverse View
Magnification X50

Lots 74A and 74B differ only by the stated differences in heat treatment.

Material Record

Type Material: Ferrovac E CG Nat, vacuum purified electrolytic iron annealed by Mfgr.,2-1/2-inch diameter bars.

Firestone Lot No.: 79, 79B

Heat Treatment: Lot 79; None
Lot 79B; one bar was heated to 1300°F for 4 hours and furnace cooled overnight.

Mechanical Properties:	79	79B
Yield Strength	31,100 psi	21,600 psi
Tensile Strength	44,100 psi	39,000 psi
Elongation in 2-inches	40%	51%
Reduction in Area	70%	86%
Rockwell Hardness	F85	F72
Grain Size	Mixed ASTM3-6	Mixed ASTM3-5

Chemical Analysis:

Carbon	.010%
Manganese	.001%
Sulfur	.005%
Silicon	.003%
Nickel	.02%
Copper	.001%
Phosphorous	.003%
Molybdenum	.001%
Chromium	.001%
Vanadium	.004%
Tungsten	.01%
Cobalt	.007%
Nitrogen	.0002%
Oxygen	.00046%
Hydrogen	.000016%

Photomicrograph:

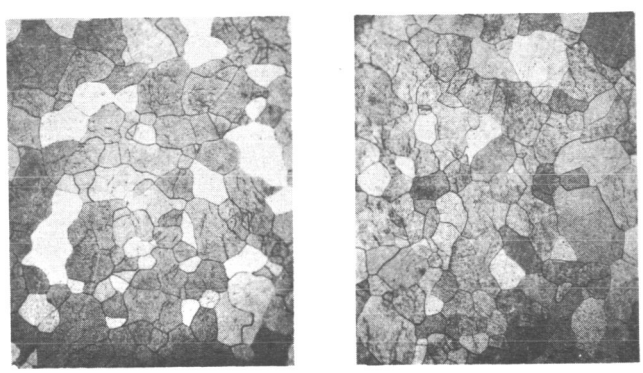

Lot 79 Lot 79B
Transverse View
Magnification x50

The Chemical Analysis was obtained from material certifications. Lots 79 and 79B differ only by the stated difference in heat treatment.

Material Record

Type Material: Battelle pure (electrolytic) iron, electron beam melted and floating-zone refined, 1-3/4-inch diameter bar.

Firestone Lot No.: 81

Heat Treatment: None

Mechanical Properties:

Grain Size	too large to classify
Rockwell Hardness	F 40-50 (H84)

Chemical Analysis:

See next page for Battelle analysis of impurities

Photograph (Full Size):

Transverse View

ANALYSIS OF BAR 102

All Analyses are ppm by Weight (1 ppm = 0.0001%)

Resistivity Ratio	Without a Magnetic Field	Maximum Ratio With a Magnetic Field
$\rho_{297\pm1.5}/\rho_{4.2\ K}$	180	540

Nonmetallic Impurities

Oxygen	1.2
Nitrogen	
Vacuum Fusion	N<0.1
Internal Friction	N<0.2
Hydrogen	0.2
Carbon	
Combustion-Conductometric	6
Internal Friction	≤4.7
Sulfur	
Mass Spectrometer	1.2

Metallic Impurities Often Detected With the Mass Spectrometer
(Impurities not detected are denoted N together with the estimated detection limits)

Aluminum	--	Nickel	2.
Arsenic	0.5	Phosphorus	0.8
Boron	0.1	Potassium	0.3
Calcium	0.4	Silicon	≤5.
Chromium	10.	Sodium	0.4
Cobalt	10.	Tantalum	4.
Columbium	0.06	Tin	N<0.12
Copper	1.2	Titanium	0.3
Germanium	≤0.9	Tungsten	0.07
Magnesium	0.4	Vanadium	N<0.03
Manganese	2.	Zinc	N<0.4
Molybdenum	0.8	Zirconium	N<0.07

Total nonmetallic impurities 7.
(Includes internal friction values for nitrogen and carbon and mass spectrometer or colorometric values for sulfur.)

Total detected metallic impurities 40
(Includes values marked ≤ except germanium, and values underlined below plus an arbitrary 2 ppm aluminum.)

Metallic Impurities not Usually Detected With the Mass Spectrometer
(Impurities detected in this bar are underlined)

Antimony	N<0.012	Holmium	N<0.01	Rubidium	N<0.05
Barium	N<0.01	Indium	N<0.04	Ruthenium	N<0.06
Beryllium	----.	Iodine	N<0.025	Samarium	N<0.04
Bismuth	0.02	Iridium	N<0.02	Scandium	N<0.08
Bromine	N<0.01	Lanthanum	N<0.008	Selenium	N<0.1
Cadmium	N<0.25	Lead	0.07	Silver	≤0.12
Cerium	N<0.008	Lithium	N<0.001	Strontium	N<0.05
Cesium	N<0.008	Lutetium	N<0.01	Tellurium	N<0.25
Dysprosium	N<0.04	Mercury	N<0.04	Terbium	N<0.01
Erbium	N<0.15	Neodymium	N<0.015	Thallium	N<0.015
Europium	N<0.02	Osmium	N<0.03	Thorium	N<0.012
Gadolinium	N<0.04	Palladium	N<0.04	Thulium	N<0.1
Gallium	N<0.2	Platinum	N<0.04	Uranium	N<0.012
Gold	N<0.012	Praseodymium	N<0.008	Ytterbium	N<0.03
Hafnium	N<0.04	Rhenium	N<0.02	Yttrium	N<0.04
		Rhodium	N<0.1		

APPENDIX D

DEVELOPMENT OF DESIGN CRITERION FOR CONSTANT CROSS-SECTIONAL AREA LINER AND CONSTANT CROSS-SECTIONAL AREA EXPLOSIVE CHARGE

Determination of the curve which will generate a surface inside a conical liner such that the cross-sectional area will remain constant along the liner axis:

The lines which will generate the conical surface and the interior surface in the x, y plane can be shown as:

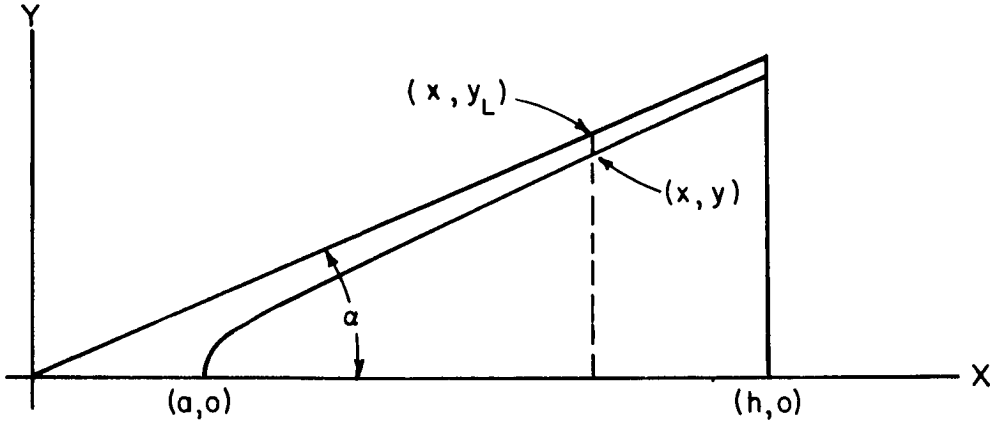

let it be required that the cross-sectional area between the surfaces be a constant, A_L, from x = a to x = h

$$\pi (y_L^2 - y^2) = A_L \qquad (53)$$

but $y_L = mx$ where $m = \tan \alpha$

thus $$\pi\left[(mx)^2 - y^2\right] = A_L$$

or $$\frac{x^2}{A_L/\pi m^2} - \frac{y^2}{A_L/\pi} = 1$$

since m is a constant and we require that A_L be a constant we can let

$$a^2 = A_L/\pi m^2$$

$$b^2 = A_L/\pi$$

thus
$$\frac{x^2}{a^2} - \frac{y^2}{b^2} = 1 \qquad (54)$$

which is a hyperbola symmetric about the x axis and open in the positive x direction.

Determination of the curve which will generate a surface outside a conical liner such that the cross-sectional area will remain constant along the liner axis:

The lines which will generate the conical surface and the exterior surface in the x, y plane can be shown as:

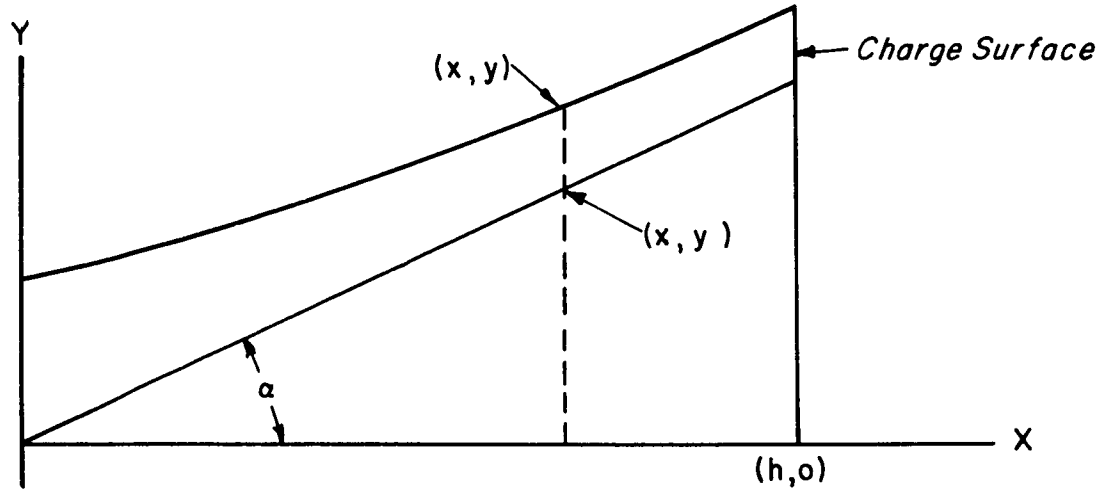

let it be required that the cross-sectional area between the two surfaces be a constant, A_c, from x = o to x = h

$$\pi(y^2 - y_L^2) = A_c \qquad (55)$$

but $y_L = mx$ where $m = \tan \alpha$

thus $$\pi\left[y^2 - (mx)^2\right] = A_c$$

or $$\frac{y^2}{A_c/\pi} - \frac{x^2}{A_c/\pi m^2} = 1$$

since m is constant and we require that A_c be a constant we can let

$$a^2 = A_c/\pi m^2$$

$$b^2 = A_c/\pi$$

thus

$$\frac{y^2}{b^2} - \frac{x^2}{a^2} = 1 \qquad (56)$$

which is a hyperbola symmetric about the y axis and open in the positive y direction.

APPENDIX E

DEVELOPMENT OF DESIGN CRITERION FOR AN EXPLOSIVE CHARGE WHOSE CROSS-SECTIONAL AREA VARIES LINEARLY

Determination of the curve which will generate a surface outside a conical surface such that the cross-sectional area will vary linearly along the conical axis:

The lines which will generate the conical surface and the exterior surface in the X, Y plane can be shown as:

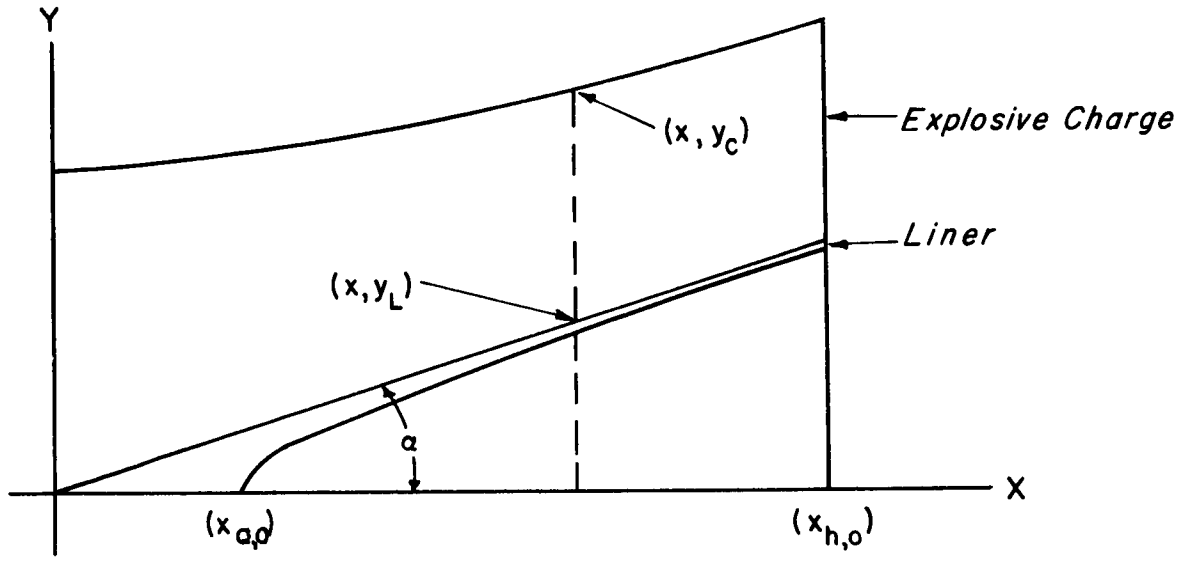

let the area between the exterior surface and conical surface be given by:

$$\pi(Y_c^2 - Y_L^2) = A(X) \tag{57}$$

let $$A(X) = MX + b \tag{58}$$

applying the following conditions to equation 58

when $X = X_a$, $A(X) = K A_o$ $K \geq 1$

when $X = X_h$, $A(X) = A_o$

$$K A_o = M X_a + b \tag{59}$$

$$A_o = M X_h + b \tag{60}$$

Solving equations 59 and 60 for M and b gives

$$M = \frac{(1 - K)A_o}{X_h - X_a} \tag{61}$$

$$b = A_o - \left[\frac{(1 - K)A_o}{X_h - X_a}\right]X_h \tag{62}$$

Substitute equations 61 and 62 into equation 58

$$A(X) = \frac{(1 - K)A_o}{X_h - X_a} X + A_o - \left[\frac{(1 - K)A_o}{X_h - X_a}\right] X_h \tag{63}$$

Substitute equation 63 into equation 57

$$\pi(Y_c^2 - Y_L^2) = \frac{(1 - K)A_o}{X_h - X_a} X + A_o - \left[\frac{(1 - K)A_o}{X_h - X_a}\right] X_h \tag{64}$$

It can be seen from the figure that

$$Y_L = mX \qquad \text{where } m = \tan \alpha \tag{65}$$

Substitute equation 65 into equation 64 and solve for the radius of the exterior surface, Y_c

$$Y_c = \left\{ m^2 X^2 + \left(\frac{1 - K}{X_h - X_a} \right) \frac{A_o}{\pi} X + \frac{A_o}{\pi} \left[1 - \left(\frac{1 - K}{X_h - X_a} \right) X_h \right] \right\}^{1/2} \qquad (66)$$

When K = 1, equation 66 reduces to the case of constant cross-sectional area along the liner axis. When K > 1, the cross-sectional area of the charge will increase linearly from the liner base to liner apex.

Equation 66 is a hyperbola symmetric about the Y-axis, when K = 1 and symmetric about an axis parallel to and translated to the right of the Y-axis for K > 1.

REFERENCES

1. Berus, E. R.; and Clark, E.L.: Development and Testing of Shaped Charge Meteoritic Simulators. Defense Research Division, The Firestone Tire and Rubber Company (Contract NAS1-4187) for National Aeronautics and Space Administration Oct. 1965.

2. Berus, E. R.; and Clark, E.L.: Development and Testing of Advanced Shaped Charge Meteoritic Simulators. Part I - Shaped Charge Design and Development. NASA CR-66215, Nov. 1966.

3. Woodall, R. L.; and Clark, E.L.: Development and Testing of Advanced Shaped Charge Meteoritic Simulators. Part II - Calibration of Flight Guns. NASA CR-66216. Nov. 1966.

4. Watson, R.W.; Becker, K.R.; and Gibson, F.C.: Stress Waves in Bounded Media. Bureau of Mines, Explosives Research Center. Quarterly Report, March 1, 1966 to May 31, 1966.

5. Argous, J.P.; Peyre, C.; and Thouvenin, J.: Observation and Study of the Conditions for Formation of Mach Detonation Waves. Fourth Symposium (International) on Detonation. ACR-126 Office of Naval Research, Department of the Navy. Oct. 12-15,1965.

6. Birkhoff, G.; MacDougall, D.P.; Pugh, E.M.; Taylor, G.: Explosives with Lined Cavities, J. of Appl. Phy. 19,563 (1948).

7. Eichelberger, R.J.: Shaped Charge Warheads: Potential Improvements and Problems. Proceedings, of Non-Nuclear Warhead Symposium. Picatinny Arsenal 29th, 30th Sep. and 1 Oct. 1964, Vol. I.

8. Walsh, J.M.; Schreffler, R. G.; Willig, F.S.: Limiting Conditions for Jet Formation in High Velocity Collisions, J. of Appl. Phy. 24,349 (1953).

Table I

NUMERICAL VALUES FOR BI-EXPLOSIVE CHARGE DESIGN PARAMETERS FOR VARIOUS EXPLOSIVE COMBINATIONS

Liner Cone Angle (deg.)	"Y" Location of P_4 (in.)	EXPLOSIVE (1) Inner	EXPLOSIVE (1) Outer	Angle θ (deg.) (2)	Effective Detonation Rate (μ_E) (km/sec)(2)
50	4.89	60/40 comp. B	75/25 octol	43.5	10.4
	3.80	50/50 pentolite	75/25 octol	33.4	12.2
	3.27	TNT	75/25 octol	24.6	14.8
	2.36	76/24 baratol	75/25 octol	-3.0	-72.2
	4.64	75/25 octol	pressed HMX	41.7	11.3
	3.87	60/40 comp. B	pressed HMX	34.2	12.7
	3.40	50/50 pentolite	pressed HMX	27.0	14.8
	3.05	TNT	pressed HMX	19.8	18.2
	2.31	76/24 baratol	pressed HMX	-4.9	-43.2
70	4.17	60/40 comp. B	75/25 octol	32.8	11.9
	3.10	50/50 pentolite	75/25 octol	22.3	16.0
	2.57	TNT	75/25 octol	13.1	24.6
	1.66	76/24 baratol	75/25 octol	-16.1	-12.1
	3.92	75/25 octol	pressed HMX	31.0	13.2
	3.17	60/40 comp. B	pressed HMX	23.2	16.4
	2.70	50/50 pentolite	pressed HMX	15.6	22.5
	2.36	TNT	pressed HMX	8.1	39.8
	1.61	76/24 baratol	pressed HMX	-18.2	-10.7

(1) The following detonation rates were used for the above computed results: Pressed HMX, 8.8 km/sec; octol, 8.3 km/sec; comp. B, 7.9 km/sec; pentolite, 7.4 km/sec; TNT, 6.8 km/sec; baratol, 4.1 km/sec.

(2) When the angle θ and the effective detonation rates are negative, the conical detonation wave will hit the bottom of the liner first and the detonation wave will sweep up toward the liner apex.

Table II

NUMERICAL VALUES FOR BI-EXPLOSIVE CHARGE DESIGN PARAMETERS FOR VARIOUS EXPLOSIVE COMBINATIONS WITH FIXED VALUES FOR THE HEIGHT OF THE INNER CHARGE, P_4

Liner Cone Angle (deg.)	"Y" Location of P_4 (in.)	EXPLOSIVE (1)		Angle θ (deg.) (2)	Effective Detonation Rate (μ_E) (km/sec) (2)
		Inner	Outer		
50	4.00	60/40 comp. B	75/25 octol	42.7	10.6
		50/50 pentolite	75/25 octol	33.6	12.1
		TNT	75/25 octol	25.5	14.3
		76/24 baratol	75/25 octol	0.1	1576.1
		75/25 octol	pressed HMX	41.1	11.4
		60/40 comp. B	pressed HMX	34.4	12.7
		50/50 pentolite	pressed HMX	27.8	14.4
		TNT	pressed HMX	21.1	17.1
		76/24 baratol	pressed HMX	-1.7	-125.4
70	3.25	60/40 comp. B	75/25 octol	31.6	12.3
		50/50 pentolite	75/25 octol	22.6	15.8
		TNT	75/25 octol	14.5	22.2
		76/24 baratol	75/25 octol	-10.9	-17.8
	4.00	75/25 octol	pressed HMX	31.1	13.2
		60/40 comp. B	pressed HMX	24.4	15.7
		50/50 pentolite	pressed HMX	17.8	19.9
		TNT	pressed HMX	11.1	28.8
		76/24 baratol	pressed HMX	-11.7	-16.6

(1) The following detonation rates were used for the above computed results: pressed HMX, 8.8 km/sec; octol, 8.3 km/sec; comp. B, 7.9 km/sec; pentolite, 7.4 km/sec; TNT, 6.8 km/sec; baratol, 4.1 km/sec.

(2) When the angle θ and the effective detonation rate are negative, the conical detonation wave will hit the bottom of the liner first and the detonation wave will sweep up toward the liner apex.

Table III

EVALUATION OF DETONATION WAVE FRONT IN THE BI-EXPLOSIVE SYSTEM
40° Liner Cavity
50° Bi-Explosive Loading Fixture

CHARGE TYPE (1)				Program Round Number	Comments
Waveshaper	Explosive Inner	Explosive Outer	θ Degrees(2)		
90° Lucite	60/40 comp. B	75/25 octol	54	923-1	Detonation wave radiographed .58" down from apex of cavity. Wave in comp. B curved, slightly convex upward.
	60/40 comp. B	75/25 octol	54	923-2	Detonation wave radiographed at same position as for Rd. 923-1. Wave has same shape.
	50/50 pentolite	75/25 octol	47	923-4	Detonation wave radiographed in pentolite at cavity apex. Wave curved, near center, convex upward.
	76/24 baratol	75/25 octol	———	923-6	Detonation wave observed in octol .90-in. from charge bottom. X-ray absorption did not permit observation in baratol.
	60/40 comp. B	75/25 octol	56	923-9	Detonation wave radiographed just at apex of conical cavity. Wave in comp. B curved convex upward.
			52	923-10	Detonation wave radiographed at same position as for Rds. 923-1, 923-2. Wave in comp. B curved convex upward.
			———	923-11	Detonation wave in comp. B radiographed at position half way between Lucite and apex of cavity. Wave curved convex upward.
			———	923-12	Detonation wave in comp. B observed just at bottom of wave-shaper, from outer edge to position about half way toward center.
			———	923-13	Detonation wave in comp. B radiographed 3/8-in. below waveshaper. Wave curved convex upward.
			———	923-14	Detonation wave radiographed at same position as for Rd. 923-11.
80° lead	60/40 comp. B	75/25 octol	———	923-15	Detonation wave radiographed in comp. B between waveshaper and apex of cavity. Center of wave intersects waveshaper.
			51	923-16	Detonation wave in comp. B radiographed just at cavity apex. Most of wave appears conical.
			49	923-17	Detonation wave in comp. B is cusped. Point of cusp is about half way between waveshaper and cavity apex.

(1) The inner explosive of the bi-explosive charge was cast around a 40° Hyperbolic Liner, then the liner was removed leaving a 40° conical cavity.

(2) Angle between conical wave front and conical cavity wall. For cases where there was no true conical wave front, a straight line was fitted to straightest portion of wave.

Table IV

COMPARISON OF THE PREDICTED AND MEASURED VALUES
FOR THE ANGLE θ IN THE BI-EXPLOSIVE SYSTEM
40° Liner Cavity
50° Bi-Explosive Loading Fixture

EXPLOSIVE		Wave Shaper Type	Predicted Angle θ (deg.)	Average Measured Angle θ (deg.)
Inner	Outer			
60/40 comp. B	75/25 octol	90° Lucite	47.7	54
		80° lead	47.7	50
50/50 pentolite	75/25 octol	90° Lucite	38.6	47

(1) θ is the angle between the conical wave front and the conical cavity wall. For cases where there was no true conical wave front, a straight line was fit to the straightest portion of the wave.

Table V

WAVESHAPER DESIGN EVALUATION FOR RIGID POLYURETHANE FOAM
40° Liner Cavity
Explosive: Inner, 60/40 Comp.B; Outer 75/25 Octol
50° Bi-Explosive Loading Fixture

Wave Shaper		Program Round Number	Position of Detonation Wave Front (1) (inches)	Time (2) (μsec.)	Comments
Drawing	Description				
DRB-23-2434 IT.5(FIG.8)	80° Apex Angle	923-21	1.37	15.6	Shock through waveshaper appears to have initiated inner explosive. Inner portion of wave front rounded convex upward.
		923-22	0.51	13.4	Shock initiation of explosive appears to have occurred along flat front.
DRB-23-2434 IT.3(FIG.8)	70° Apex Angle	923-24	NO DATA - FILM DESTROYED BY BLAST		
		923-32	0.72	13.4	Shock through waveshaper appears to have initiated inner explosive along flat front.
DRB-23-2434 IT.1(FIG.8)	60° Apex Angle	923-25	1.27	14.4	Shock wave through waveshaper appears to have initiated inner explosive. Upper portion of wave front rounded concave upward.
		923-33	0.57	13.3	Same condition as for Round 923-22 except that rarefaction front is seen behind shock induced detonation front.
DRB-23-2542 (FIG. 10)	43° Apex Angle (truncated)	923-35	1.31	14.8	No evidence of detonation of inner explosive through waveshaper.
		923-36	1.59	16.4	No evidence of detonation of inner explosive through waveshaper.

(1) The wave position is located relative to the base of the waveshaper and is measured to the furthest point of axial propogation of the detonation wave in the octol outer charge.
(2) Time is measured relative to initiation of booster at rear of charge.

Table VI

PRELIMINARY HYPERBOLIC LINER TESTS IN THE BI-EXPLOSIVE SYSTEM
40°, .030-in. Wall Hyperbolic Liner, Dwg. DRB-23-2073-1
Explosive: Outer, 75/25 Octol
50° Bi-Explosive Loading Fixture
Aluminum Adaptor Plate

LINER			Wave Shaper	Inner Explosive Charge	Program Round Number	Pressure (microns)	PELLET			
Type	Wall Thkns.	Material					Approx. Mass (grams)	Velocity (km/sec) Tip	Velocity (km/sec) Tail	Comments
40° Hyperbolic	.030	Nickel 200 (Lot 57, annealed)	90° Lucite	comp. B	923-3	Atm.	2.1	11.9	———	Jet integrity indeterminate.
				pentolite	923-5	Atm.	2.3	11.7	———	Jet integrity indeterminate.
				baratol	923-7	Atm.	2 (est.)	10.1	———	Not cohesive.
				comp. B	923-8	40	———	11.39	———	Not cohesive.
			80° lead	comp. B	923-23(1)	63	———	11.8	11.5	Not cohesive.
		Ni 270 (Lot 62,as received)	80° lead	comp. B	923-19	71	———	11.5	10.9	Not cohesive.
		Forma Iron (Lot 66,as received)	80° lead	comp. B	923-18	Atm.	———	>10.9	10.9	Not cohesive
					923-20	Atm.	———	———	———	Not cohesive.
					923-26	Atm.	———	11.9	———	Not cohesive.

(1) This liner was modified so that the external conic angle was 39° 38' instead of 40° 0'; therefore, the liner base wall thickness was .020-inch.

Table VII

INVESTIGATION OF 50°, 60°, AND 70° CONICAL LINER DESIGNS
80° Lead Waveshaper
Aluminum Adaptor Plate

LINER				EXPLOSIVE		Program (2)Round Number	Pressure (microns)	JET		
Angle (degrees)	Wall Thkns. (inches)	Material (1)	Drawing Number	Inner	Outer			Tip Velocity (km/sec)	Approx. Mass (g.)	Comments
50°	.030	Forma Iron (Lot 66)	DRB-23-2416 It. 1	60/40 comp. B	75/25 octol	923-28	Atm.	11.7	2.0	Jet integrity indeterminate.
						923-30	200	>11.6	---	Jet expanding radially.
		Nickel 200 (Lot 50)	DRB-23-2416 It. 1	60/40 comp. B	75/25 octol	923-42	Atm.	11.1	6.0	Jet tip dispersing radially.
						923-45	68	11.34	---	Radial dispersion of large fragments.
	.050	Forma Iron (Lot 66)	DRB-23-2416 It. 3	60/40 comp. B	75/25 octol	923-27	Atm.	10.77	5.0	Jet integrity indeterminate.
						923-29	120	10.7	---	Jet tip dispersing radially.
		Nickel 200 (Lot 50)	DRB-23-2416 It. 3	60/40 comp. B	75/25 octol	923-43	Atm.	10.0	4.0	Segmented and cohesive.
						923-44	65	10.23	---	Segmented and cohesive.
60°	.040	Ingot Iron (Lot 60)	DRB-23-1912 -2 M.P.	60/40 comp. B	75/25 octol	940-1	Atm.	10.68	3.4	Appeared to be cohesive.
						940-2	Atm.	10.64	3.8	Appeared to be cohesive.
70°	.015	Nickel 270 (Lot 62)	DRB-23-2429B It. 5	60/40 comp. B	75/25 octol	946-8	Atm.	10.8.	3.0	Jet tip dispersing radially
	.020	Nickel 270 (Lot 62)	DRB-23-2429B It. 4	60/40 comp. B	75/25 octol	946-7	Atm.	12.49	2.7	Jet fragmenting, tip elements cohesive.
	.030	Forma Iron (Lot 66)	DRB-23-2429B It. 1	60/40 comp. B	75/25 octol	924-5	Atm.	>10.5	2.0	Jet integrity indeterminate.
						924-8	120	11.1	---	Segmented and cohesive.
					PBX 9404	939-1	Atm.	12.2	3.0	Segmented and cohesive.
				75/25 octol	PBX 9404	939-2	Atm.	12.5	3.0	Segmented and cohesive.
						939-4	65	12.47	---	Segmented and cohesive.
		Nickel 200 (Lot 57A)	DRB-23-2429B It. 1	60/40 comp. B	75/25 octol	924-1	Atm.	10.1	1.7	Segmented and cohesive.
						924-4	66	10.3	---	Segmented and cohesive.
				75/25 octol	PBX 9404	939-3	Atm.	11.9	3.0	Segmented and cohesive.
						939-5	70	11.87	---	Segmented and cohesive.
	.050	Forma Iron (Lot 66)	DRB-23-2429B It. 3	60/40 comp. B	75/25 octol	924-6	Atm.	9.8	2.0	Segmented and cohesive.
						924-9	67	9.5	---	Segmented and cohesive.
				75/25 octol	75/25 octol	924-7	Atm.	9.8	2.0	Segmented and cohesive.
		Nickel 200 (Lot 57A)	DRB-23-2429B It. 3	60/40 comp. B	75/25 octol	924-2	Atm.	9.2	2.5	Segmented and cohesive.
						924-3	70	-----	---	Segmented and cohesive.

(1) Liners were machined from "As Received" materials.
(2) Rounds for Program 924 were loaded in the 70° bi-explosive loading fixture; all other programs used the 50° bi-explosive fixture.

Table VIII

COMPARISON OF LINEAR AND NON-LINEAR LINER DESIGNS FOR 70° LINERS
70° Forma Iron (lot 73, As-Received) Hyperbolic Liners
Explosive: Inner, 60/40 Comp.B; Outer, 75/25 Octol
80° Lead Waveshaper
50° Bi-Explosive Loading Fixture
Aluminum Adaptor Plate

LINER			Program Round Number	Pressure (microns)	JET PELLET		
Wall Thkns. (inches)	Area Ratio and(1) Type Variation	Drawing Number			Velocity(2) (km/sec)	Mass (grams)	Comments
.020	1.48 Non-Linear	DRB-23-2524-A	946-1	Atm.	10.47	1.16	Pellet segmenting - some radial expansion.
			946-5	65	10.71	———	Pellet fragmenting - some radial expansion.
.015	1.95 Non-Linear	DRB-23-2525-A	946-2	Atm.	10.97	0.96	Exhibits some velocity gradient.
			946-6	65	11.16	———	Pellet fragmented, expanding radially.
.020	1.39 Linear	DRB-23-2520-A	946-3	Atm.	10.65	2.4	Pellet expanding radially.
.015	1.78 Linear	DRB-23-2521-A	946-4	Atm.	11.07	1.8	Pellet expanding radially.

(1) Ratio of Liner cross-section area at internal apex to cross-sectional area at base.
(2) All velocities are measured at the jet tip.
(3) All masses have been estimated by treating the hyperbolic pellet as a cylinder of measured length and approximated diameter. The mass was taken at the first radiographed position where the pellet is being formed.

Table IX

COMPARISON OF LINEAR DESIGN LINERS WITH DIFFERING AREA RATIOS
70°, .020-in. Wall Forma Iron (Lot 73B, Annealed) Hyperbolic Liner
Explosive: Inner, 60/40 Comp.B; Outer, 75/25 Octol
80° Lead Waveshaper
50° Bi-Explosive Loading Fixture
Aluminum Adaptor Plate
Pressure: Atmospheric

LINER		Program	JET PELLET		
Area Ratio and(1) Type Variation	Drawing Number	Round Number	Velocity (km/sec)	Mass (grams)	Comments
1.75 Linear	DRB-23-2537	964-1	10.72	2.02	Pellet broken into dust-like pieces at about 27-inches of travel. Radial expansion is evident. Velocity gradient along the pellet is not observable.
2.00 Linear	DRB-23-2539	964-2	11.01	1.75	Pellet broken into dust-like pieces at about 27-inches of travel. Radial expansion is evident. Velocity gradient along the pellet is not observable.

(1) Ratio of liner cross-sectional area at internal apex to cross-sectional area at base.

Table X

EVALUATION OF 70° CONSTANT CROSS-SECTIONAL AREA DESIGN LINERS
70°, .020-in. Wall Ferrovac (Lot 79B, Annealed) Iron Hyperbolic Liner Dwg. DRB-23-2537-A
43° Rigid Polyurethane Foam Waveshaper
50° Bi-Explosive Loading Fixture
Aluminum Adaptor Plate

EXPLOSIVE		Program Round Number	Pressure (microns)	JET PELLET		
Inner	Outer			Velocity (km/sec)	Mass (grams)	Comments
60/40 comp. B	75/25 octol	974-1	Atm.	10.26	0.58	Jet dispersing radially. Appears to have reverse velocity gradient.
75/25 octol	HMX	974-2	2	>10.82	_____	Jet severely fragmented. Dispersing radially.
75/25 octol	HMX	974-3	1	11.30	_____	Jet severely fragmented. Dispersing radially.

Table XI

COMPARISON OF 50°, 60°, and 70° ELECTRON BEAM MELTED IRON HYPERBOLIC LINERS
Non-Linear Design EBM Iron (Lot 74B/ Annealed) Hyperbolic Liner
(Cross-Sectional Area Ratio: 1.48:1)
80° Lead Waveshaper
50° Bi-Explosive Loading Fixture
Aluminum Adaptor Plate

LINER			EXPLOSIVE		Program Round Number	Pressure (microns)	JET PELLET			
Wall Thkns. (inches)	Angle (degrees)	Drawing Number	Inner	Outer			Velocity (km/sec)	Gradient (km/sec)	Mass (grams)	Comments
.020	70°	DRB-23-2524A	60/40 comp. B	75/25 octol	965-1	Atm.	10.56	———	1.36	Pellet appears cohesive.
					965-2	15	10.54(1)	28	———	Pellet fragmenting - 3 cohesive pieces.
			75/25 octol	PBX9404(2)	965-3	Atm.		———	1.87	Jet integrity indeterminate.
					965-4	14	11.20(1)	.43	———	Pellet fragmenting, pieces cohesive.
	60°	DRB-23-2543	60/40 comp. B	75/25 octol	965-9	17	11.02(1)	.23	———	Pellet fragmented, some radial expansion.
			75/25 octol	HMX	965-12	17	11.24	.21	———	
			75/25 octol	PBX9404(2)	965-5	Atm.	11.47	———	2.31	Pellet expanding radially.
					965-8	17	11.52(1)	.38	———	Pellet fragmented, expanding radially.
	50°	DRB-23-2544	60/40 comp. B	75/25 octol	965-7	Atm.	11.59	———	2.03	Pellet expanding radially.
					965-11	12	11.43(1)	.15	———	Pellet fragmented, asymmetric expansion.
			75/25 octol	PBX9404(2)	965-6	Atm.	11.88	———	2.46	Pellet expanding radially.
					965-10	16	11.79(1)	.46	———	Pellet fragmented, asymmetric expansion.

(1) Velocity given is an Average velocity over the broken "pellet" taken from the tip to the tail of the pellet. Previous tables and atmospheric data in this table give velocities for the tip most piece only, but since the linear velocity differencial has been decreased, the average now becomes the significant number to examine.
(2) 94% HMX, 3% Nitrocellulose, 3% CEF (tris β -chloroethylphosphate) pressed into cylinders and machined by BRL.

Table XII

MATERIAL COMPARISON FOR ELECTRON BEAM MELTED IRON VERSUS BATTELLE PURE IRON
USING SECTIONED HYPERBOLIC LINER DESIGN
70°, .020-in. Wall Non-Linear Hyperbolic Liner Dwg. DRB-23-2598
(Cross-Sectional Area Ratio: 1.48:1)
Explosive: Inner, 75/25 Octol; Outer, HMX
43° Rigid Polyurethane Foam Waveshaper
50° Bi-Explosive Loading Fixture
Aluminum Adaptor Plate

LINER (1)		Program Round Number	Pressure (microns)	JET PELLET		
1/4-in. Base Section	Main Section			Velocity (km/sec)	Mass (grams)	Comments
EBM Iron (Lot 74B, Forged and annealed)	EBM Iron (Lot 74B, Forged and annealed)	975-3	Atm.	11.09	1.51	Jet fragmenting.
		975-1	5	11.33	———	Jet fragmented.
	Battelle Pure Iron (Lot 81, as received)	975-4	Atm.	11.03	1.25	Jet fragmenting.
		975-2	30	10.94	———	Jet fragmented. 7 major pieces.

(1) Two piece liner with cemented joint.

Table XIII

PRELIMINARY TESTS OF 50° NICKEL HYPERBOLIC LINER DESIGNS
50° Nickel 270 (Lot 62, As-Received) Hyperbolic Liner
80° Lead Waveshaper
50° Bi-Explosive Loading Fixture
Aluminum Adaptor Plate

LINER			EXPLOSIVE		Program		JET PELLET			
Wall Thkns. (inches)	Area Ratio and(1) Type Variation	Drawing Number	Inner	Outer	Round Number	Pressure (microns)	Velocity (km/sec)	Gradient (km/sec)	Mass (grams)	Comments
.030	1.00 Constant	DRB-23-2439	60/40 comp. B	75/25 octol	950-1	Atm.	10.53 (Tip)	0.28	1.85	Pellet is broken into 3 major solid sections. Radial expansion does not appear to exist.
.020	1.48 Non-Linear	DRB-23-2544	60/40 comp. B	75/25 octol	950-2	14	11.19 (Average)	0.20	———	Pellet is broken into 3 major solid sections. Radial expansion does not appear to exist.
.020	1.48 Non-Linear	DRB-23-2544	75/25 octol	HMX	950-3	75	11.77 (Tip)	———	———	Pellet is broken into 4 major solid sections. The segments are not quite as solid as for 950-1 or 950-2.

(1) Ratio of liner cross-sectional area at internal apex to cross-sectional area at base.

Table XIV

COMPARISON OF .020, .018, AND .016-INCH WALL 50° NICKEL HYPERBOLIC LINERS
50° Nickel 270 (Lot 62, As-Received) Hyperbolic Liner
43° Rigid Polyurethane Foam Waveshaper
50° Bi-Explosive Loading Fixture

LINER				EXPLOSIVE		Program Round Number	Pressure (microns)	JET PELLET	
Wall Thkns. (inches)	Area Ratio and(1) Type Variation	Drawing Number	Adapter Material	Inner	Outer			Velocity (km/sec)	Comments
.020	1.48 Non-Linear	DRB-23-2544	Steel	60/40 comp. B	75/25 octol	973-2 (2)	4	11.25	Integral Jet.
			Steel	60/40 comp. B	75/25 octol	973-3	3	11.05	Jet Fragmented.
.018	1.64 Non-Linear	DRB-23-2439 MP	Aluminum	75/25 octol	HMX	976-1	3	11.80	Jet Fragmented.
			Steel	75/25 octol	HMX	976-2	5	11.85	Jet Fragmented.
.016	1.84 Non-Linear	DRB-23-2439 MP	Aluminum	75/25 octol	HMX	976-4	4	12.08	Jet Fragmented.
			Steel	75/25 octol	HMX	976-3	28	12.13	Jet Fragmented
.020	1.00 Constant	DRB-23-2574	Steel	75/25 octol	HMX	976-5	0.5	11.79	Jet Fragmented

(1) Ratio of liner cross-sectional area at internal apex to cross-sectional area at base.
(2) The jet pellet had a mass of 1.28 grams.

Table XV

COMPARISON OF CYLINDRICAL AND TAPERED SKIRT TYPE INHIBITOR DESIGNS FOR 50° HYPERBOLIC LINERS
50° Nickel 270 (Lot 62, As-Received) Skirted Hyperbolic Liner
43° Rigid Polyurethane Foam Waveshaper
50° Bi-Explosive Loading Fixture

LINER						EXPLOSIVE		Program Round Number	Pressure (microns)	JET PELLET	
Skirt		Design Wall Thkns.(in.)	Area Ratio and(1) Type Variation(2)	Drawing Number	Adapter Material	Inner	Outer			Velocity(3) (km/sec)	Comments
Description	Thkns.(in.)										
Inside Tapered	.058	.016	1.84 Non-Linear	DRB-23-2579	Aluminum	75/25 octol	HMX	976-6	7	12.33	Jet fragmented and dispersing radially.
		.020	1.48 Non-Linear	DRB-23-2586	Steel	75/25 octol	HMX	976-7	5	11.80	Jet fragmented and dispersing radially.
Inside Cylindrical	.154	.016	1.84 Non-Linear	DRB-23-2578	Aluminum	60/40 comp. B	75/25 octol	976-9	4	11.85	Jet fragmented and dispersing radially.
		.020	1.48 Non-Linear	DRB-23-2585	Steel	60/40 comp. B	75/25 octol	976-10	3	11.74	Jet fragmented and dispersing radially.

(1) Values given omit skirt dimensions (See Figs. 42 and 43).
(2) Ratio of liner cross-sectional area at internal apex to cross-sectional area at base.
(3) Velocities given are jet tip velocities.

Table XVI

NICKEL AND IRON MATERIAL PROPERTIES STUDY
40°, .030-in. Wall Hyperbolic Liner Dwg. DRB-23-2073-1
Explosive: 65/35 Octol
Aluminum Adaptor Plate

LINER MATERIAL					Program Round Number	Pressure (microns)	JET PELLET		
Type	Lot No.	Elongation (in 2-in.)	Hardness (Rockwell)	Grain Structure			Velocity (km/sec)	Mass (grams)	Comments
Nickel Type 270 (As Received)	62	56%	B52	>ASTM1	922-3	60	9.53	1.68	Integral jet pellet.
					922-5	58	9.42	1.58	Integral jet pellet.
Nickel Type 270 (Annealed) (2)	62B	63%	B23	>ASTM1	922-4 (1)	58	9.42	1.58	Segmented - two cohesive pieces.
					922-6	61	9.52	1.54	Segmented - two cohesive pieces.
Ingot Iron (As Received)	59	25%	B69	Mixed	922-7	59	9.47	———	Fragmented - radial and axial dispersion.
					922-17 (3)	60	9.43	———	Fragmented - radial and axial dispersion.
Ingot Iron (Annealed) (4)	59A	———	B58	Mixed	922-8	58	9.55	———	Fragmented - radial and axial dispersion.
					922-10	62	9.53	———	Fragmented - radial and axial dispersion.
Forma (Uddeholm) Iron (As Received)	66	55%	B35	ASTM6	922-11	62	9.63	———	Fragmented - radial and axial dispersion.
					922-14	55	9.82	———	Fragmented - radial and axial dispersion.
EBM Iron (decarb.) (5)	64	———	B0-B31	ASTM7	922-12	61	9.58	———	Segmented - four cohesive pieces.
					922-18 (3)	60	9.31	1.62	0.11 g. fragment leading solid pellet.
C-1020 Steel (Annealed) (6)	51	———	B65-B67	ASTM7	922-16	68	9.81	———	Fragmented - large radial dispersion.
EBM Iron (As Received)	74A	———	B21	Too Large to Classify	922-19 (3)	13	9.55	———	Fragmented - expanding radially.
EBM Iron (Forged & Annealed) (7)	74B	53%	F63-F67	ASTM1	922-20 (3)	14	9.36	1.23	Fragmented - one large cohesive piece.
					922-23 (3)	18	9.25	———	Fragmented - one large cohesive piece.
Ferrovac E-CGA (As Received)	79	40%	F85	ASTM3-6	922-21 (3)	15	9.23	1.69	Cohesive - one large, one small segment.
					922-22 (3)	17	9.26	1.64	Cohesive - one large, one small segment.

(1) The annealed nickel 270 formed an unstable pellet which broke into two solid pieces. The velocity given for these two shots is the velocity of the leading piece; the mass given is the total mass of the two pieces.
(2) Annealed at 1500°F for 30 minutes and water quenched.
(3) Cast in 11°59' single angle loading fixture. All other rounds cast in standard 10°9' single angle loading fixture.
(4) Annealed at 1300°F for 1 hour and slow cooled.
(5) The material was received as a 1010 steel which was made by combining high purity carbon with high purity Electrolytic iron using the Electron Beam Melting Process. The carbon was then removed after rough machining by ARMCO Steel Corporation's decarburation process.
(6) Annealed at 1300°F for 30 minutes and air cooled.
(7) The material was received as high purity Electron Beam Melted Iron which was then forged to a smaller diameter and annealed twice in bar form at 1710°F for 1 hour and air cooled.

Table XVII

MONO-EXPLOSIVE CHARGE CONFIGURATION STUDY
40°, .020-in. Wall Nickel 200 (Lot 57A, As-Received) Hyperbolic Liner Dwg. DRB-23-2171
Explosive: 65/35 Octol
Aluminum Adaptor Plate

CHARGE		Program Round Number	Section (1)	Pressure (microns)	PELLET			
Loading Fixture Drawing	Type				Velocity (km/sec)	A to B Velocity Differential (km/sec)	Mass (grams)	Comments
DRC-11-2054	Hyperbolic H=1	931-6	A B	62	10.04 9.72	0.32	1.20 1.09	Segmented - two pieces; about equal in size.
DRC-11-2165	Hyperbolic H=1.125	931-7	A B	63	10.31 9.77	0.54	1.09	Segmented - two pieces; leading piece longest.
DRC-11-2166	Hyperbolic H=1.250	931-4	A B	65	10.37 9.99	0.38	1.27 1.22	Segmented - two pieces; equal in size.
DRB-N-3-3 MP It. 4	ϕ =0°	931-13	B	150	10.70(3)	———	.80	Single pellet surrounded by large fragments.
DRC-11-2163	ϕ =4°	931-1	A B	67	10.45 10.34	0.11	2.14(2) 0.98	Segmented - two pieces; leading piece longest.
DRC-11-2162	ϕ =6°	931-2	A B	60	10.45 10.34	0.11	1.37	Segmented - two pieces; rear piece longest.
DRC-11-2161	ϕ =8°	931-3	A B	300	10.20 10.13	0.07	1.34 0.41	Segmented - two pieces; leading piece has bulbous center section.
DRC-11-2040	ϕ =10°9' (original)	931-8	A B	62	10.04 9.92	0.12	1.24	Segmented - two pieces; leading piece longest.
DRC-11-2238	ϕ =10°57'	931-11	A B	90	9.92 9.85	0.07	1.36 1.51	Segmented - two pieces; about equal in size.
DRC-11-2238	ϕ =11°16'	931-10	A B	150	10.05 9.90	0.15	1.11 1.38	Segmented - two pieces; about equal in size.
DRC-11-2239	ϕ =11°59'	931-9	———	75	9.78	0.00	2.68	Single pellet with bulbous center section.
DRC-11-2239	ϕ =11°59'	931-12	———	54	9.90	0.00	2.32	Single pellet with bulbous center section.
DRC-11-2239	ϕ =11°59'	931-14(4)	———	Atm.	10.00	0.00	2.32	Single pellet with bulbous center section.
DRC-11-2267	ϕ =13°	931-15	———	60	9.90	0.00	2.36	Single pellet with bulbous center section - slight reverse gradient.

(1) Pellets which broke into two segments have been sub-headed with the letters "A" and "B". "A" is the leading segment.
(2) The Mass value 2.14 was not well determined due to insufficient radiographic data.
(3) The velocity value 10.70 was estimated using trailing debris and information from the NAS 1-521[illegible] contract. The pellet was not viewed at station 2 due to a timing error.
(4) Round 931-14 was fired at the open test site for collapse information. The mass data given is for a pellet travel of 9.16-inches. The velocity was taken over a 24-inch interval.

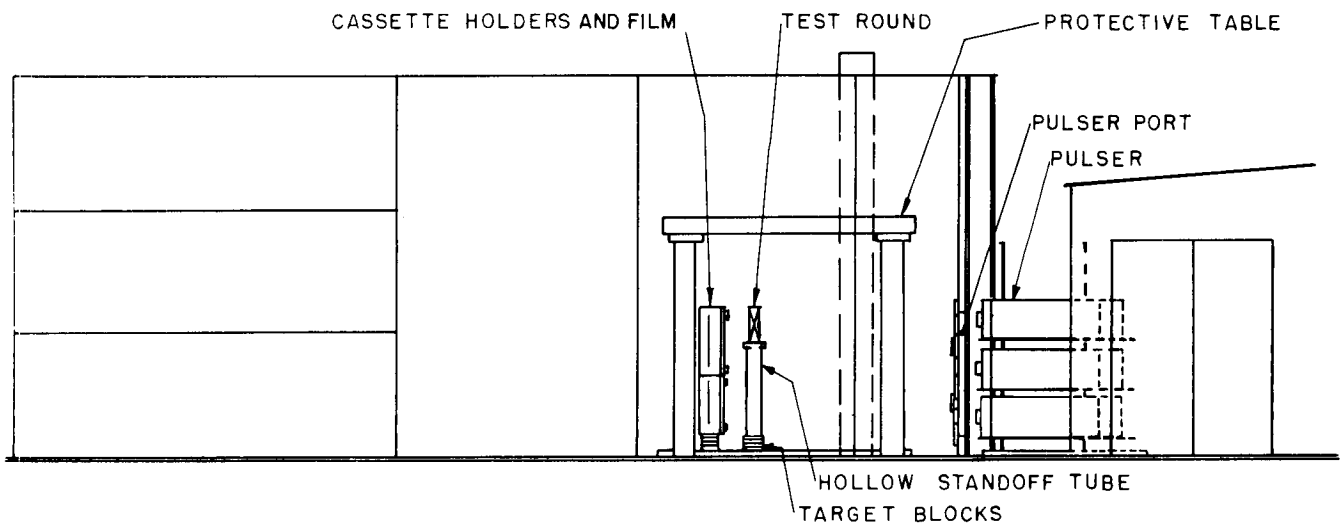

Fig. la. Side view sketch of the open test site facility.

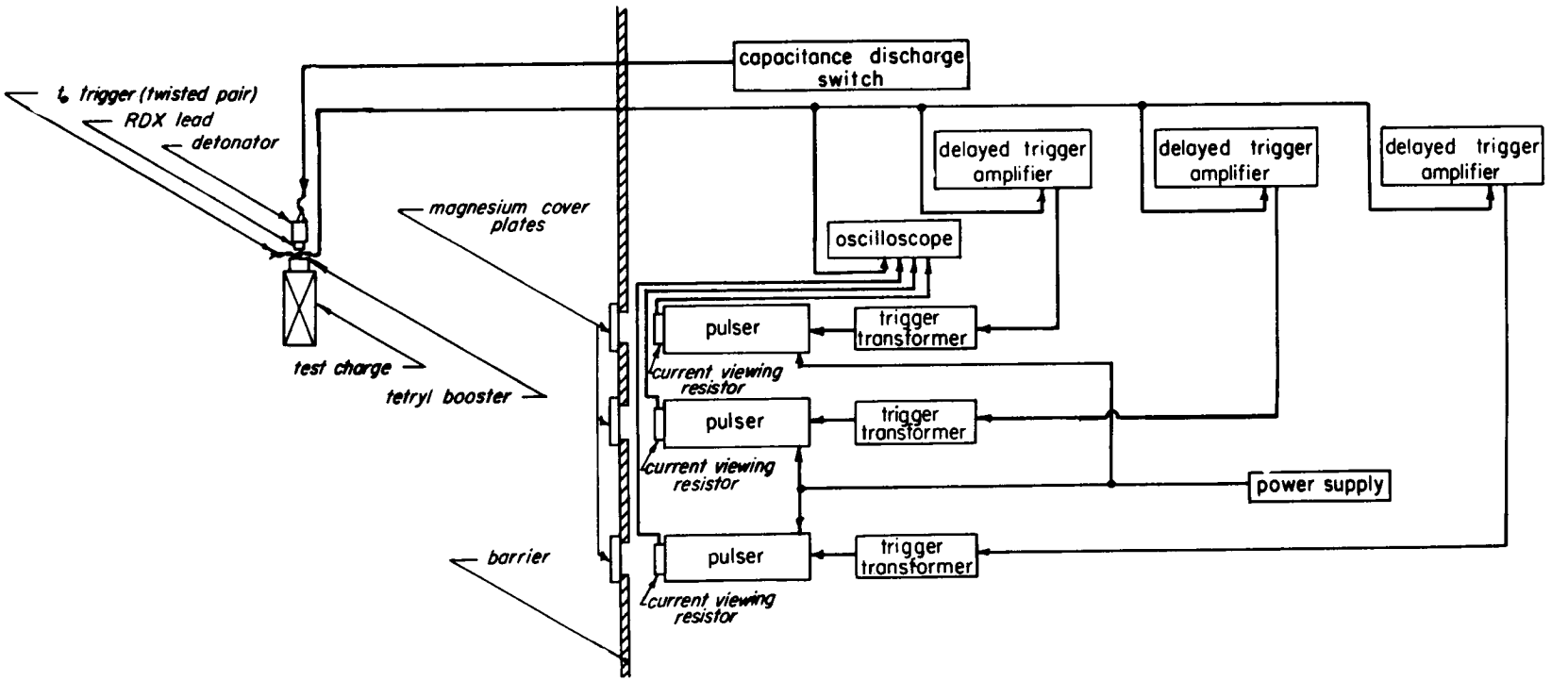

Fig. 1b. Side view block diagram of the electrical equipment for the open test site facility.

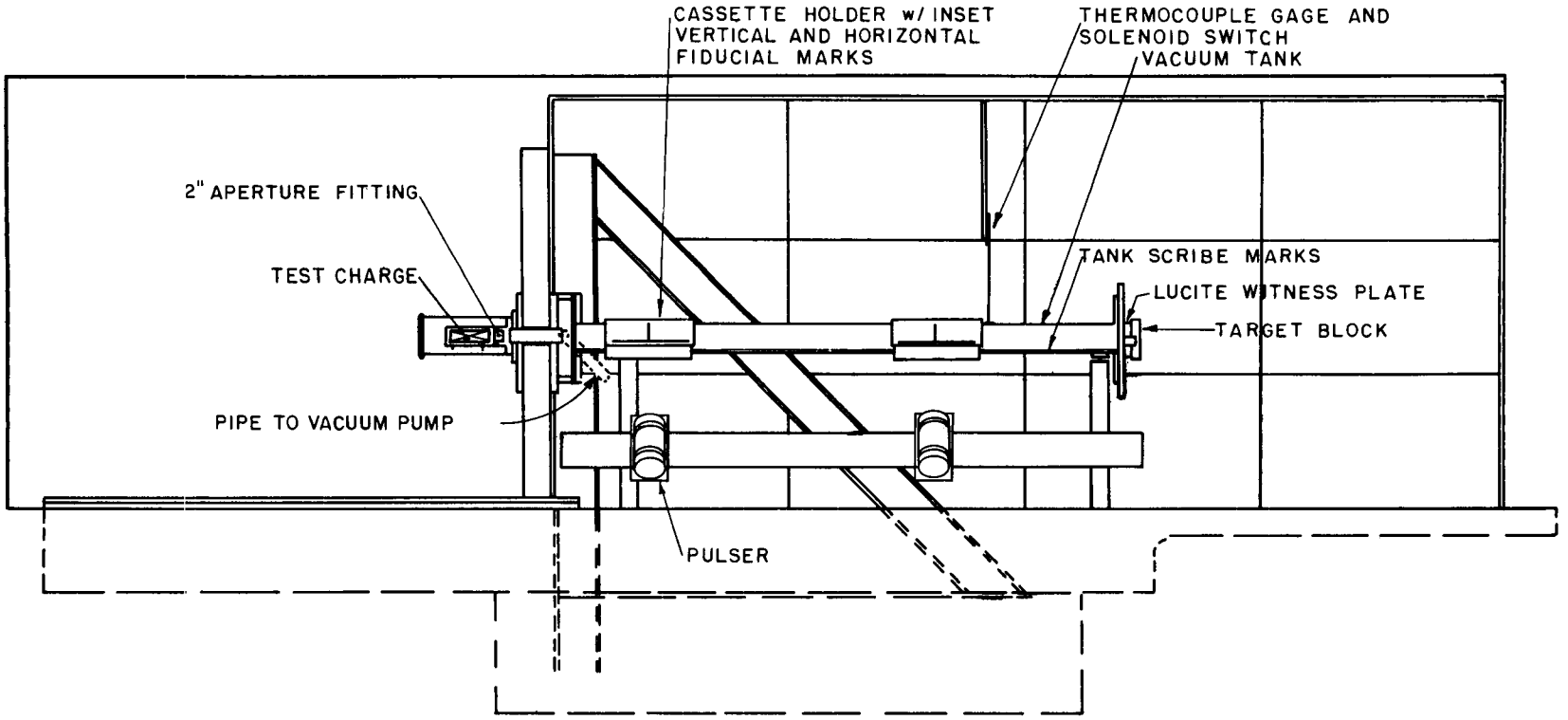

Fig. 2a. Side view sketch of the NASA vacuum test site facility.

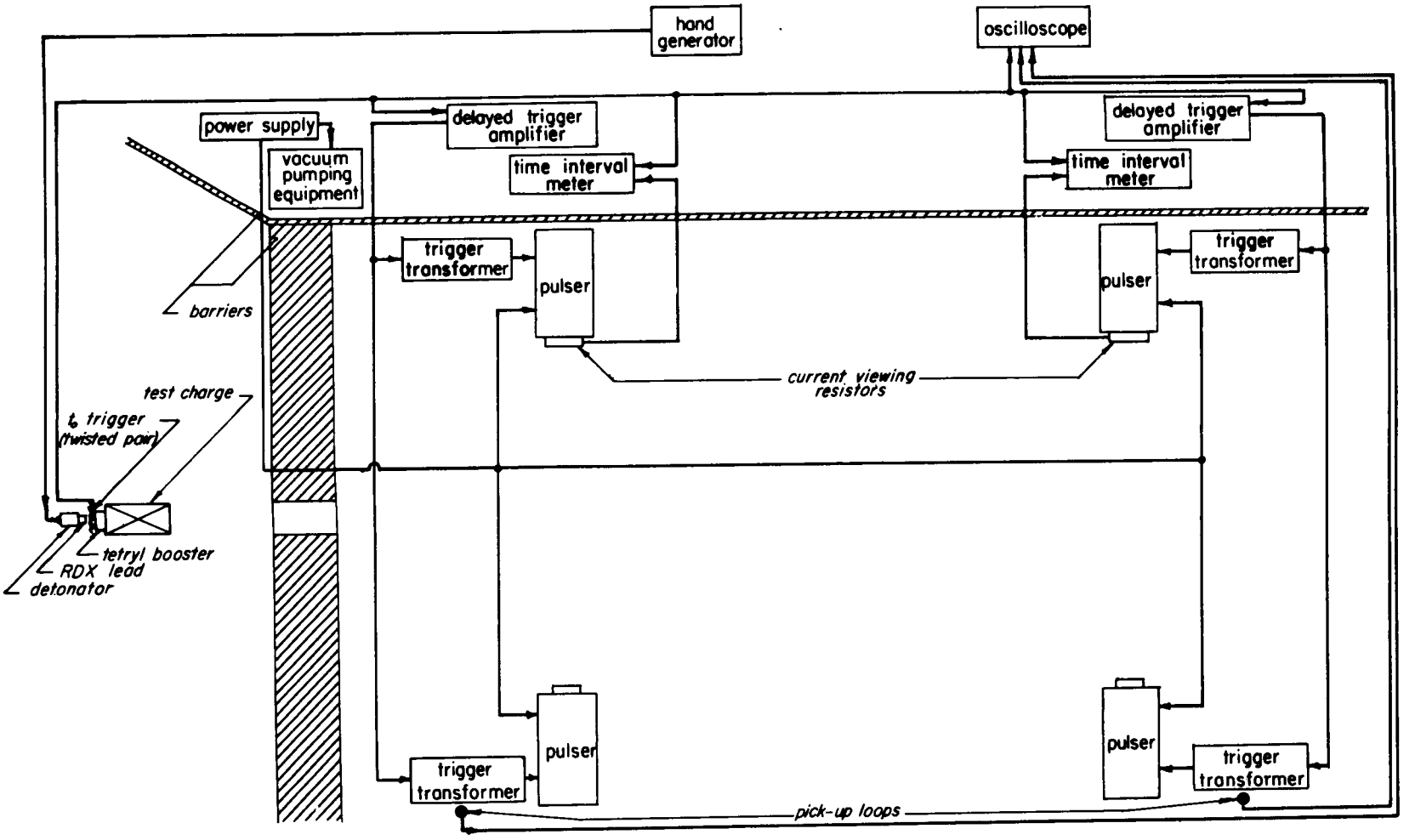

Fig. 2b. Top view block diagram of the electrical equipment for the NASA vacuum open test site facility.

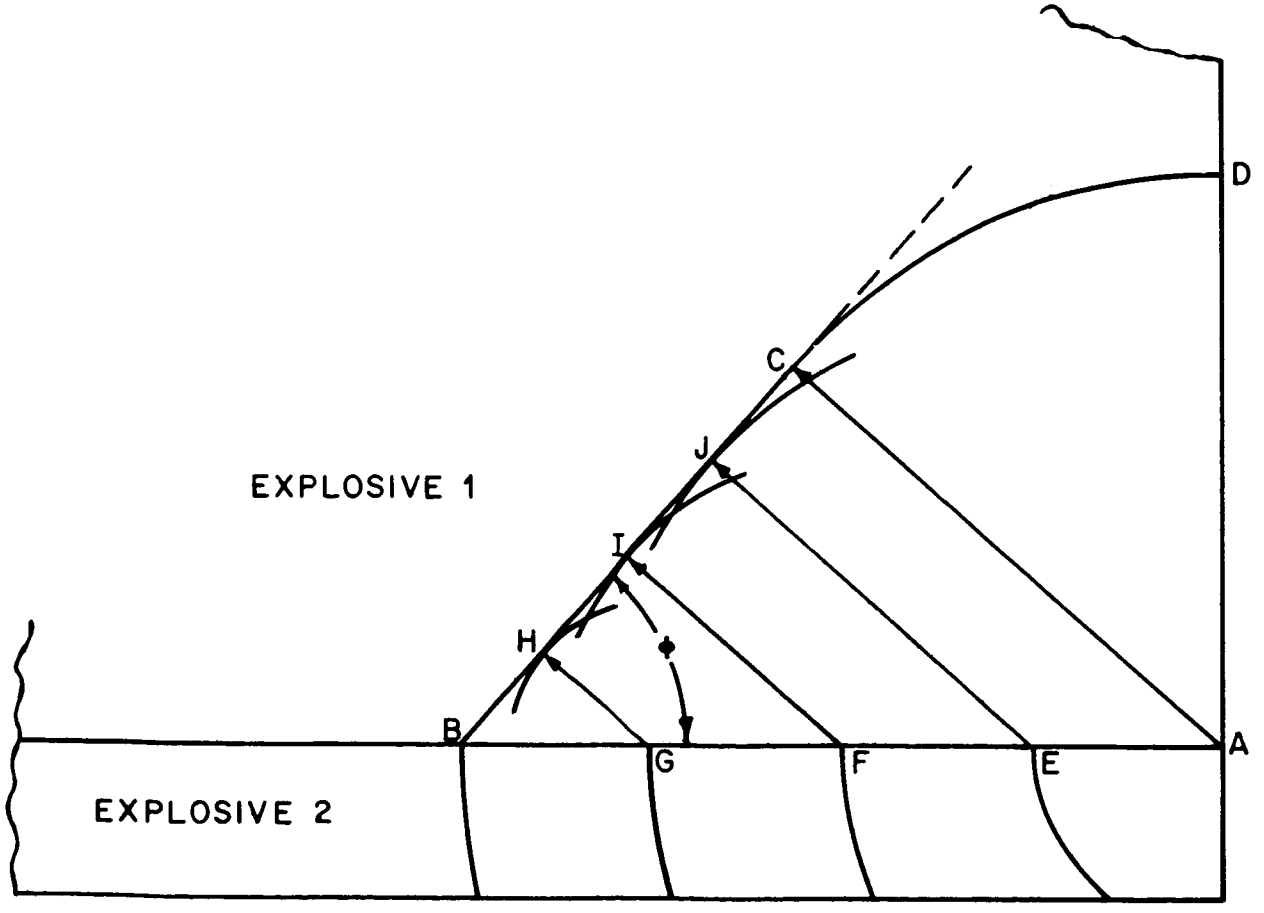

$u_1 < u_2$

where A = Initiation Point of Detonation Wave

u_1 = Detonation Rate of Explosive 1

u_2 = Detonation Rate of Explosive 2

Fig. 3. Schematic of linear wave front development in a bi-explosive charge.

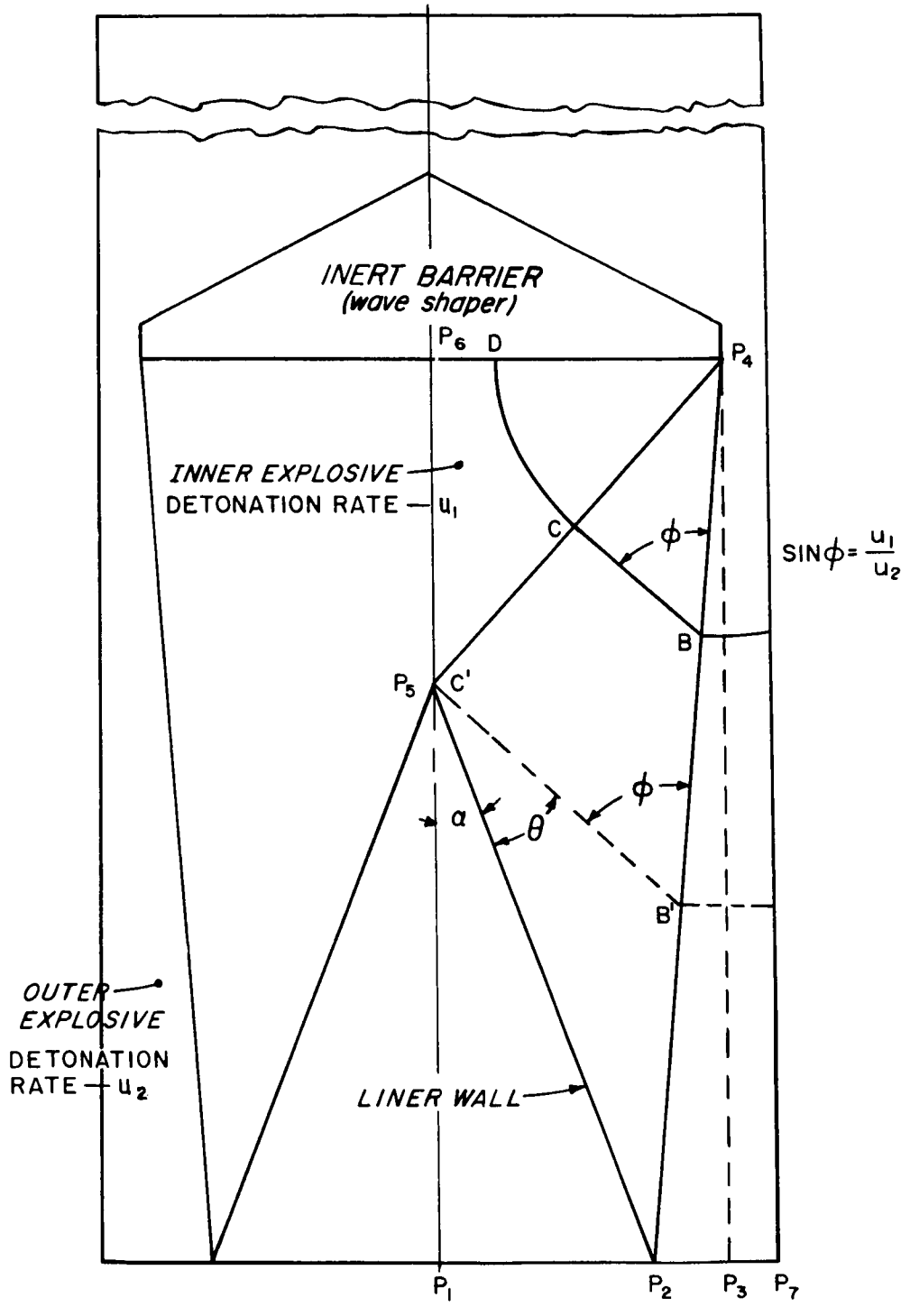

Fig. 4. Schematic of bi-explosive concept applied to cylindrical charge.

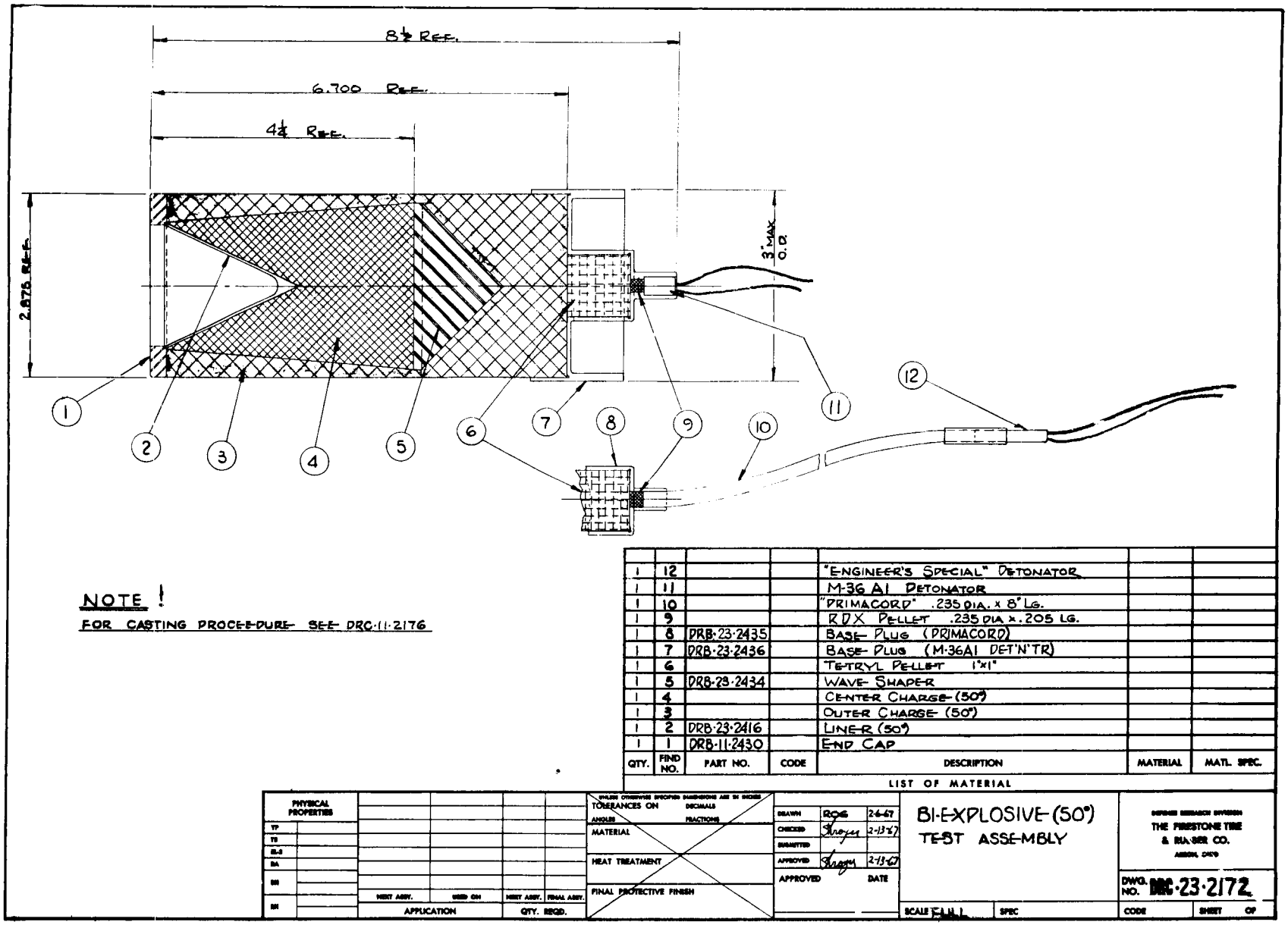

NOTE !

FOR CASTING PROCEDURE SEE DRC-11-2176

QTY.	FIND NO.	PART NO.	CODE	DESCRIPTION	MATERIAL	MATL. SPEC.
1	12			"ENGINEER'S SPECIAL" DETONATOR		
1	11			M-36 A1 DETONATOR		
1	10			"PRIMACORD" .235 DIA. x 8" LG.		
1	9			RDX PELLET .235 DIA x .205 LG.		
1	8	DRB-23-2435		BASE PLUG (PRIMACORD)		
1	7	DRB-23-2436		BASE PLUG (M-36A1 DET'N'TR)		
1	6			TETRYL PELLET 1"x1"		
1	5	DRB-23-2434		WAVE SHAPER		
1	4			CENTER CHARGE (50°)		
1	3			OUTER CHARGE (50°)		
1	2	DRB-23-2416		LINER (50°)		
1	1	DRB-11-2430		END CAP		

LIST OF MATERIAL

PHYSICAL PROPERTIES — YP, YS, EL-2, RA, BB, BH

APPLICATION — NEXT ASSY. | USED ON

QTY. REQD. — NEXT ASSY. | FINAL ASSY.

UNLESS OTHERWISE SPECIFIED DIMENSIONS ARE IN INCHES
TOLERANCES ON DECIMALS
ANGLES FRACTIONS
MATERIAL
HEAT TREATMENT
FINAL PROTECTIVE FINISH

DRAWN	ROG	2-6-67
CHECKED	[illegible]	2-13-67
SUBMITTED		
APPROVED	[illegible]	2-13-67
APPROVED		DATE

BI-EXPLOSIVE-(50°)
TEST ASSEMBLY

SCALE FULL | SPEC | CODE | SHEET OF

THE FIRESTONE TIRE & RUBBER CO.
AKRON, OHIO

DWG. NO. DRC-23-2172

Fig. 5. 50° design bi-explosive test assembly.

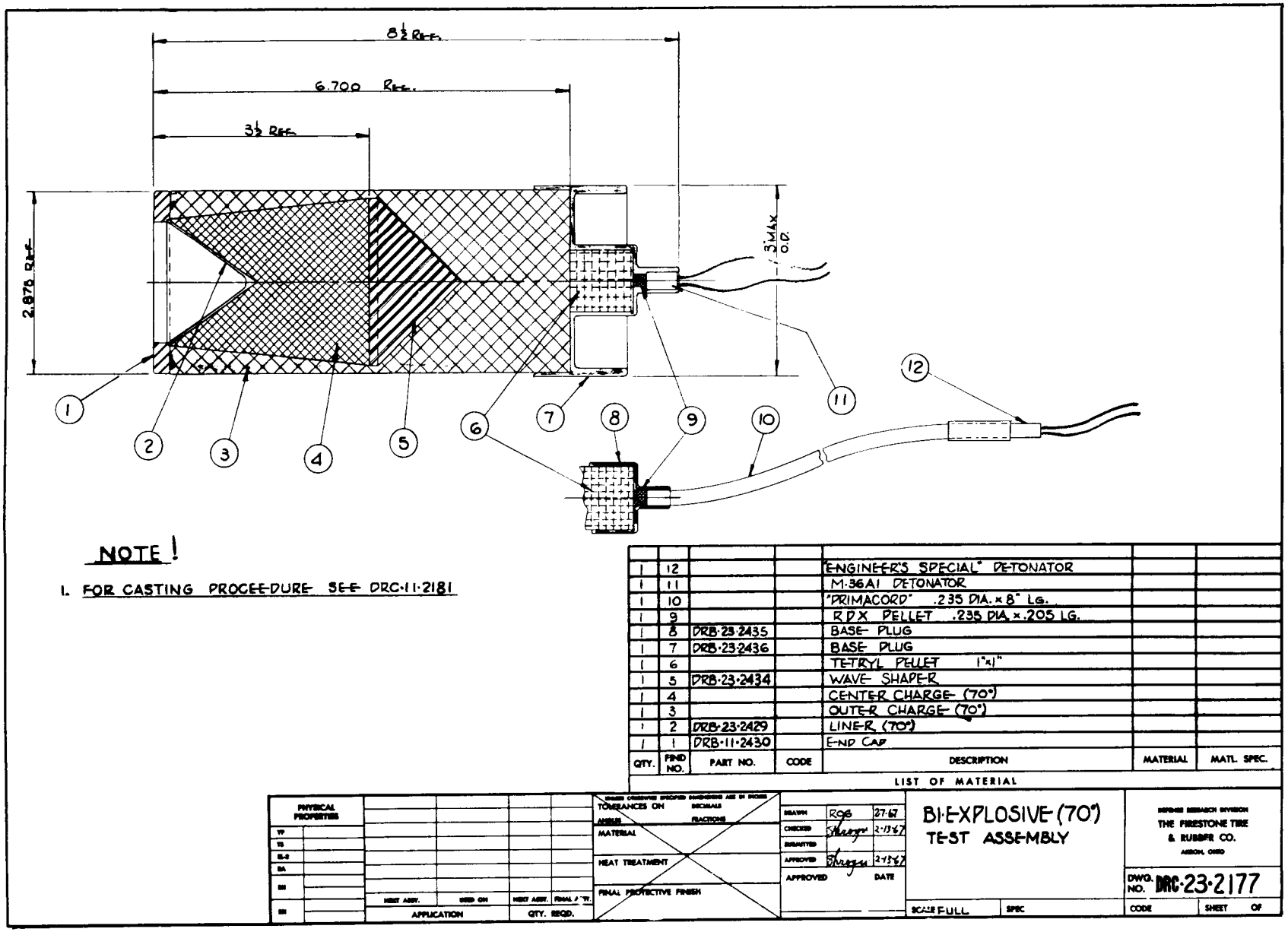

Fig. 6. 70° design bi-explosive test assembly.

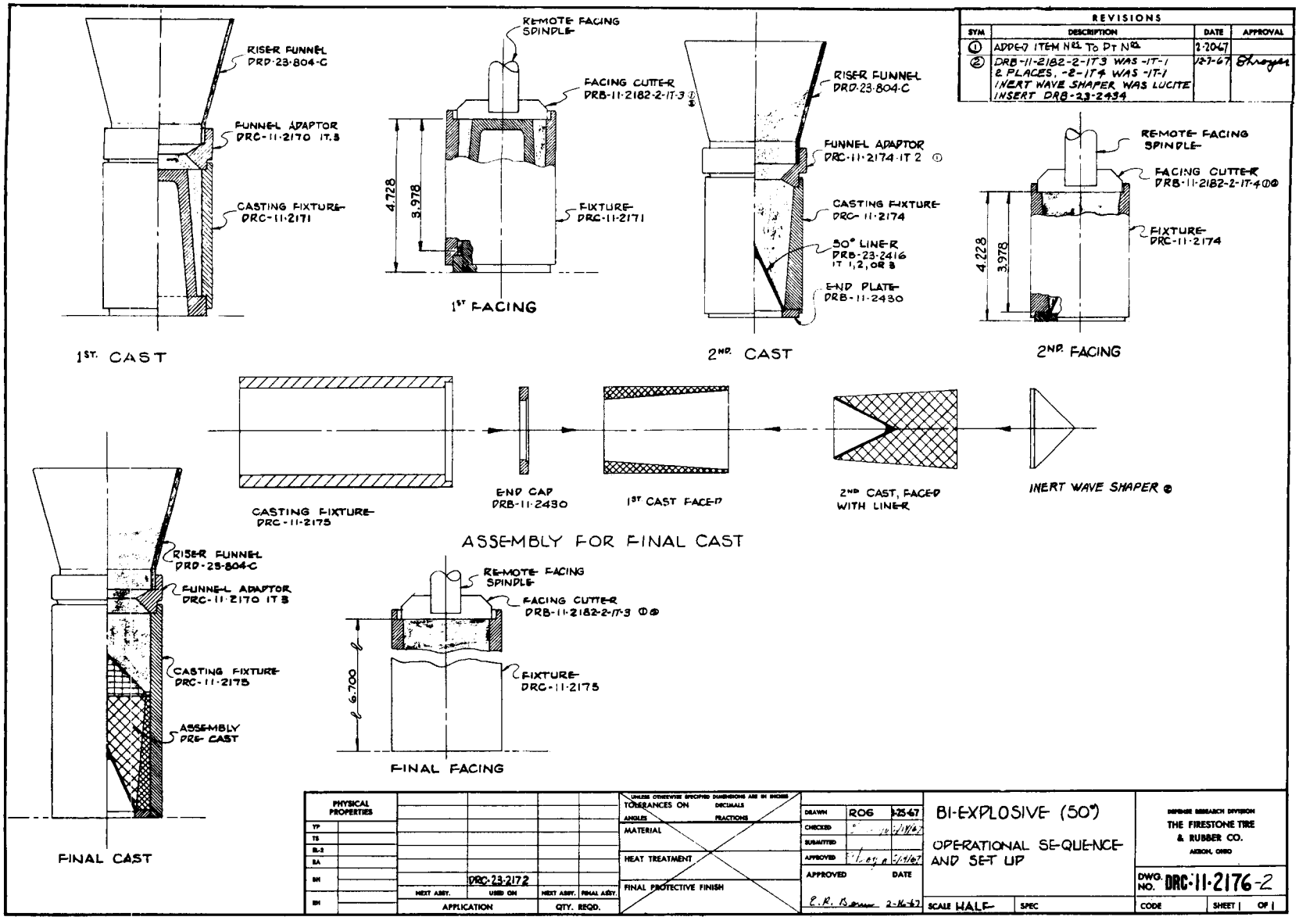

Fig. 7. Loading procedure for bi-explosive charges.

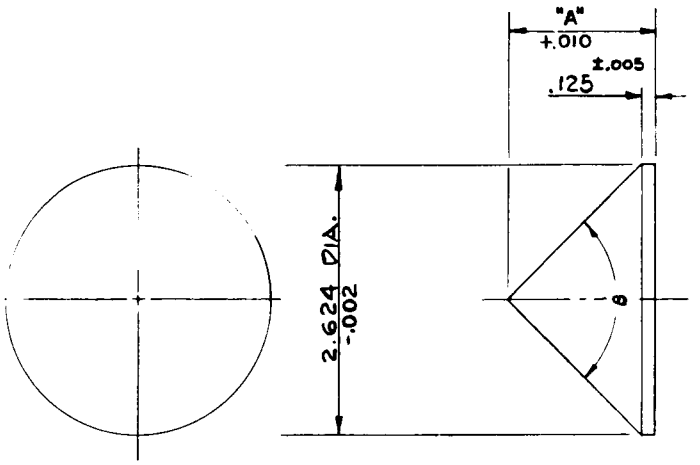

Item no.	β deg.	"A"
1	60	2.397
2	65	2.184
3	70	1.999
4	75	1.835
5	80	1.688
6	85	1.557
7	90	1.437

NOTE !
1: BREAK ALL CORNERS $\frac{1}{64}$ R
2: 2.624/2.622 DIA. MUST BE CONCENTRIC WITH CONE-POINT

PHYSICAL PROPERTIES: YP, TS, EL-2, RA, BH, BH

DRC-23-2177
DRC-23-2172
NEXT ASSY. | USED ON | NEXT ASSY. | FINAL ASSY.
APPLICATION | QTY. REQD.

UNLESS OTHERWISE SPECIFIED DIMENSIONS ARE IN INCHES
TOLERANCES ON DECIMALS ± .010
ANGLES ± ½° FRACTIONS ± 1/64
MATERIAL LUCITE HC-218 HEAT RESISTANT
HEAT TREATMENT
FINAL PROTECTIVE FINISH

DRAWN	ROG	1-25-67
CHECKED	Stroyan	2-13-67
SUBMITTED		
APPROVED	Stroyan	2-13-67
APPROVED		DATE
P. R. Bacon		2-16-67

LUCITE INSERT FOR BI-EXPLOSIVE 50° & 70° LINERS

DEFENSE RESEARCH DIVISION
THE FIRESTONE TIRE & RUBBER CO.
AKRON, OHIO

DWG. NO. DRB-23-2434

SCALE FULL | SPEC | CODE | SHEET 1 OF 1

Fig. 8. Sharp apex wave shaper designs used for Lucite, lead, and rigid polyurethane foam.

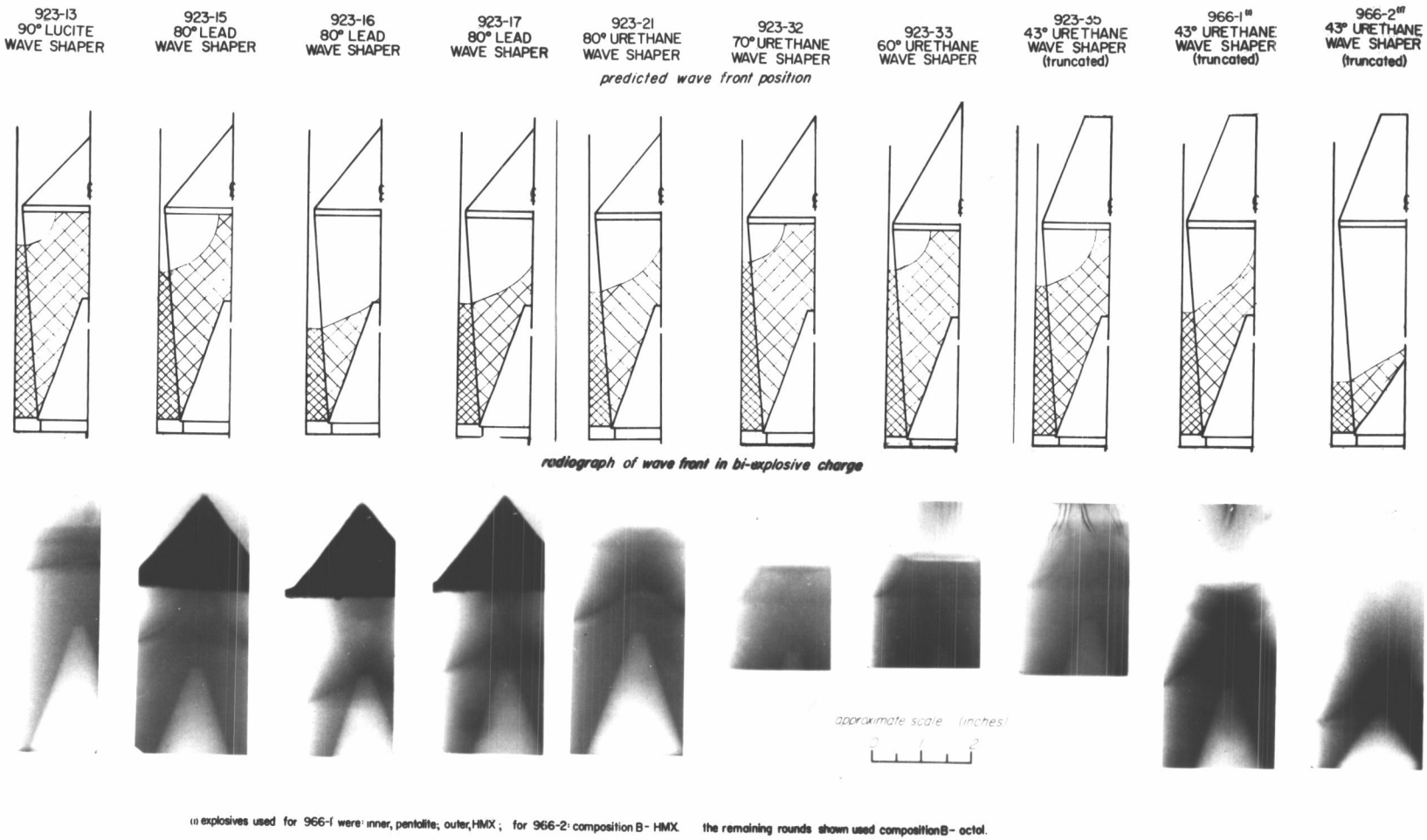

Fig. 9. Effects of wave shaper design and material on the detonation front in bi-explosive charges.

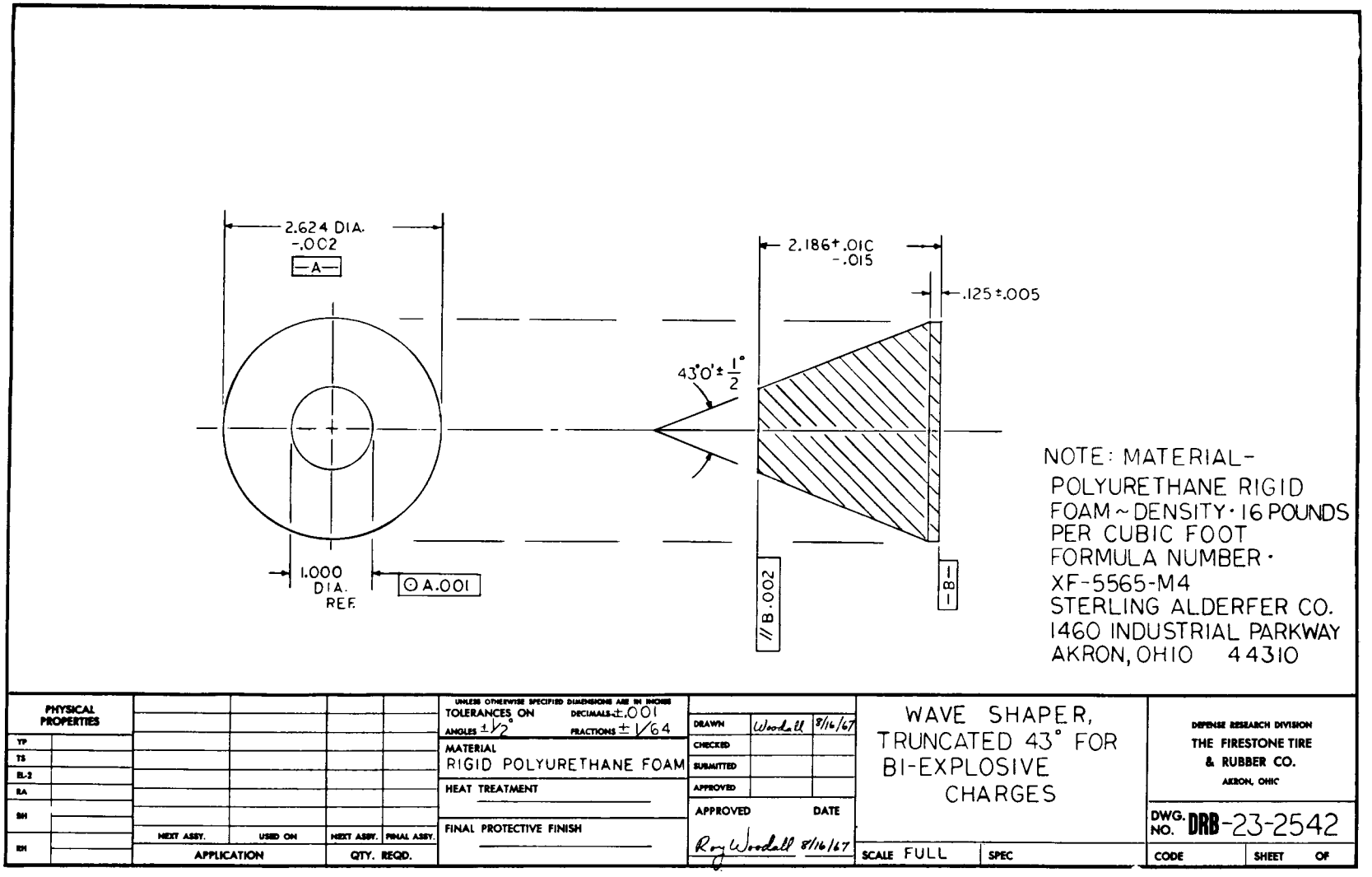

Fig. 10. Truncated 43° wave shaper design used for rigid polyurethane foam.

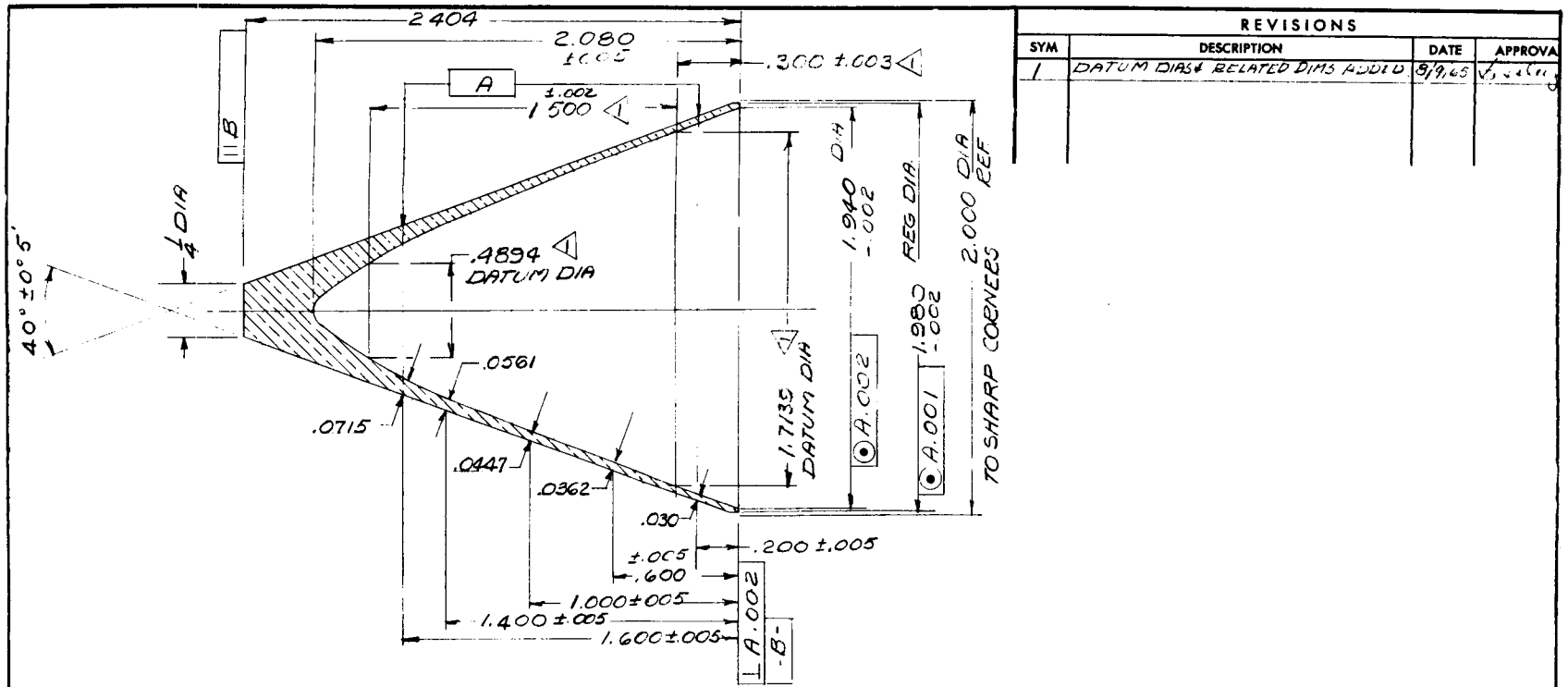

REVISIONS			
SYM	DESCRIPTION	DATE	APPROVA
1	DATUM DIAS & RELATED DIMS ADDED	9/9/65	

NOTE

1. WALL THICKNESS MEASURED PERPENDICULAR TO OUTSIDE SURFACE OF LINER SHALL NOT VARY MORE THAN ±.002
2. IN ANY GIVEN PLANE PERPENDICULAR TO ℄ OF PART, WALL THICKNESS SHALL NOT VARY MORE THAN .002 IN 360°
3. FINISH ✓3/
4. FOR INSIDE CONTOUR USE TRACER TEMPLATE DRB-10-2074

NEXT ASSY.	USED ON	NEXT ASSY.	FINAL ASSY.
APPLICATION		QTY. REQD.	

UNLESS OTHERWISE SPECIFIED DIMENSIONS ARE IN INCHES
TOLERANCES ON DECIMALS ±.010
ANGLES ±1/2° FRACTIONS ± 1/64

MATERIAL TO BE SPECIFIED ON ORDER

HEAT TREATMENT

FINAL PROTECTIVE FINISH

DRAWN	Livsey	3/29/65
CHECKED		
SUBMITTED		
APPROVED		

APPROVED DATE
S.R. Dixon 4-13-65

LINER,
40° HYPERBOLIC

SCALE 2:1 SPEC

DEFENSE RESEARCH DIVISION
THE FIRESTONE TIRE & RUBBER CO.
AKRON, OHIO

DWG. NO. DRB-23-2073-1

CODE SHEET OF

Fig. 11. 40°, .030-inch wall hyperbolic liner.

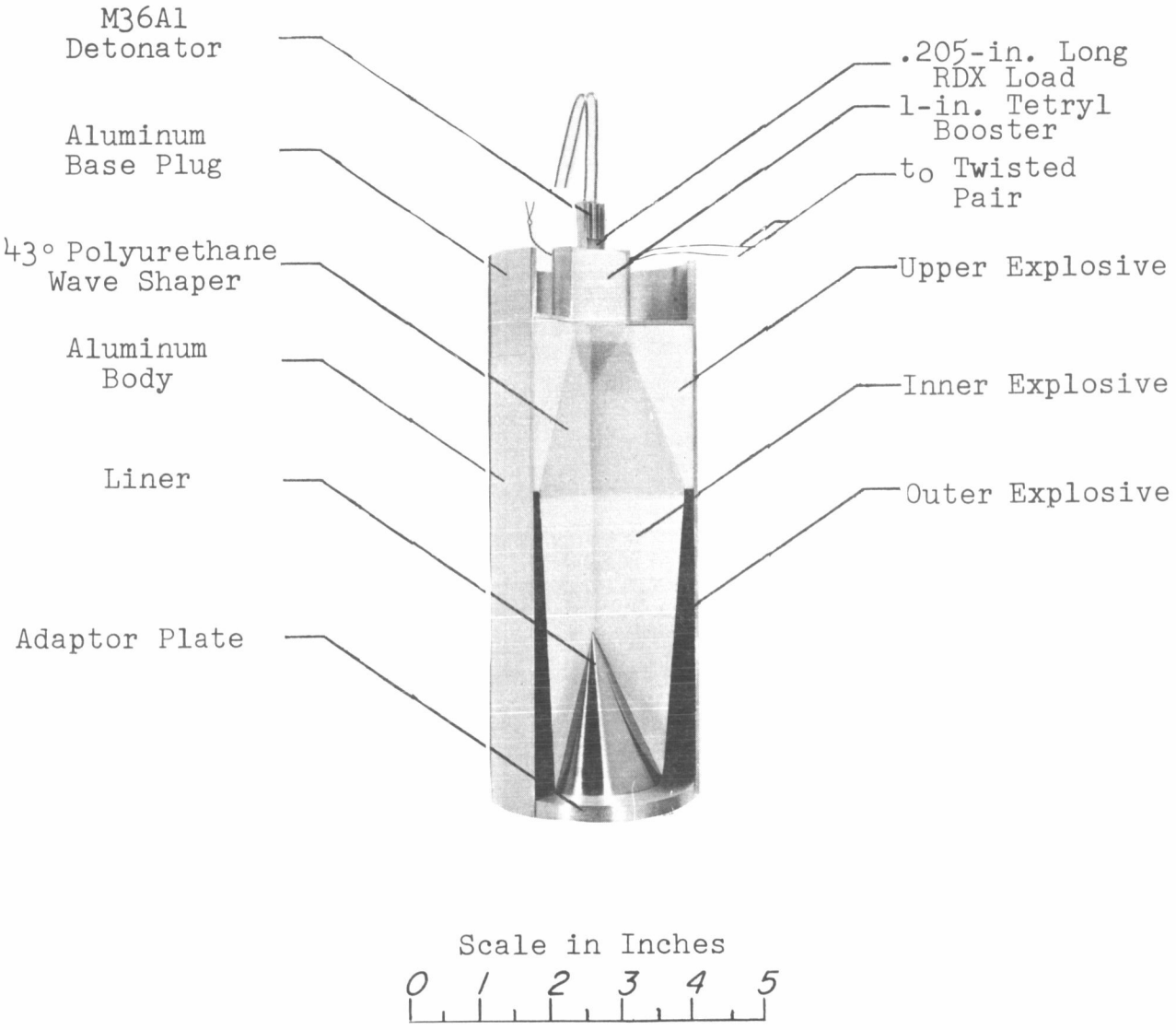

Fig. 12. Photograph of sectioned model of final bi-explosive test assembly.

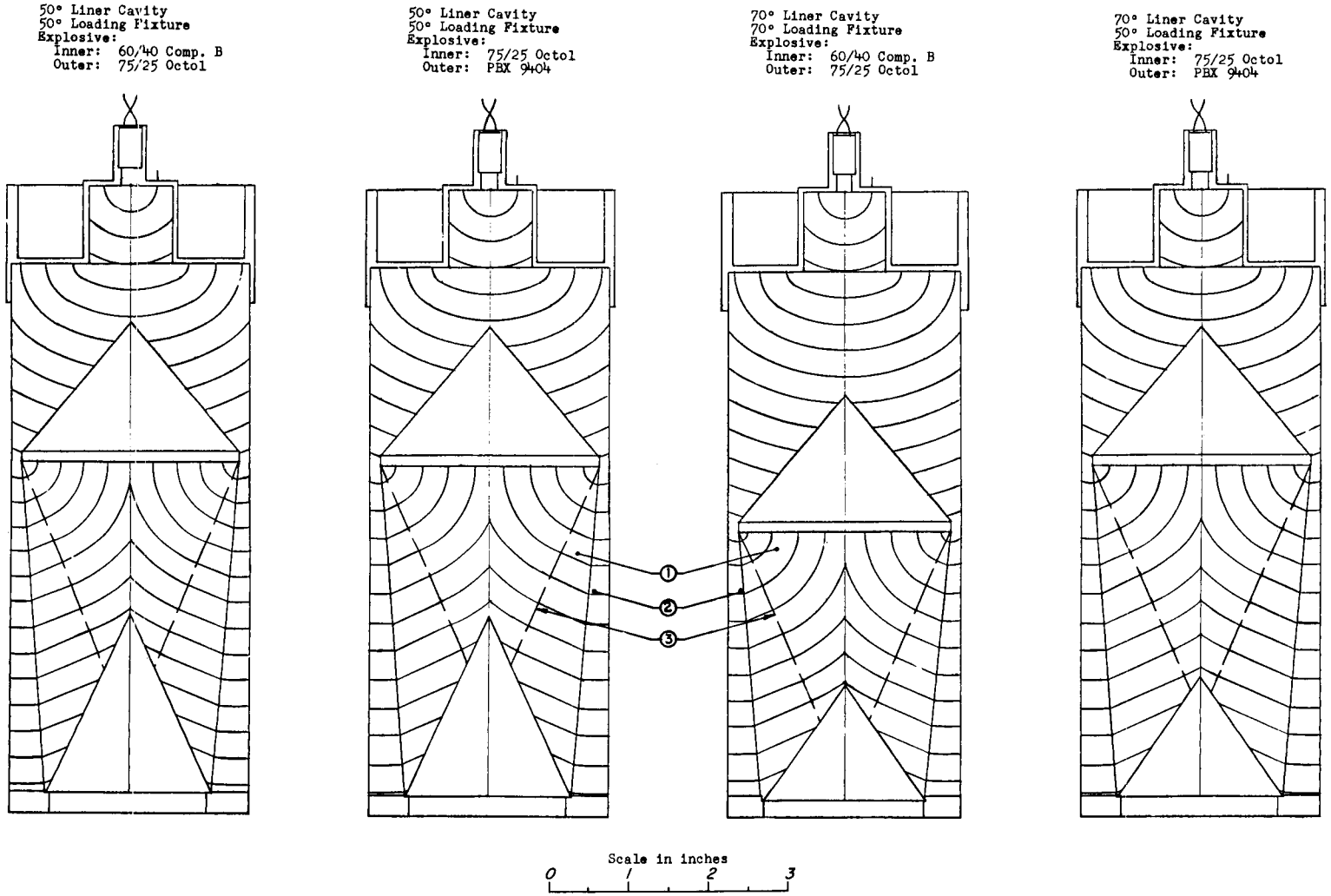

① Inner Explosive.

② Outer Explosive.

③ Intersection between true conical and non-conical detonation waves in the inner explosive.

Fig. 13. Schematic of predicted detonation wave fronts shown at one microsecond intervals for various bi-explosive designs.

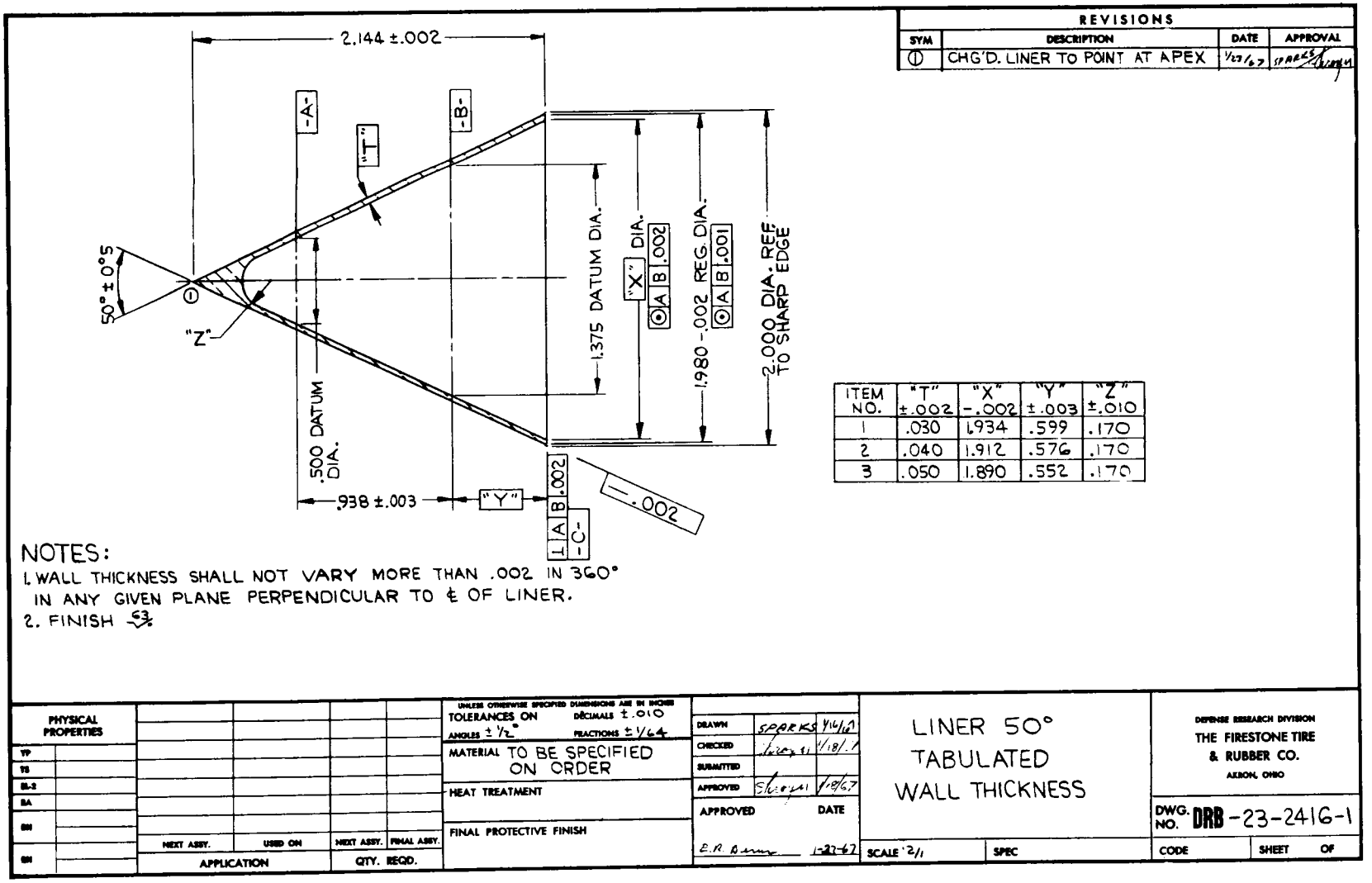

Fig. 14. 50° conical liner design.

EXPLOSIVE: INNER, COMP. B; OUTER, OCTOL
80° LEAD WAVE SHAPER
ALUMINUM ADAPTOR PLATE

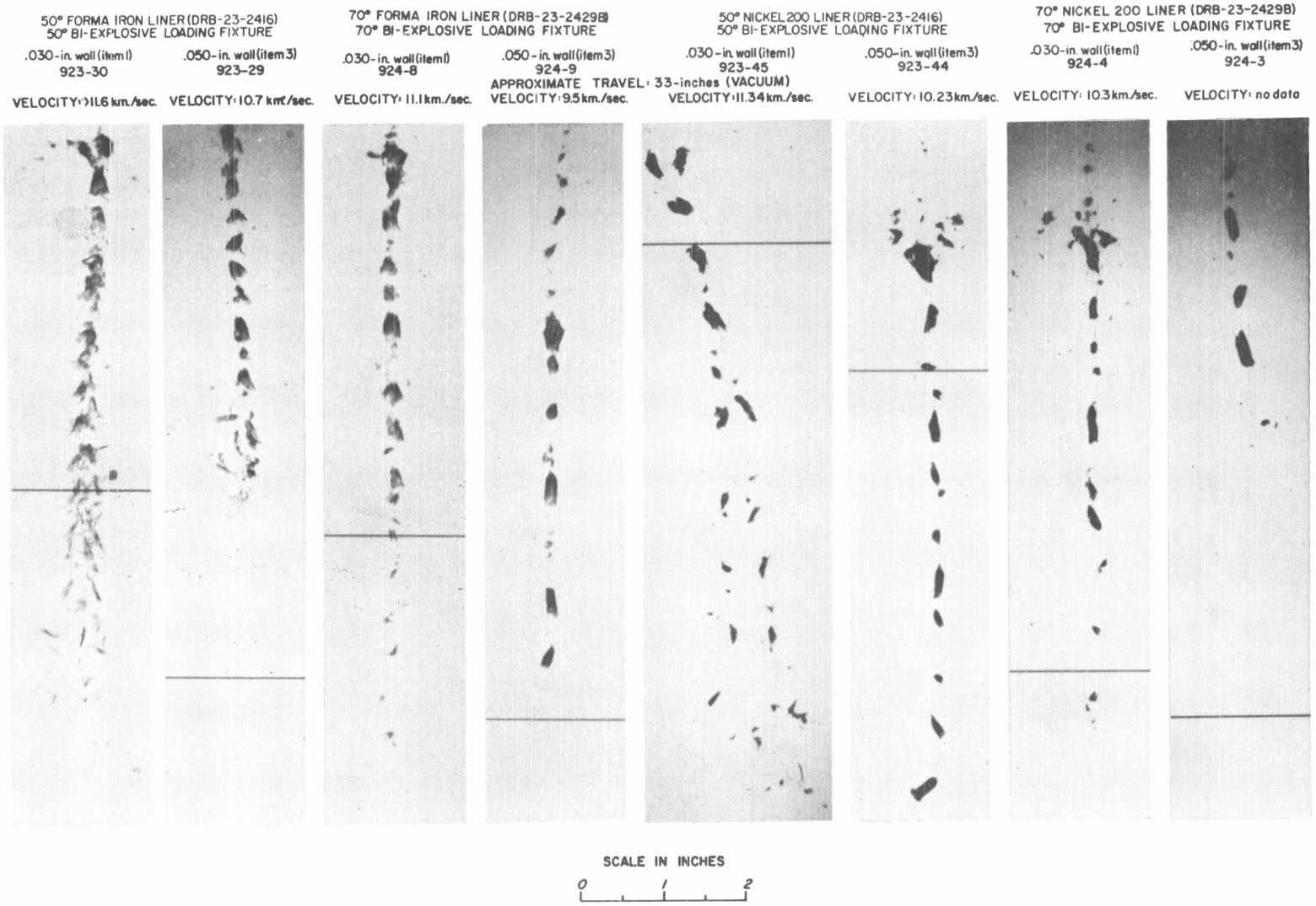

Fig. 15. Comparison of jets produced by 50° and 70° conical liners tested in the bi-explosive system.

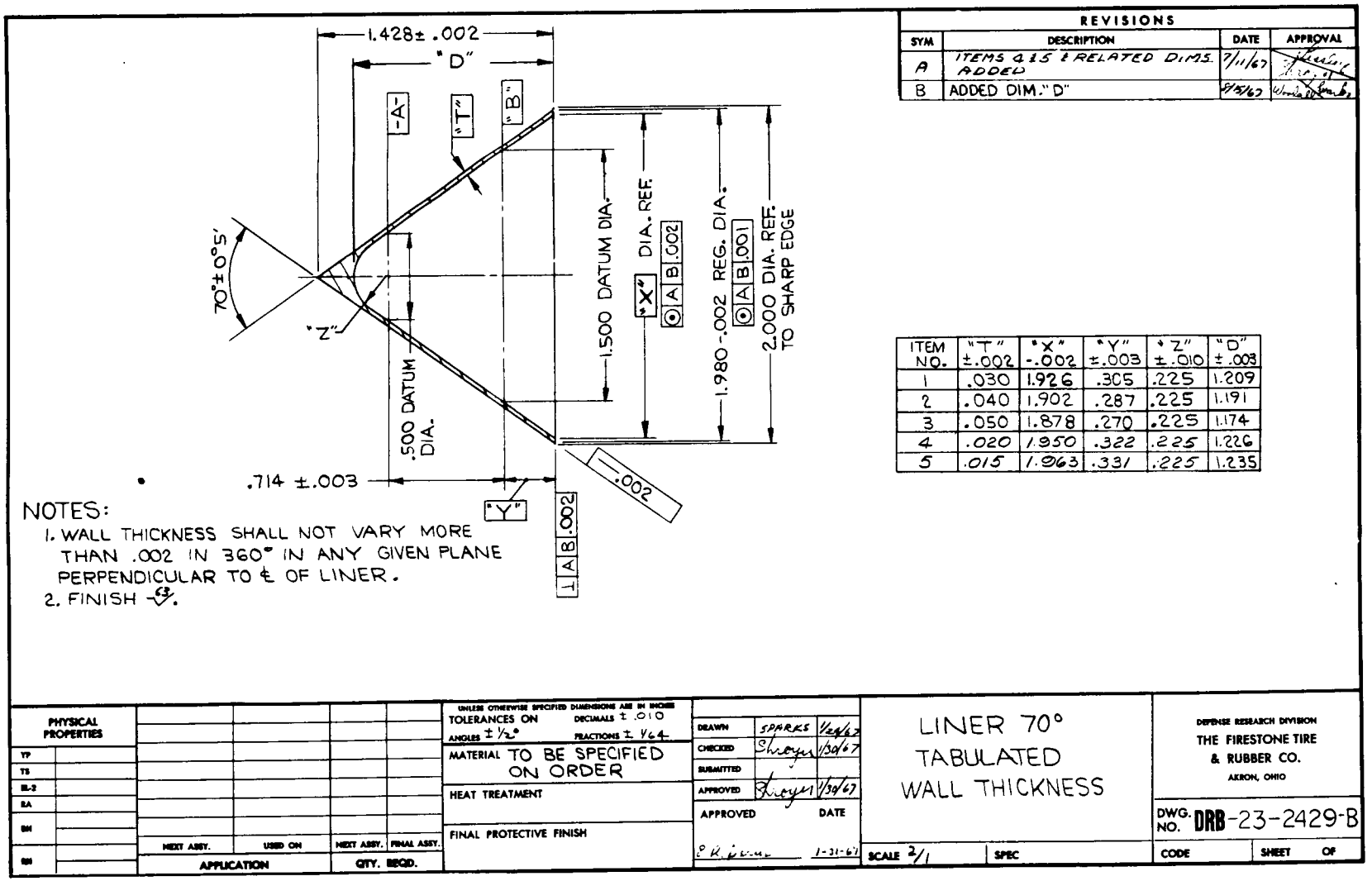

REVISIONS			
SYM	DESCRIPTION	DATE	APPROVAL
A	ITEMS 4 & 5 & RELATED DIMS. ADDED	7/11/67	
B	ADDED DIM. "D"	8/25/67	

ITEM NO.	"T" ±.002	"X" -.002	"Y" ±.003	"Z" ±.010	"D" ±.003
1	.030	1.926	.305	.225	1.209
2	.040	1.902	.287	.225	1.191
3	.050	1.878	.270	.225	1.174
4	.020	1.950	.322	.225	1.226
5	.015	1.963	.331	.225	1.235

PHYSICAL PROPERTIES: YP, TS, EL-2, RA, BH, SH

UNLESS OTHERWISE SPECIFIED DIMENSIONS ARE IN INCHES
TOLERANCES ON ANGLES ± ½° DECIMALS ± .010 FRACTIONS ± 1/64

MATERIAL TO BE SPECIFIED ON ORDER

HEAT TREATMENT

FINAL PROTECTIVE FINISH

DRAWN	SPARKS	1/24/67
CHECKED	Stroyer	1/30/67
SUBMITTED		
APPROVED	Stroyer	1/30/67
APPROVED		DATE
		1-31-67

APPLICATION: NEXT ASSY. | USED ON
QTY. REQD.: NEXT ASSY. | FINAL ASSY.

LINER 70° TABULATED WALL THICKNESS

DEFENSE RESEARCH DIVISION
THE FIRESTONE TIRE & RUBBER CO.
AKRON, OHIO

DWG. NO. DRB-23-2429-B

SCALE 2/1 | SPEC | CODE | SHEET OF

Fig. 16. 70° conical liner design.

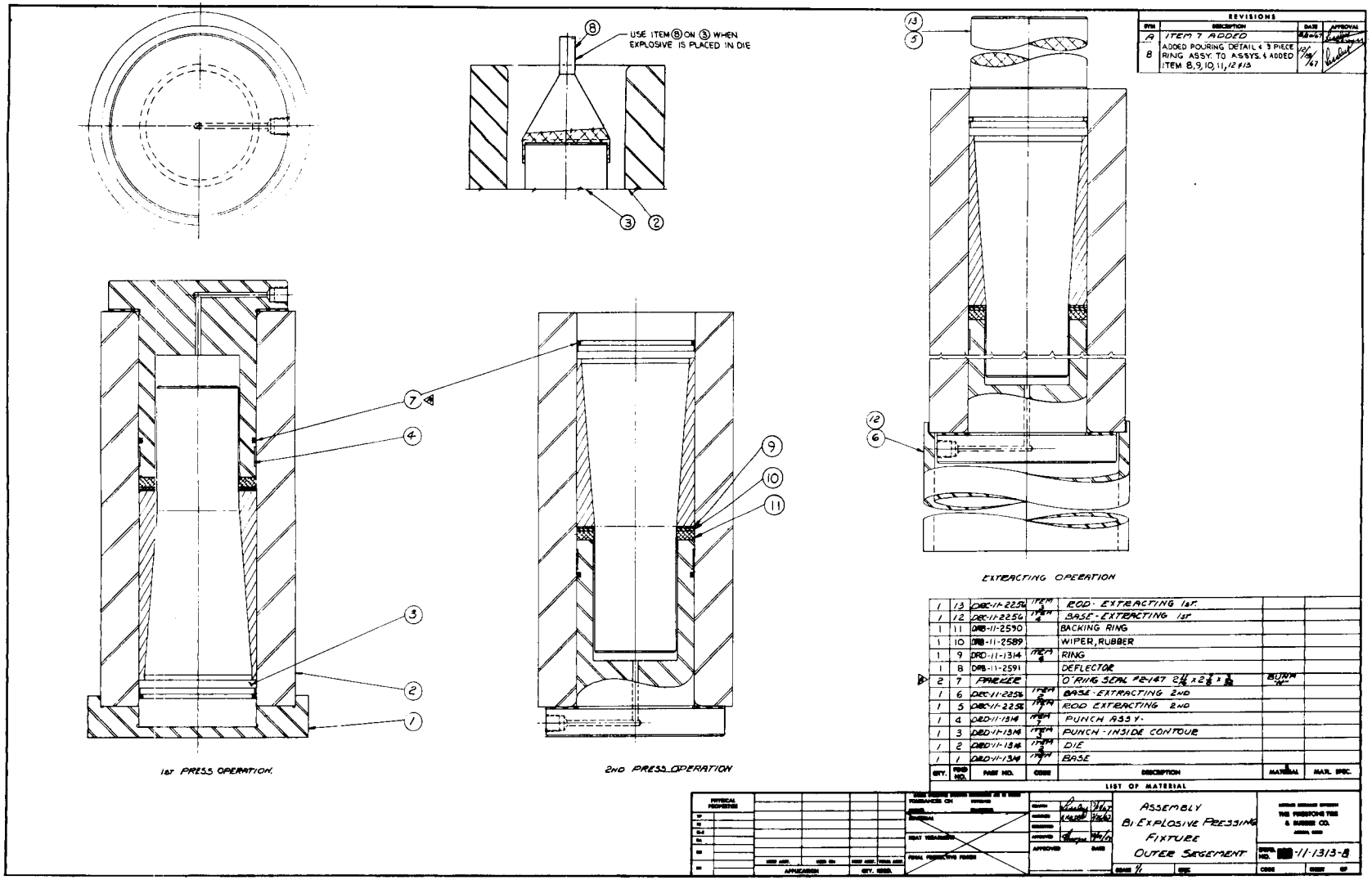

Fig. 17. Press loading fixture used to produce HMX outer sleeves.

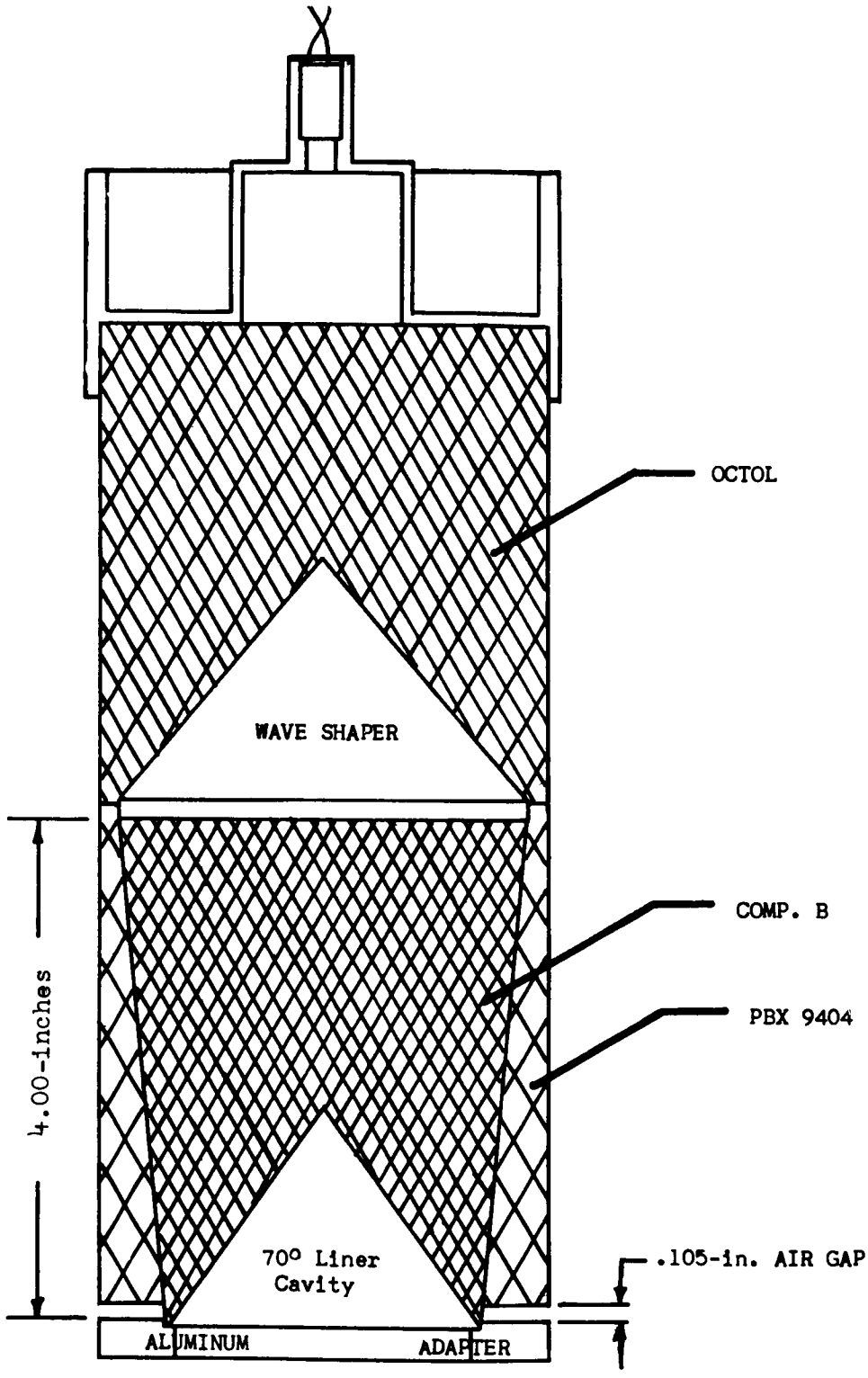

Fig. 18. Sketch of bi-explosive test assembly showing .105-inch air gap at base of pressed PBX9404.

70°, .030-INCH WALL CONICAL LINER (DRB-23-2429B)
EXPLOSIVE: INNER, 75/25 OCTOL; OUTER: PBX 9404
50° BI-EXPLOSIVE LOADING FIXTURE
80° LEAD WAVE SHAPER
ALUMINUM ADAPTOR PLATE

Forma Iron Liner
939-4
Travel: 33-in. (Vacuum)
Velocity: 12.5 km/sec

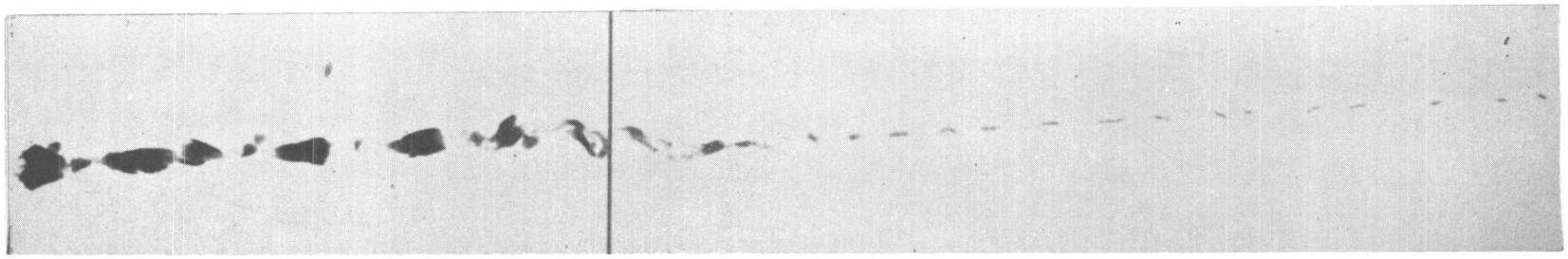

Nickel 200 Liner
939-5
Travel: 33-in. (Vacuum)
Velocity: 11.9 km/sec

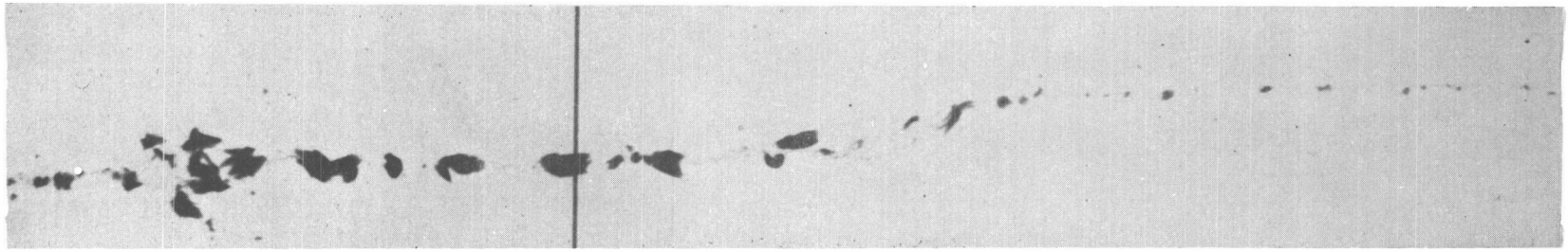

Scale in Inches
0 1 2

Direction of Travel ⟶

Fig. 19. Comparison of iron and nickel jets produced by 70°, .030-inch wall conical liners using octol/PBX9404 bi-explosive charges.

70°,.030-INCH WALL CONICAL FORMA IRON LINER DWG. DRB-23-2429B It.1
50° BI-EXPLOSIVE LOADING FIXTURE
80° LEAD WAVE SHAPER
ALUMINUM ADAPTOR PLATE

Explosive:
Inner: 60/40 Comp. B
Outer: PBX 9404
939-1
Travel: 2, 28-in. (Air)
Velocity: 12.2 km/sec

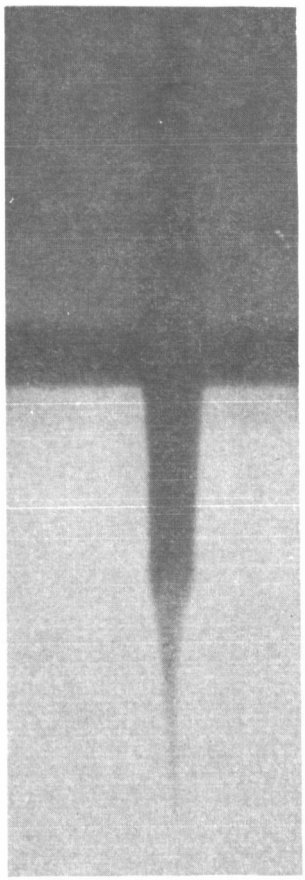

Scale in inches
0 1 2

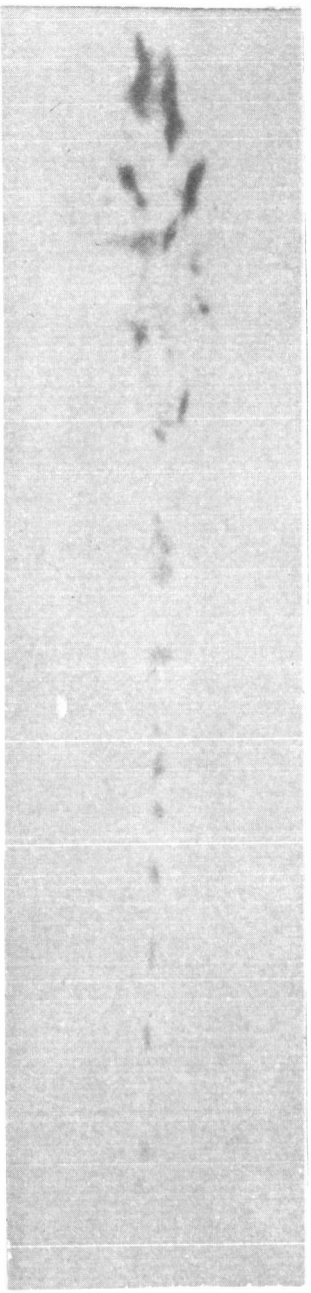

Fig. 20. Jet produced by 70°, .030-inch wall conical liner using comp.B/PBX9404 bi-explosive charge.

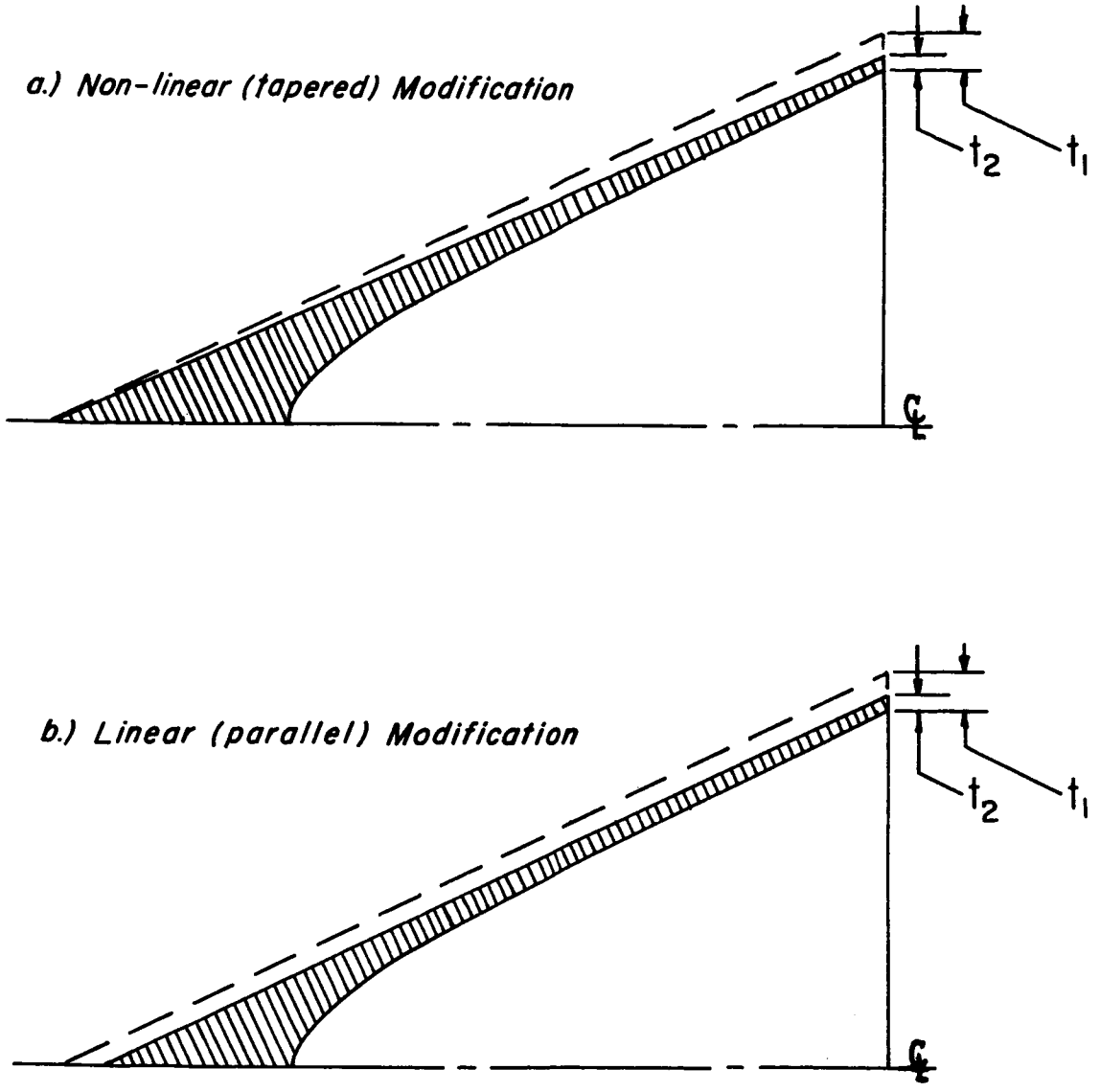

$t_1 \equiv$ the wall thickness (at base) for a constant cross-sectional area liner

$t_2 \equiv$ the wall thickness (at base) for a modified liner

Fig. 21. Sketches of the two types of modifications made on the constant cross-sectional area liner design.

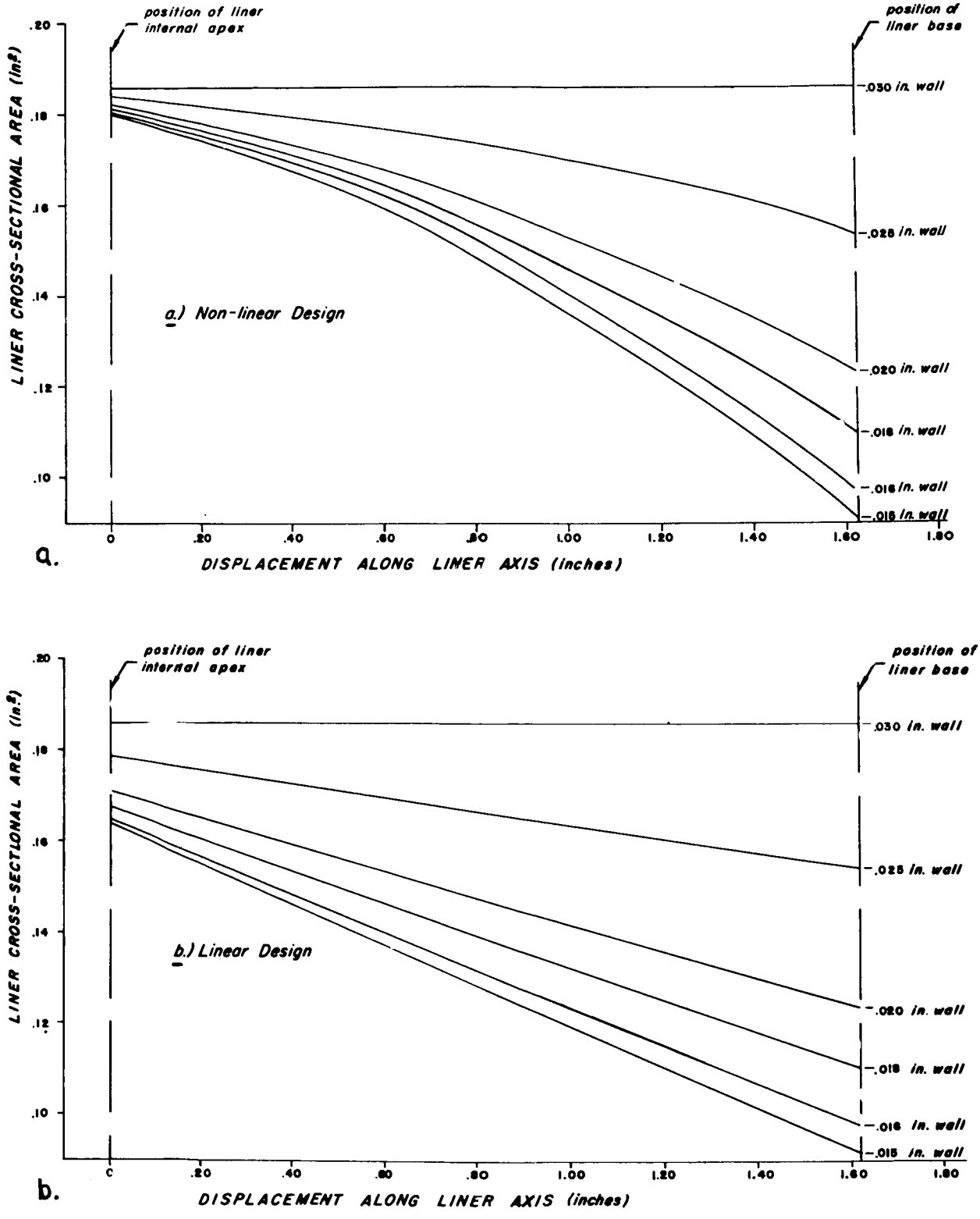

Fig. 22. Variation in cross-sectional area for the linear and non-linear liner modifications versus displacement along liner axis.

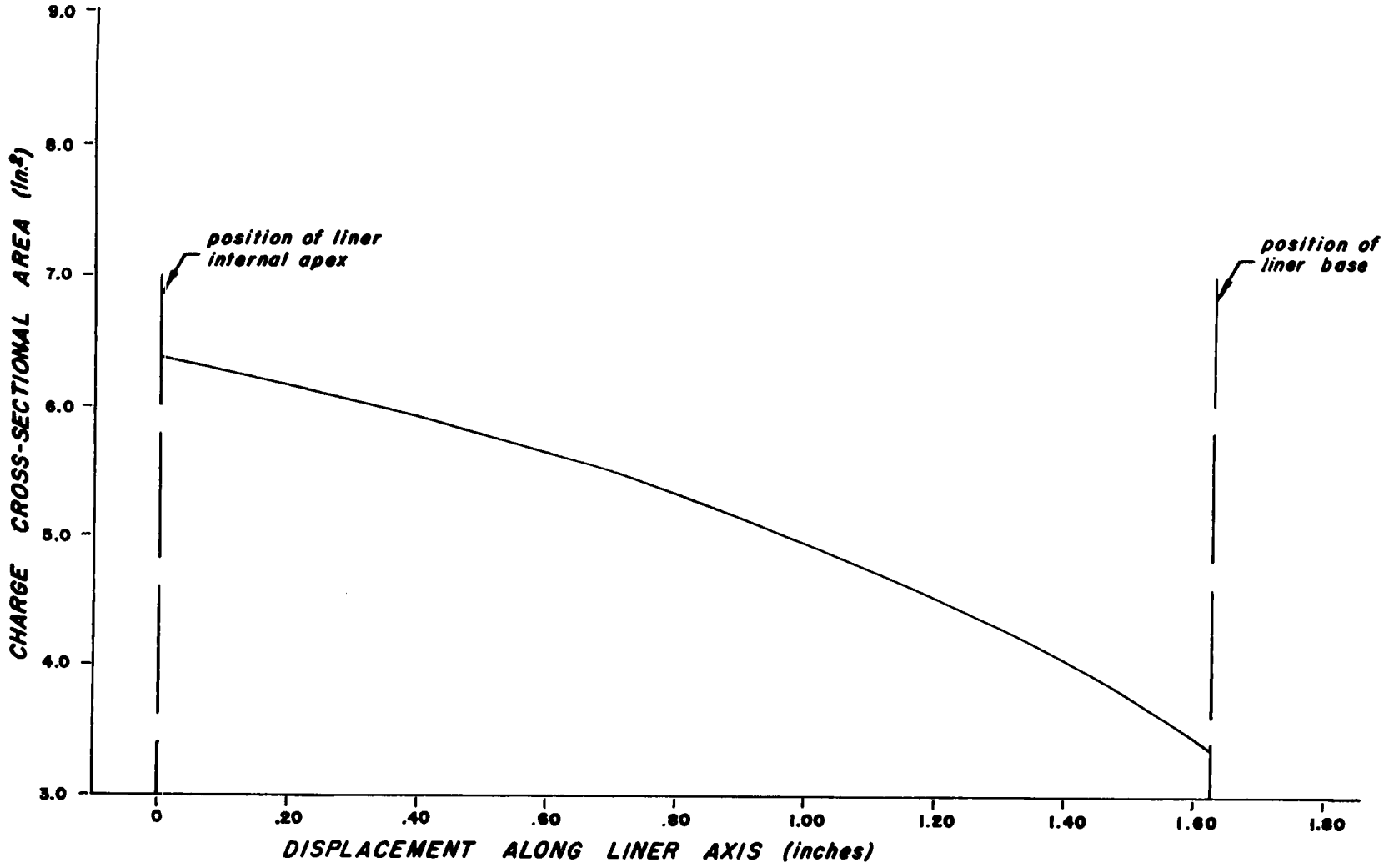

Fig. 23. Variation in cross-sectional area for the bi-explosive charge versus displacement along liner axis.

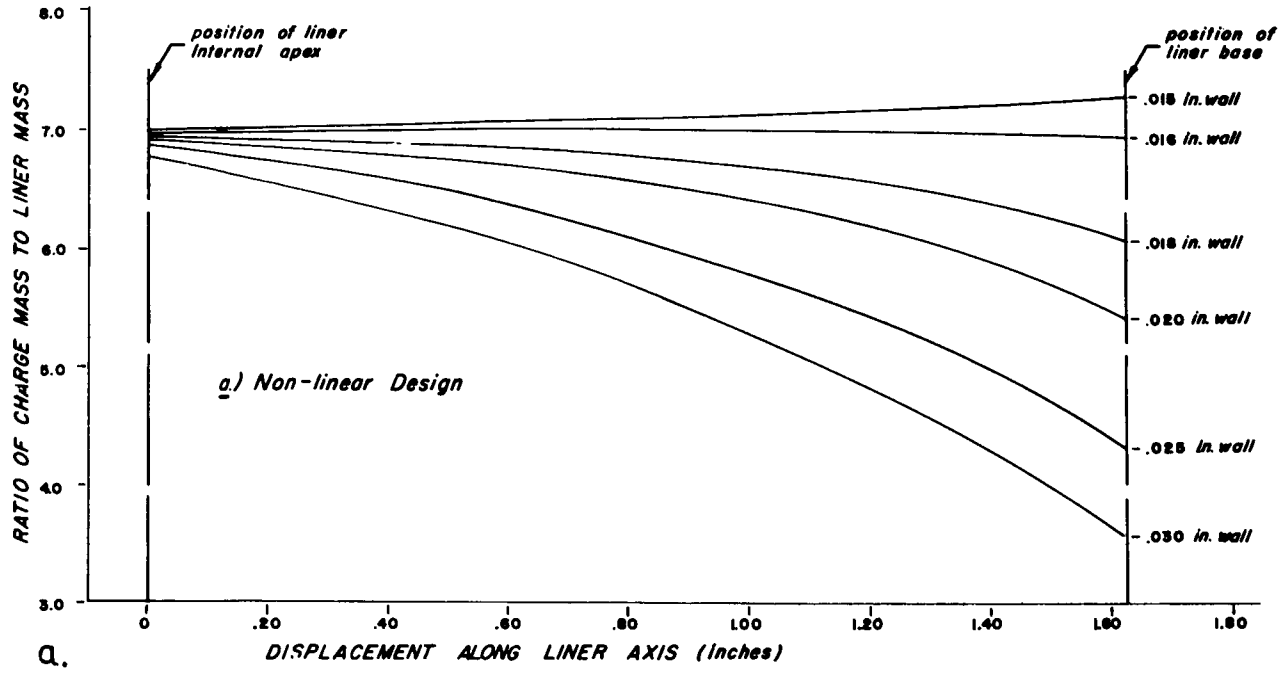

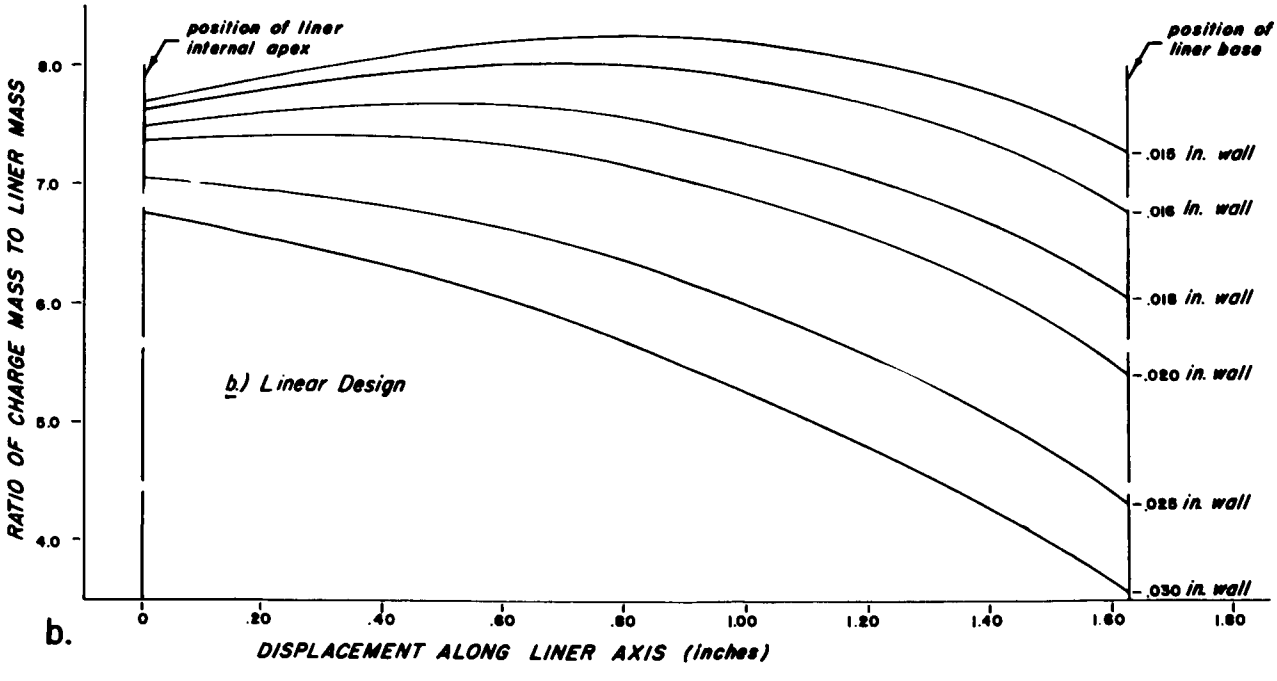

Fig. 24. Variation in C/M for bi-explosive systems using linear and non-linear designs versus displacement along liner axis.

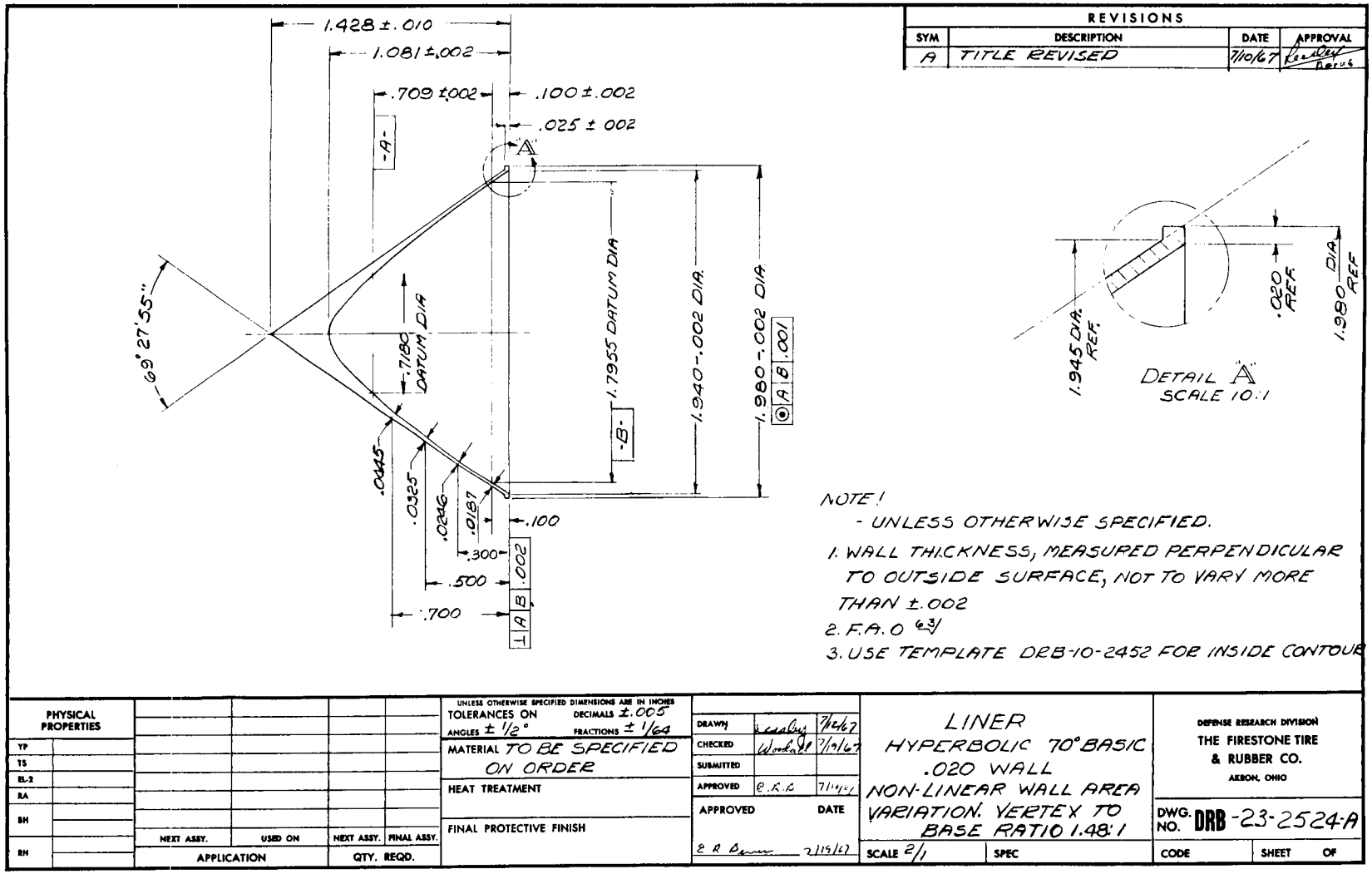

Fig. 25. 70°, .020-inch non-linear liner design (ratio: 1.48:1).

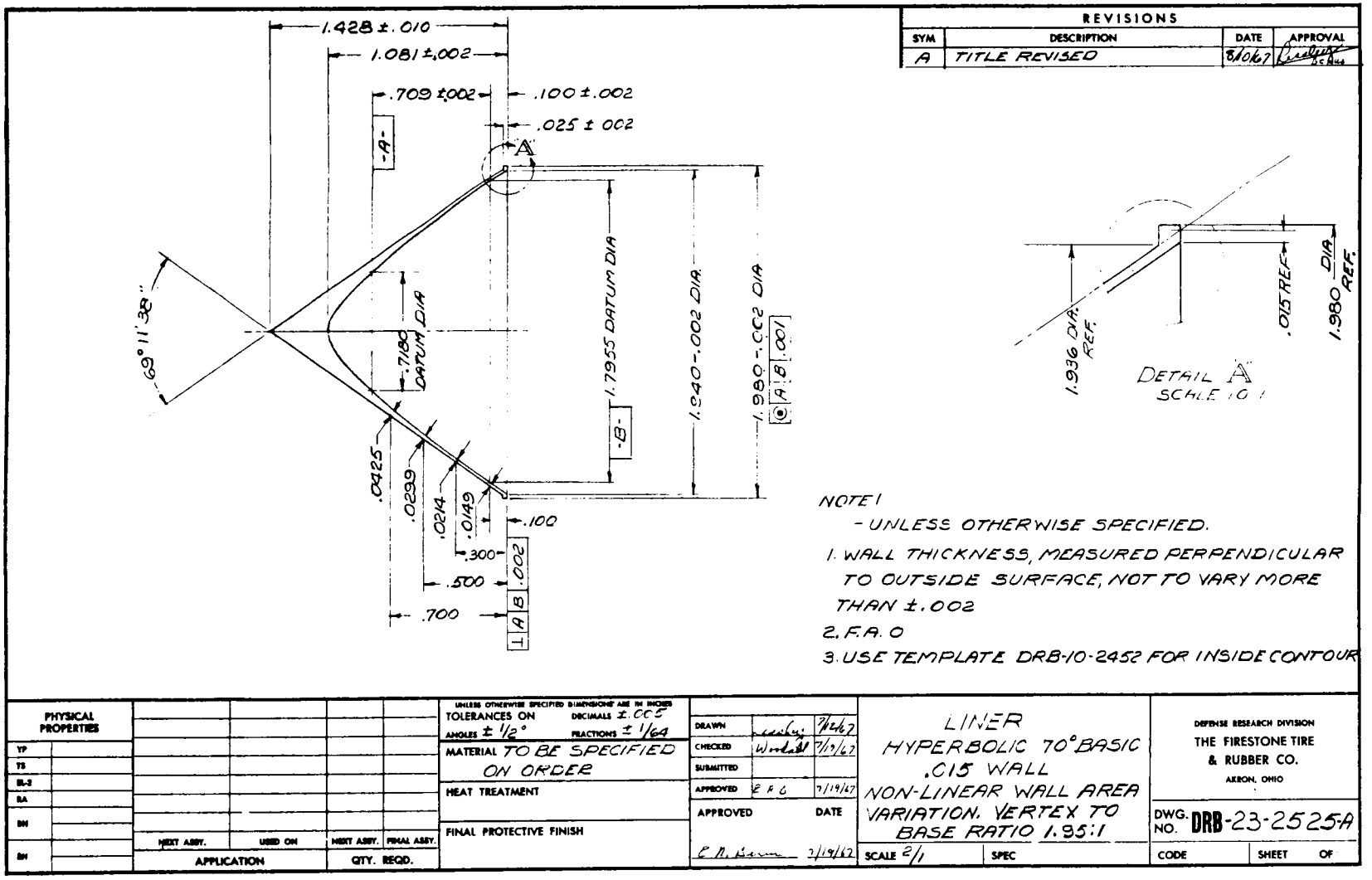

Fig. 26. 70°, .015-inch non-linear liner design (ratio: 1.95:1).

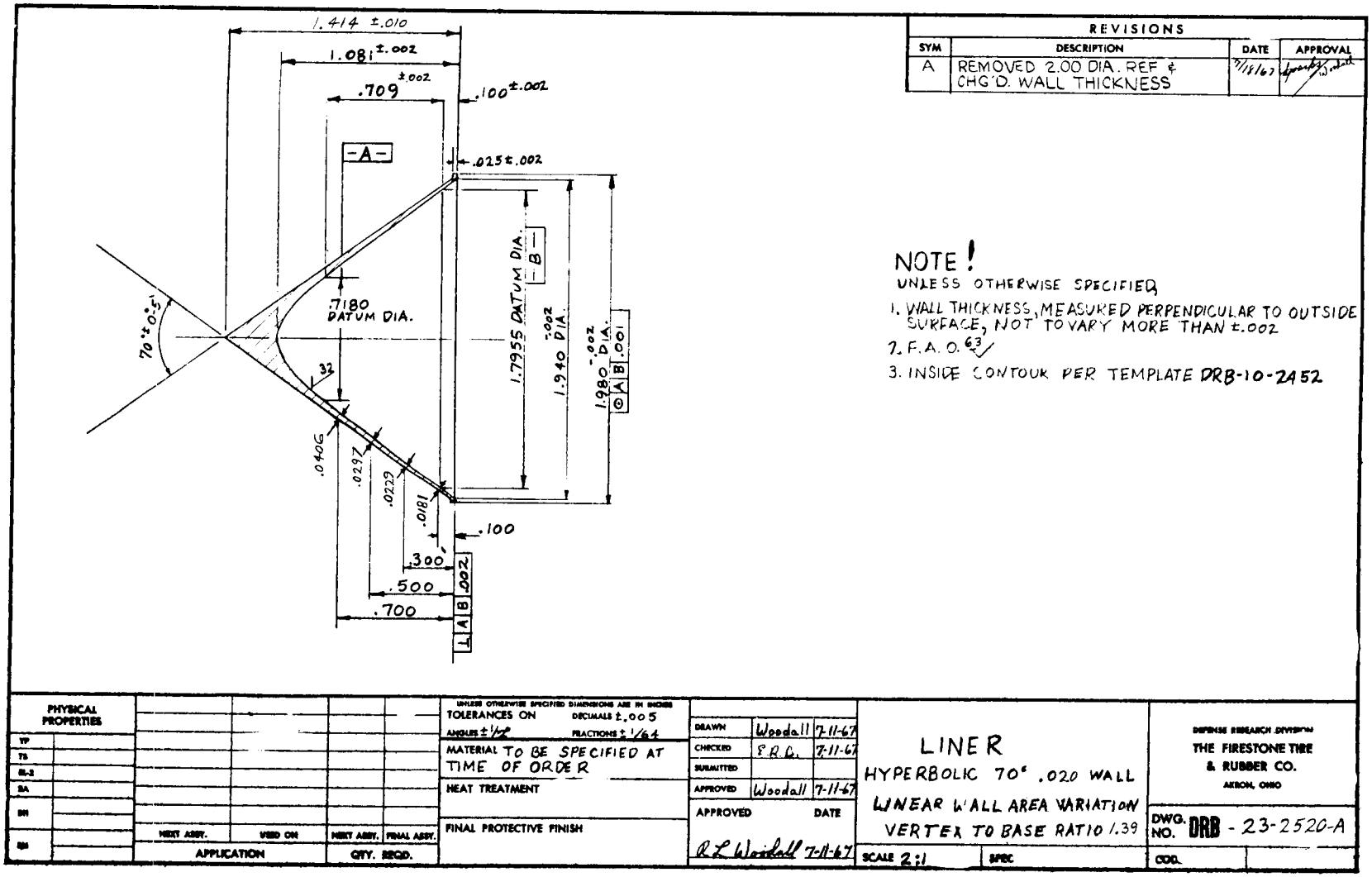

Fig. 27. 70°, .020-inch linear liner design (ratio: 1.39:1).

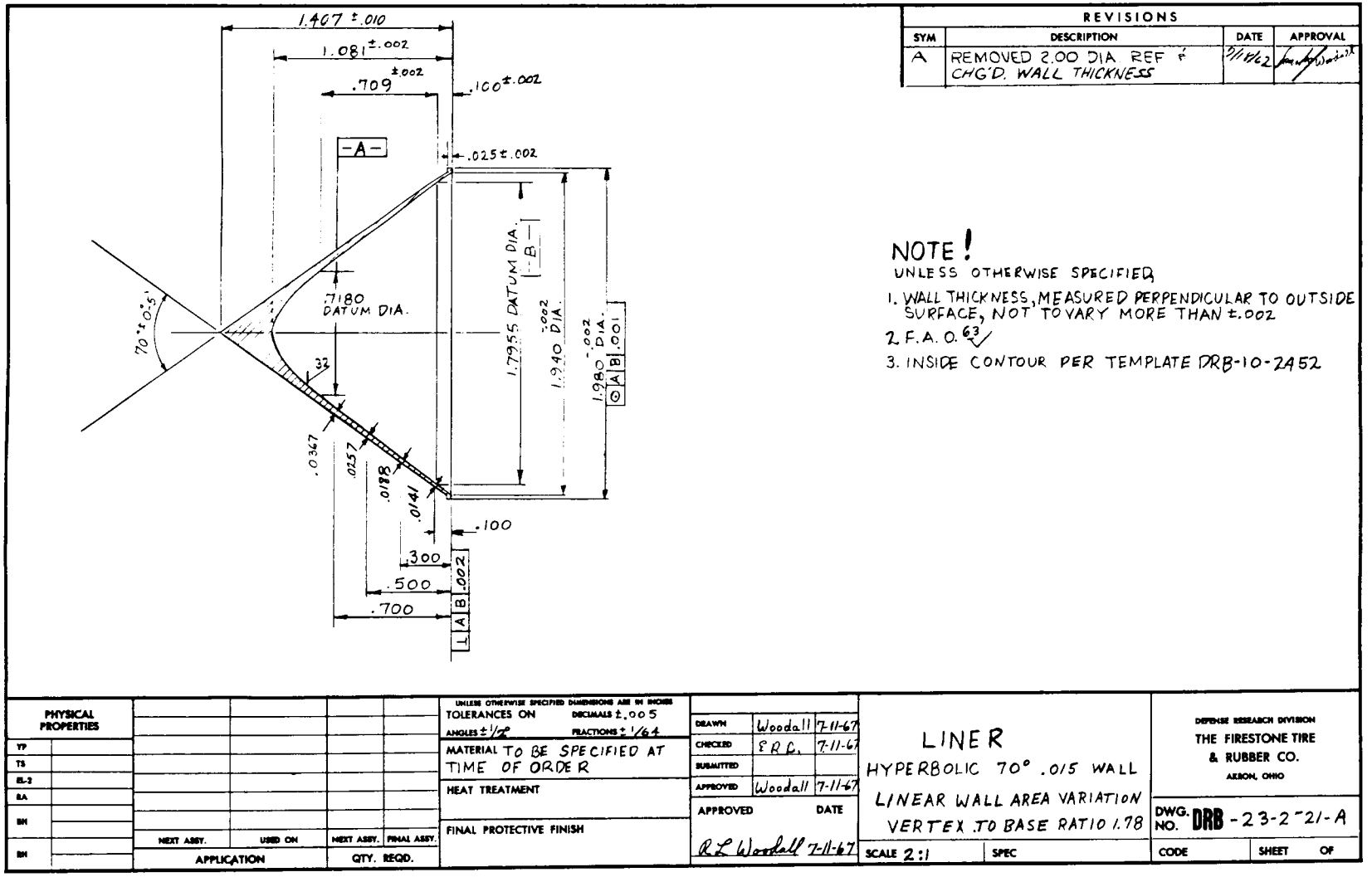

REVISIONS			
SYM	DESCRIPTION	DATE	APPROVAL
A	REMOVED 2.00 DIA REF & CHG'D. WALL THICKNESS	7/11/62	

NOTE!
UNLESS OTHERWISE SPECIFIED
1. WALL THICKNESS, MEASURED PERPENDICULAR TO OUTSIDE SURFACE, NOT TO VARY MORE THAN ±.002
2. F.A.O. 63
3. INSIDE CONTOUR PER TEMPLATE DRB-10-2452

PHYSICAL PROPERTIES	
YP	
TS	
EL-2	
RA	
BH	
BH	

NEXT ASSY.	USED ON	NEXT ASSY.	FINAL ASSY.
APPLICATION		QTY. REQD.	

UNLESS OTHERWISE SPECIFIED DIMENSIONS ARE IN INCHES
TOLERANCES ON DECIMALS ±.005
ANGLES ±½° FRACTIONS ± 1/64
MATERIAL TO BE SPECIFIED AT TIME OF ORDER
HEAT TREATMENT
FINAL PROTECTIVE FINISH

DRAWN	Woodall	7-11-67
CHECKED	E.R.L.	7-11-67
SUBMITTED		
APPROVED	Woodall	7-11-67

APPROVED DATE
R L Woodall 7-11-67

LINER
HYPERBOLIC 70° .015 WALL
LINEAR WALL AREA VARIATION
VERTEX TO BASE RATIO 1.78

SCALE 2:1 | SPEC

DEFENSE RESEARCH DIVISION
THE FIRESTONE TIRE & RUBBER CO.
AKRON, OHIO

DWG. NO. DRB-23-2-21-A
CODE | SHEET OF

Fig. 28. 70°, .015-inch linear liner design (ratio: 1.78:1).

70°, .020-INCH WALL FORMA IRON HYPERBOLIC LINER
EXPLOSIVE: INNER, 60/40 COMP. B; OUTER, 75/25 OCTOL
50° BI-EXPLOSIVE LOADING FIXTURE
80° LEAD WAVE SHAPER
ALUMINUM ADAPTER PLATE

Non-Linear Liner (DRB-23-2524)
946-1
Travels: 2, 10-inches (air)
Velocity: 10.47 km/sec

Linear Liner (DRB-23-2520A)
946-3
Travels: 1, 8-inches (air)
Velocity: 10.65 km/sec

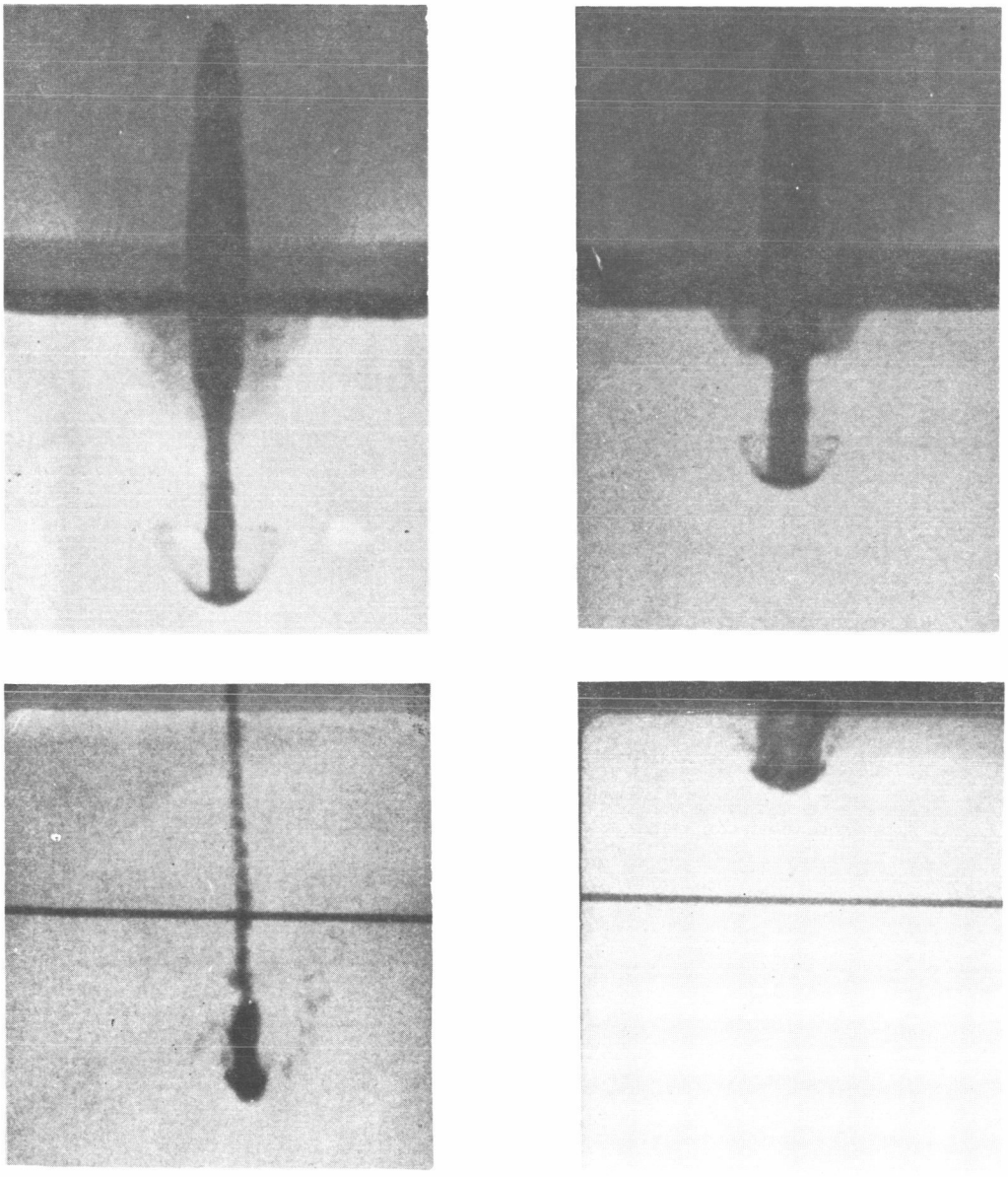

Fig. 29. Comparison of jets produced by linear and non-linear liner designs in bi-explosive systems.

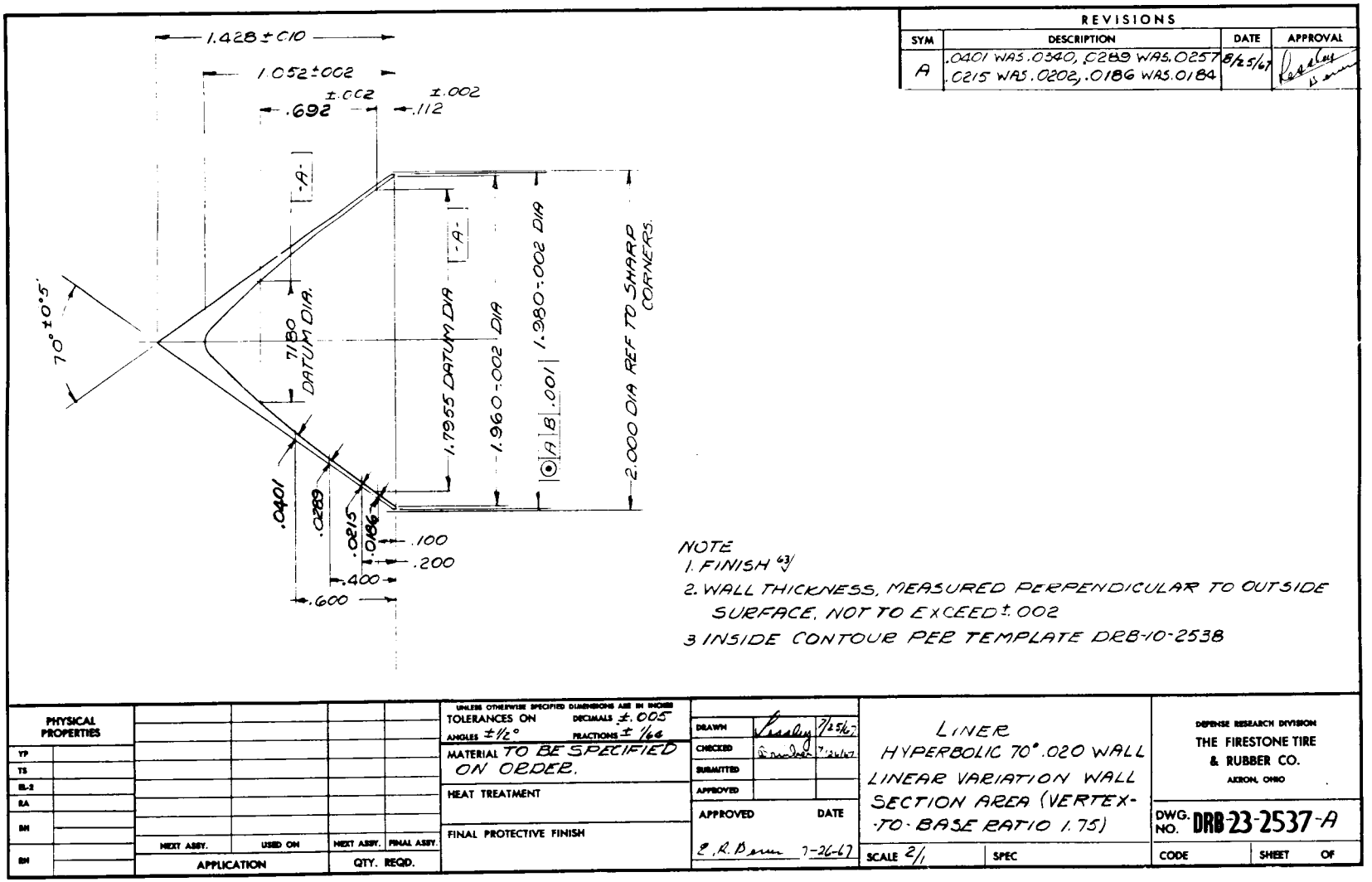

Fig. 30. 70°, .020-inch linear liner design (ratio: 1.75:1).

70°.,020-INCH WALL HYPERBOLIC FERROVAC IRON LINER DRB-23-2537A
50° BI-EXPLOSIVE LOADING FIXTURE
43° RIGID POLYURETHANE FOAM WAVE SHAPER
ALUMINUM ADAPTOR PLATE

Explosive:
Inner: 60/40 Comp. B
Outer: 75/25 Octol
974-1
Travel: 2,10-in. (Air)
Velocity: 10.26 km/sec

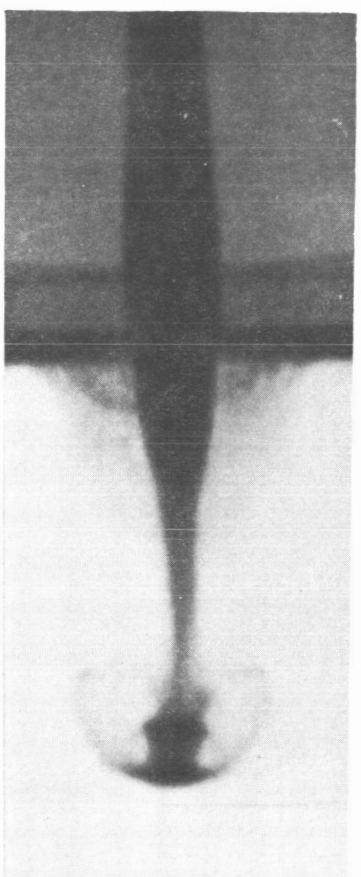

Scale in inches

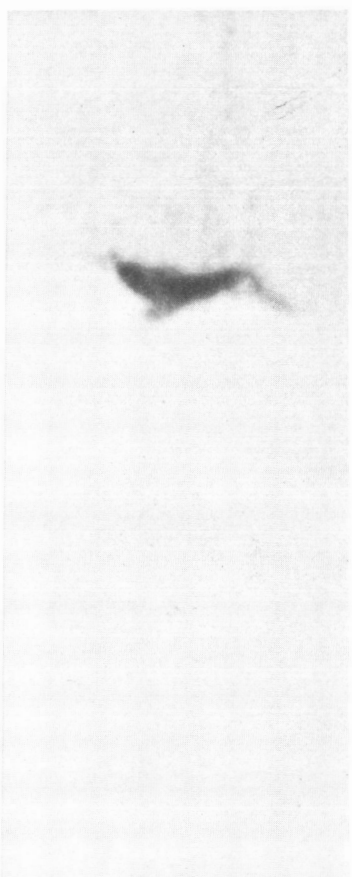

Fig. 31. Jet produced by 70°, .020-inch linear liner design (ratio: 1.75:1).

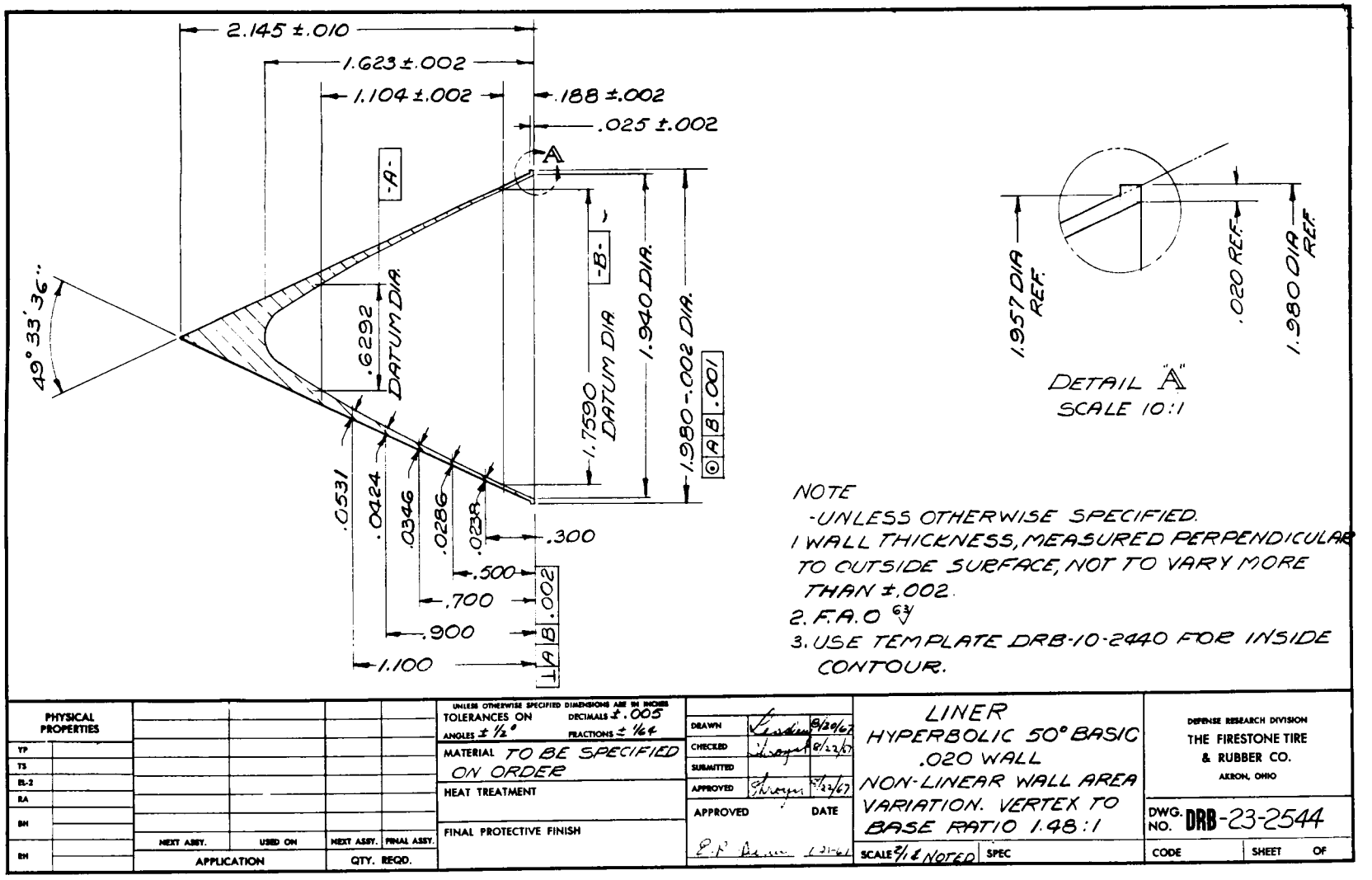

Fig. 32. 50°, .020-inch non-linear liner design (ratio: 1.48:1).

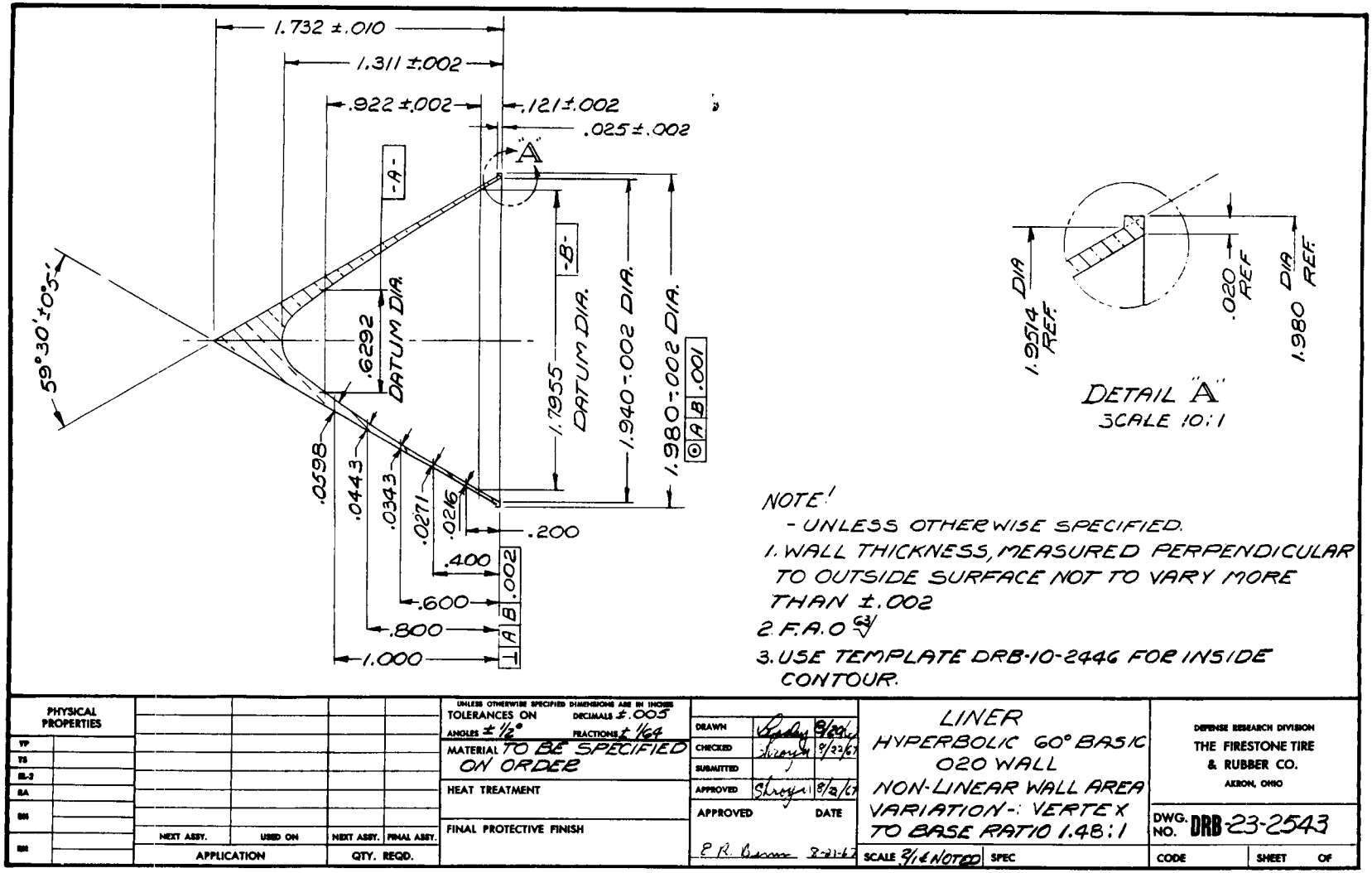

Fig. 33. 60°, .020-inch non-linear liner design (ratio: 1.48:1).

ELECTRON BEAM MELTED (EBM) IRON HYPERBOLIC LINER
EXPLOSIVE: INNER, 60/40 COMP. B; OUTER, 75/25 OCTOL
50° BI-EXPLOSIVE LOADING FIXTURE
80° LEAD WAVE SHAPER
ALUMINUM ADAPTER PLATE

70°, .020-in. Wall Liner
Dwg. DRB-23-2524A
965-2
Travel: 32-in.(vacuum)
Velocity: 10.54 km/sec

60°,.020-in. Wall Liner
Dwg. DRB-23-2543
965-9
Travel: 33-in. (vacuum)
Velocity: 11.02 km/sec

50°,.020-in. Wall Liner
Dwg. DRB-23-2544
965-11
Travel: 32-in. (vacuum)
Velocity: 11.43 km/sec

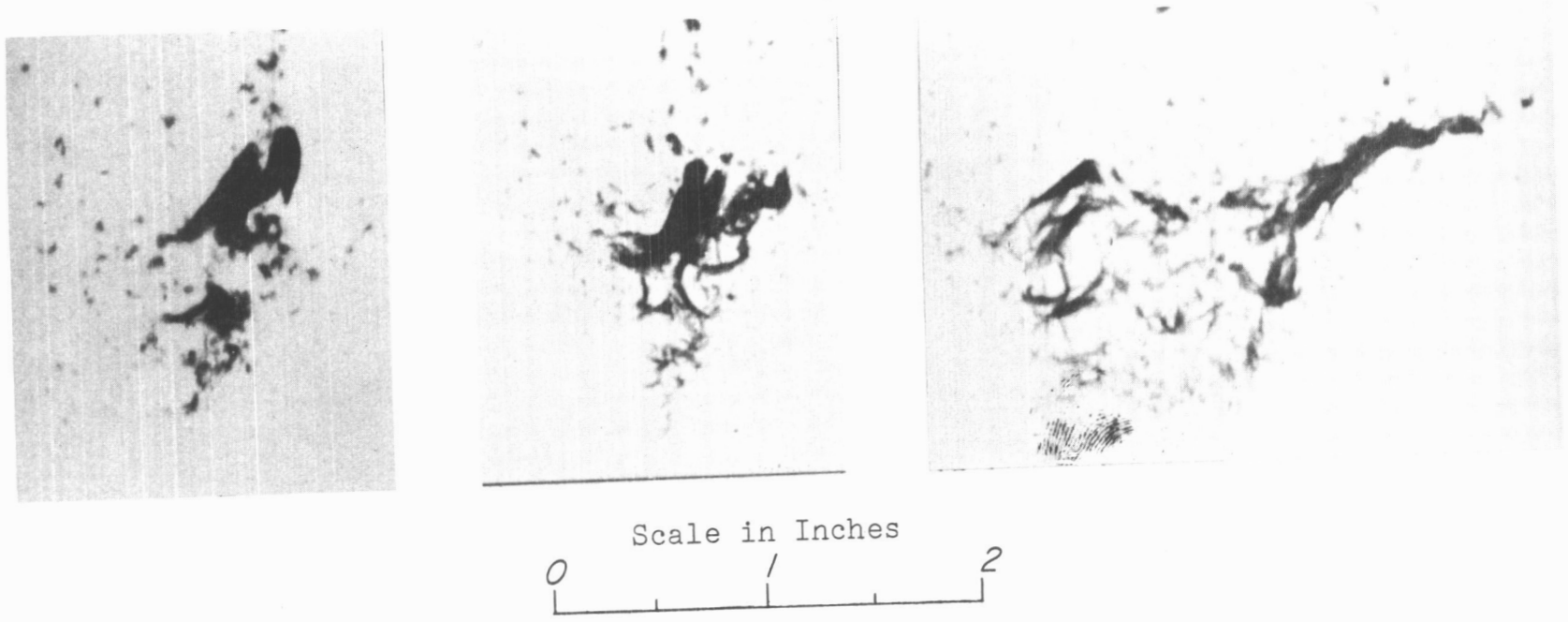

Fig. 34. Comparison of jets produced by 50°, 60°, and 70° electron beam melted hyperbolic liners.

HYPERBOLIC EXPLOSIVE VARIATION TESTS
60°, .020-inch WALL EBM IRON LINER DWG. DRB-23-2543
50° BI-EXPLOSIVE LOADING FIXTURE
80° LEAD WAVE SHAPER - ALUMINUM ADAPTOR PLATE

Explosive:
Inner: 60/40 comp.B
Outer 75/25 octol
965-9
Travel: 33-in. (vacuum)
Velocity: 11.02 km/sec

Explosive:
Inner: 75/25 octol
Outer: PBX 9404
965-8
Travel: 33-in. (vacuum)
Velocity: 11.52 km/sec

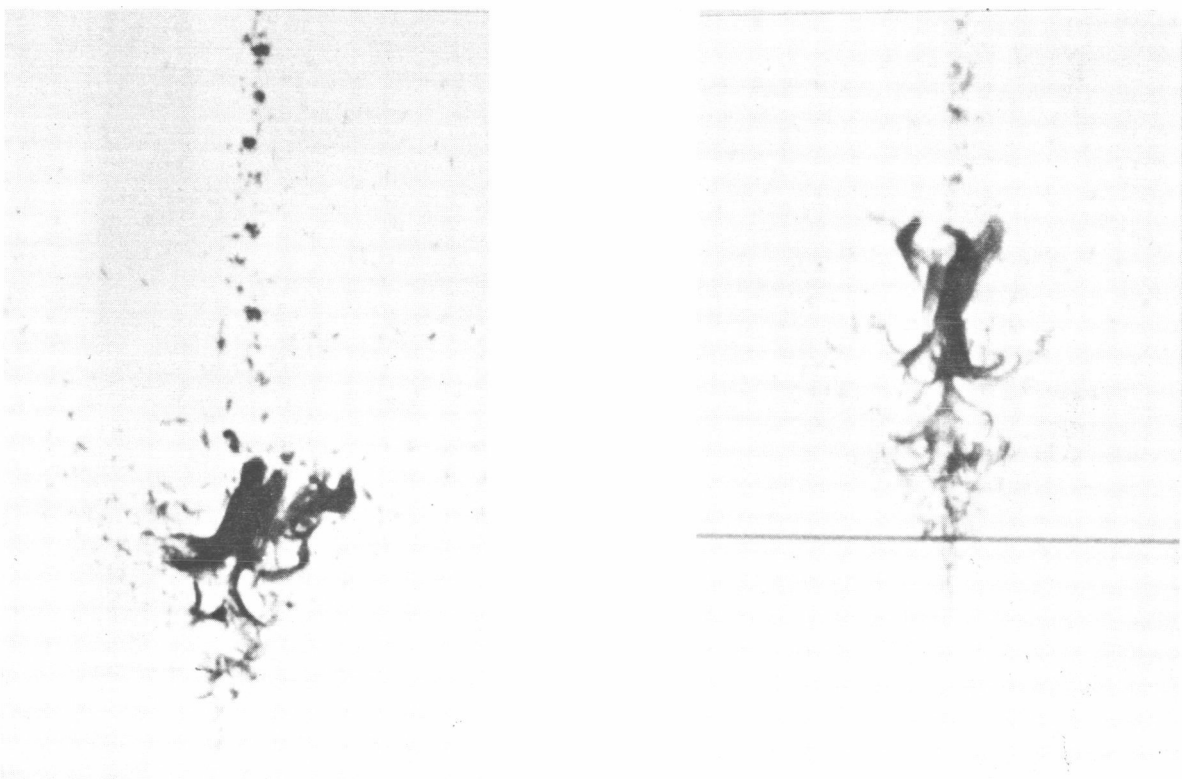

Scale in Inches

Fig. 35. Comparison of jets produced using comp.B/octol and octol/PBX9404 bi-explosive charges.

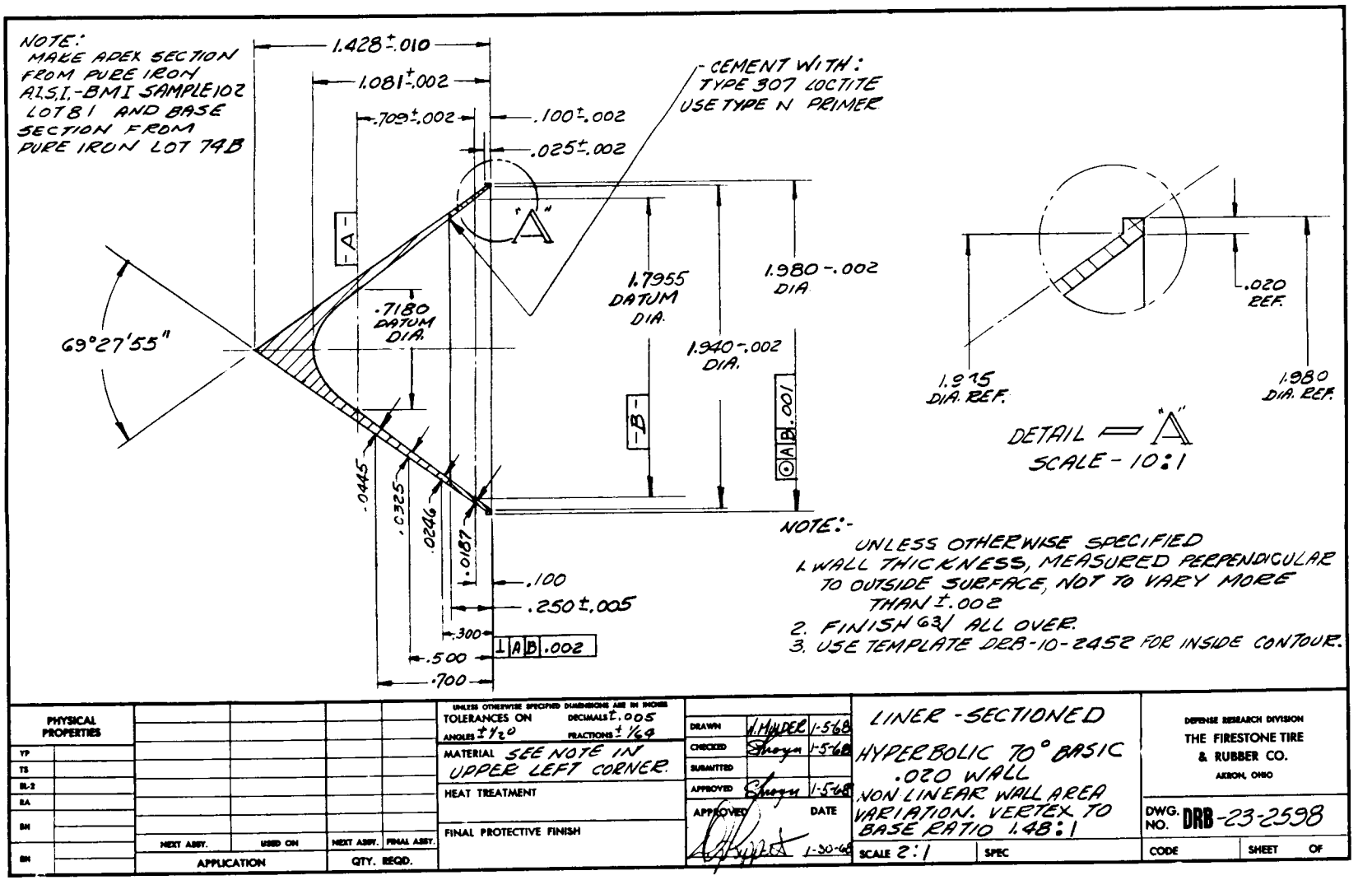

Fig. 36. Sectioned 70°, .020-inch liner used to test the battelle pure iron.

70°,.020-INCH WALL SECTIONED HYPERBOLIC LINER DRB-23-2598
BASE (1/4-INCH) SECTION MATERIAL: EBM IRON
EXPLOSIVE: INNER, 75/25 OCTOL; OUTER, HMX
50° BI-EXPLOSIVE LOADING FIXTURE
43° RIGID POLYURETHANE FOAM WAVE SHAPER
ALUMINUM ADAPTER PLATE

Main(Upper)Section Material:
EBM Iron
975-1
Travel: 35-in. (Vacuum)
Velocity: 11.33 km/sec

Main(Upper)Section Material:
Battelle Pure Iron
975-2
Travel: 32-in. (Vacuum)
Velocity: 10.94 km/sec

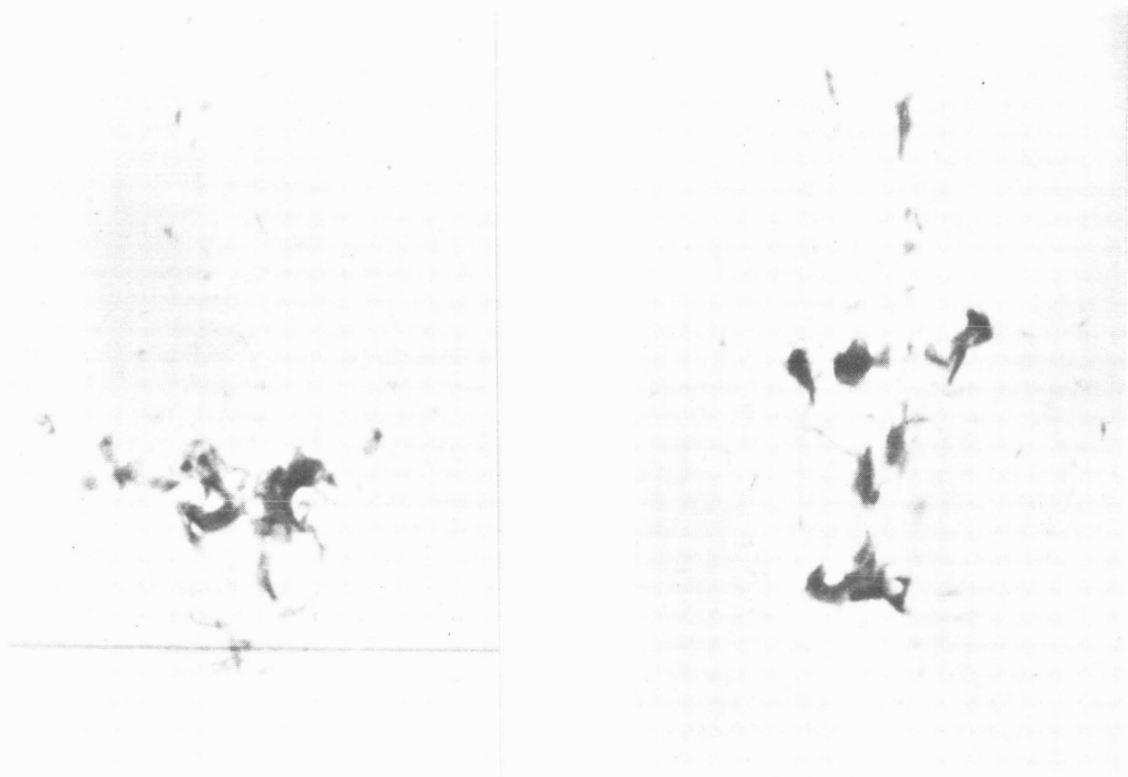

Scale in inches
0 1 2

Fig. 37. Comparison of jets produced by sectioned liners using Battelle pure iron and electron beam melted iron.

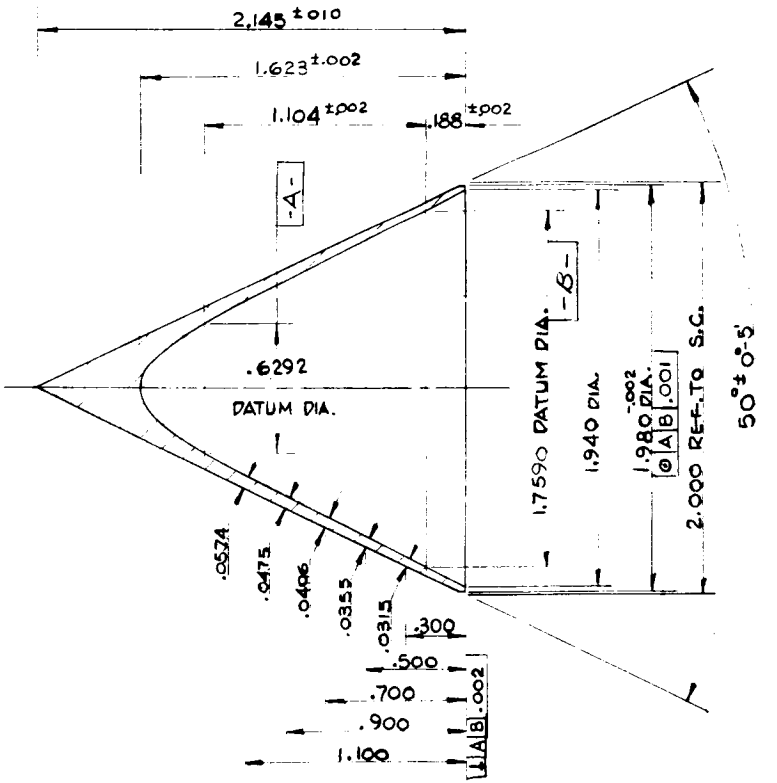

REVISIONS			
SYM	DESCRIPTION	DATE	APPROVAL

NOTE ! UNLESS OTHERWISE SPECIFIED,

1. WALL THICKNESS, MEASURED PERPENDICULAR TO OUTSIDE SURFACE, **NOT** TO VARY MORE THAN ±.002
2. F.A.O. 63 ✓
3. INSIDE CONTOUR PER TEMPLATE DRB-10-2440

PHYSICAL PROPERTIES					
YP					
TS					
EL-2					
EA					
BH					
BH					
	NEXT ASSY.	USED ON	NEXT ASSY.	FINAL ASSY.	
	APPLICATION		QTY. REQD.		

UNLESS OTHERWISE SPECIFIED DIMENSIONS ARE IN INCHES
TOLERANCES ON DECIMALS ± .005
ANGLES ± ½° FRACTIONS ± 1/64

MATERIAL TO BE SPECIFIED AT TIME OF ORDER

HEAT TREATMENT

FINAL PROTECTIVE FINISH

DRAWN	ROG	2-8-67
CHECKED	Kirby	4/21/67
SUBMITTED		
APPROVED	[illegible]	4/21/67
APPROVED	DATE	
E. R. Bean	3/1/67	

LINER
HYPERBOLIC .030 WALL 50°

SCALE 2:1 | SPEC

DEFENSE RESEARCH DIVISION
THE FIRESTONE TIRE & RUBBER CO.
AKRON, OHIO

DWG. NO. DRB-23-2439

CODE | SHEET | OF

Fig. 38. 50°, .030-inch wall hyperbolic liner design.

50° NICKEL 270 HYPERBOLIC LINER
EXPLOSIVE: INNER, 60/40 COMP. B; OUTER, 75/25 OCTOL
50° BI-EXPLOSIVE LOADING FIXTURE

.030-in.Wall(DRB-23-2439)	.020-in. Wall(DBR-23-2544)	.020-in.Wall (DRB-23-2544)
80° Lead Wave Shaper	80° Lead Wave Shaper	43° Polyurethane Wave Shaper
Aluminum Adapter Plate	Aluminum Adapter Plate	Steel Adapter Plate
950-1	950-2	973-2
Travel: 25-in. Air	Travel: 32-in.(vacuum)	Travel: 31-in. (vacuum)
Velocity: 10.51 km/sec	Velocity: 11.19 km/sec	Velocity: 11.25 km/sec

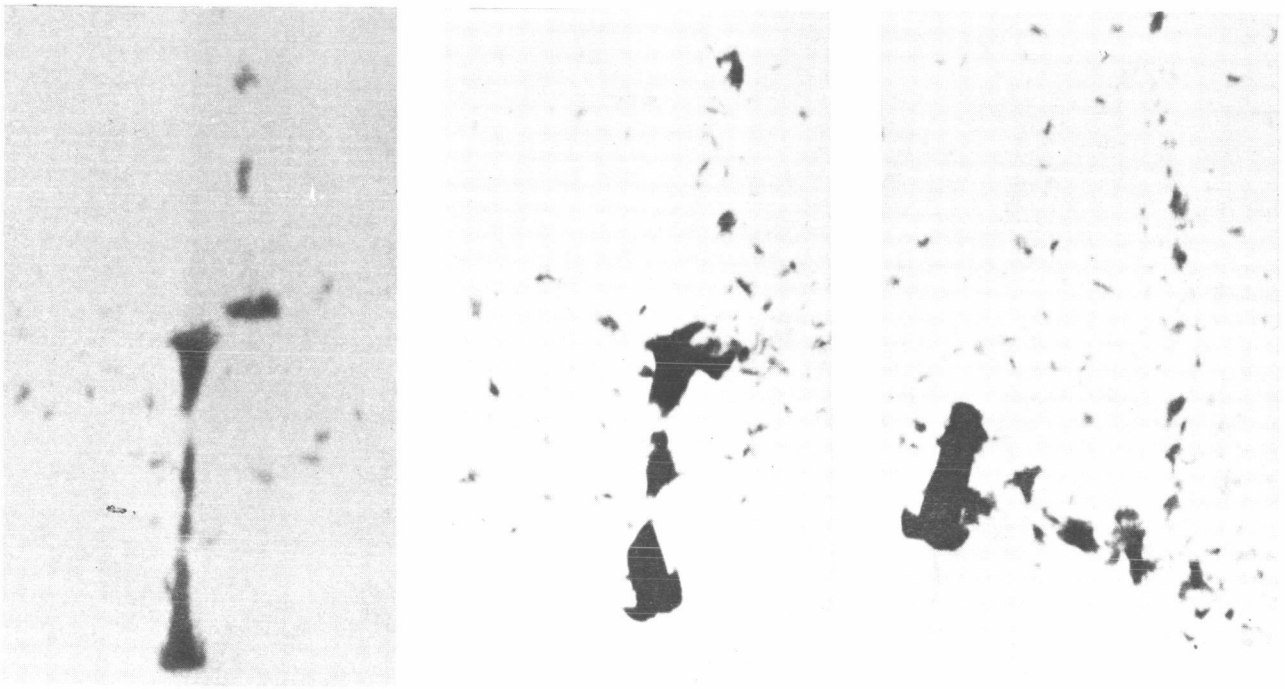

Fig. 39. Improvement of nickel jet by various design charges.

HYPERBOLIC EXPLOSIVE VARIATION TESTS
50°, .020-INCH WALL NICKEL 270 LINER DWG. DRB-23-2544
50° BI-EXPLOSIVE LOADING FIXTURE
80° LEAD WAVE SHAPER
ALUMINUM ADAPTER PLATE

Explosive:
Inner: 60/40 Comp. B
Outer: 75/25 Octol
950-2
Travel: 32-in.(vacuum)
Velocity: 11.19 km/sec

Explosive:
Inner: 75/25 Octol
Outer: HMX
950-3
Travel: 31-in.(vacuum)
Velocity: 11.77 km/sec

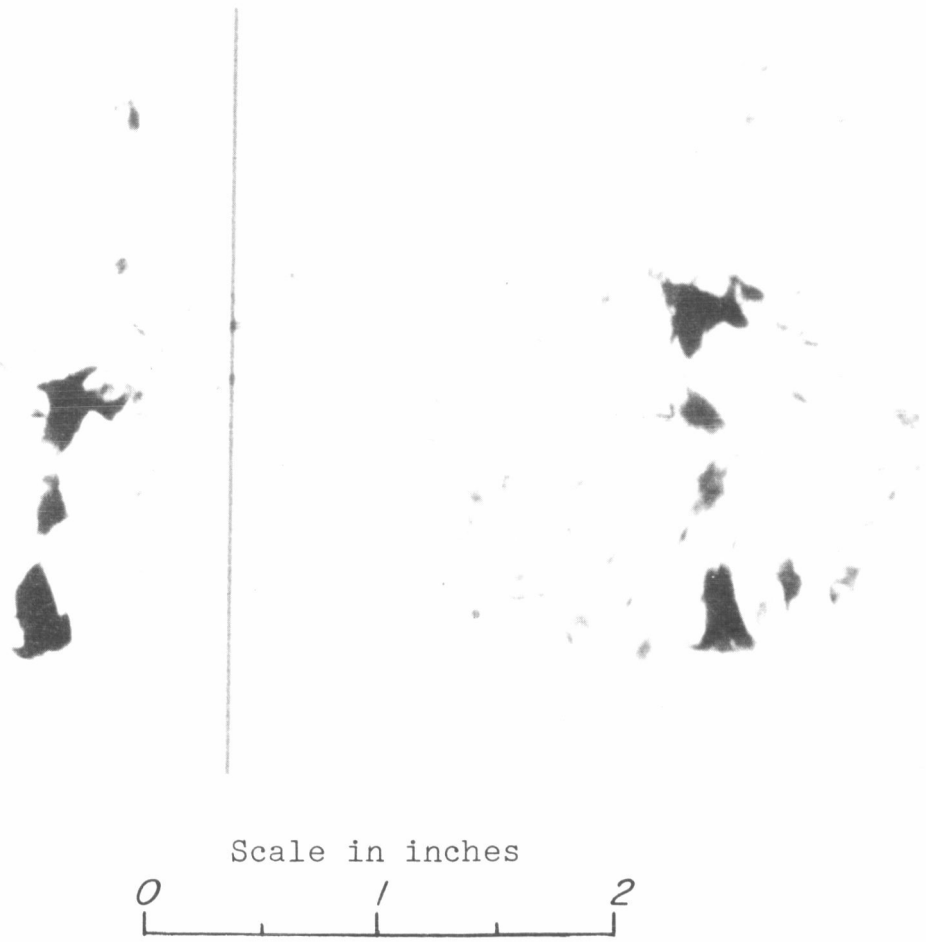

Fig. 40. Comparison of nickel jets produced using comp.B/ octol and octol/HMX bi-explosive charges.

50°, .020-INCH WALL NICKEL 270 LINER DWG. DRB-23-2544
EXPLOSIVE: INNER, 60/40 COMP. B; OUTER 75/25 OCTOL
50° BI-EXPLOSIVE LOADING FIXTURE
43° POLYURETHANE WAVE SHAPER
STEEL ADAPTER PLATE

973-2
Travel: 31-in.(vacuum)
Velocity: 11.25 km/sec

973-3
Travel: 33-in.(vacuum)
Velocity: 11.25 km/sec

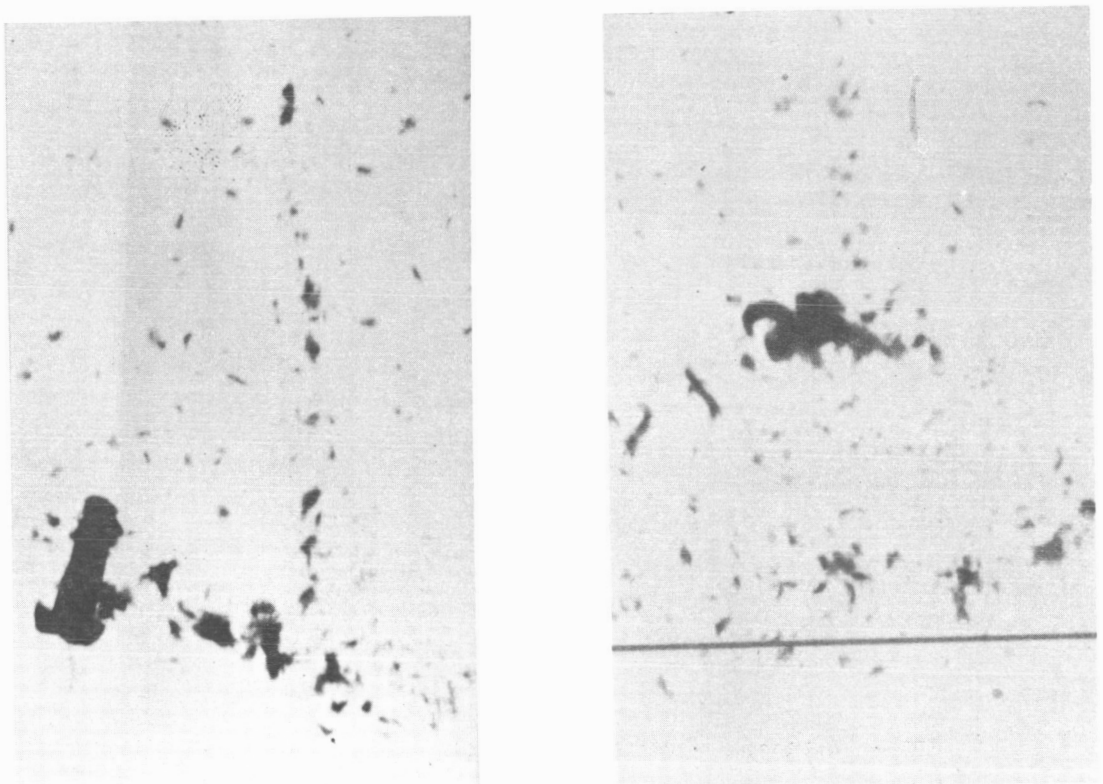

Fig. 41. Comparison of two nickel jets produced by 50°, .020-inch hyperbolic liners assembled with iron adaptors.

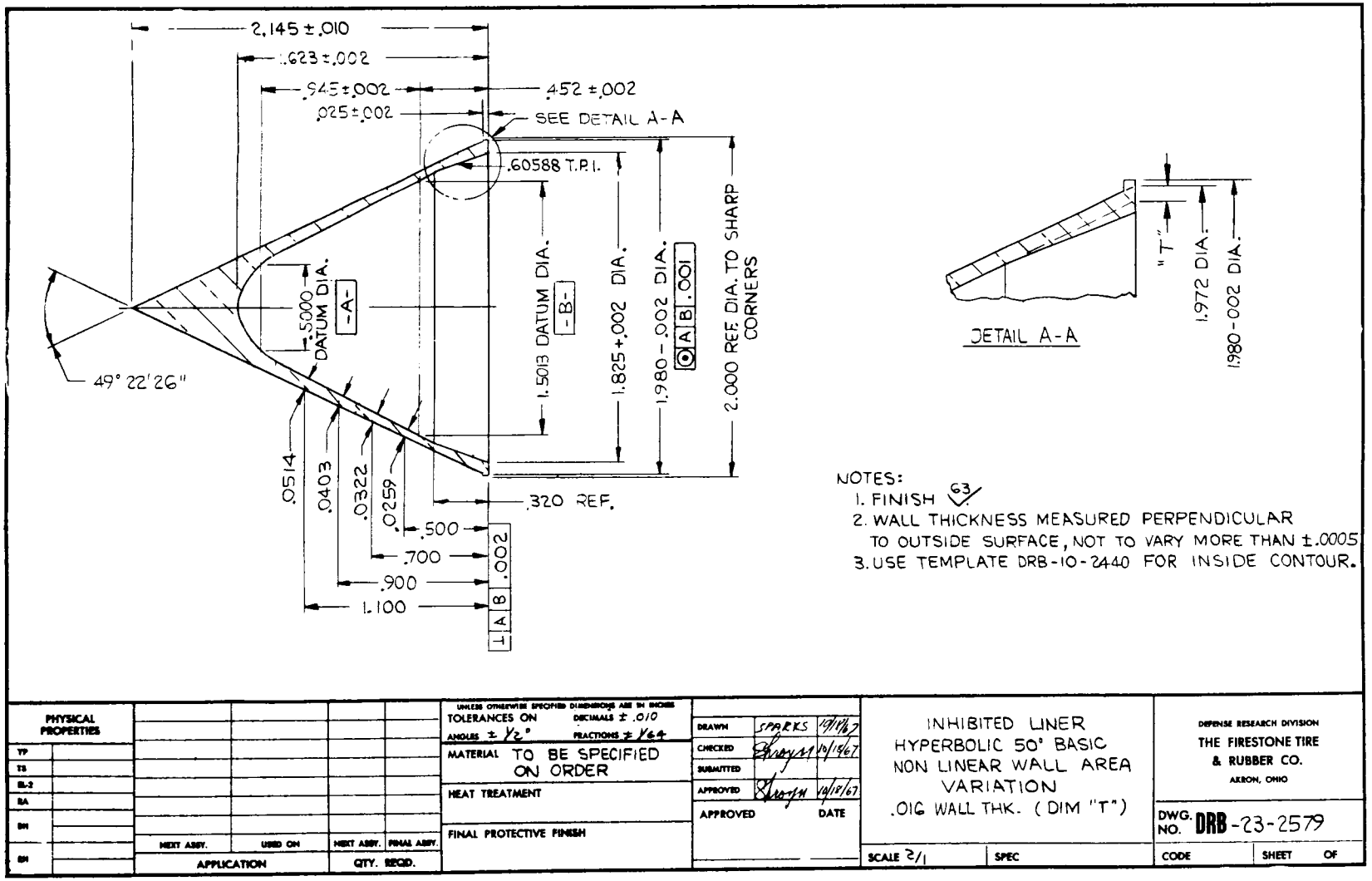

Fig. 42. 50° liner with tapered internal skirt type inhibitor.

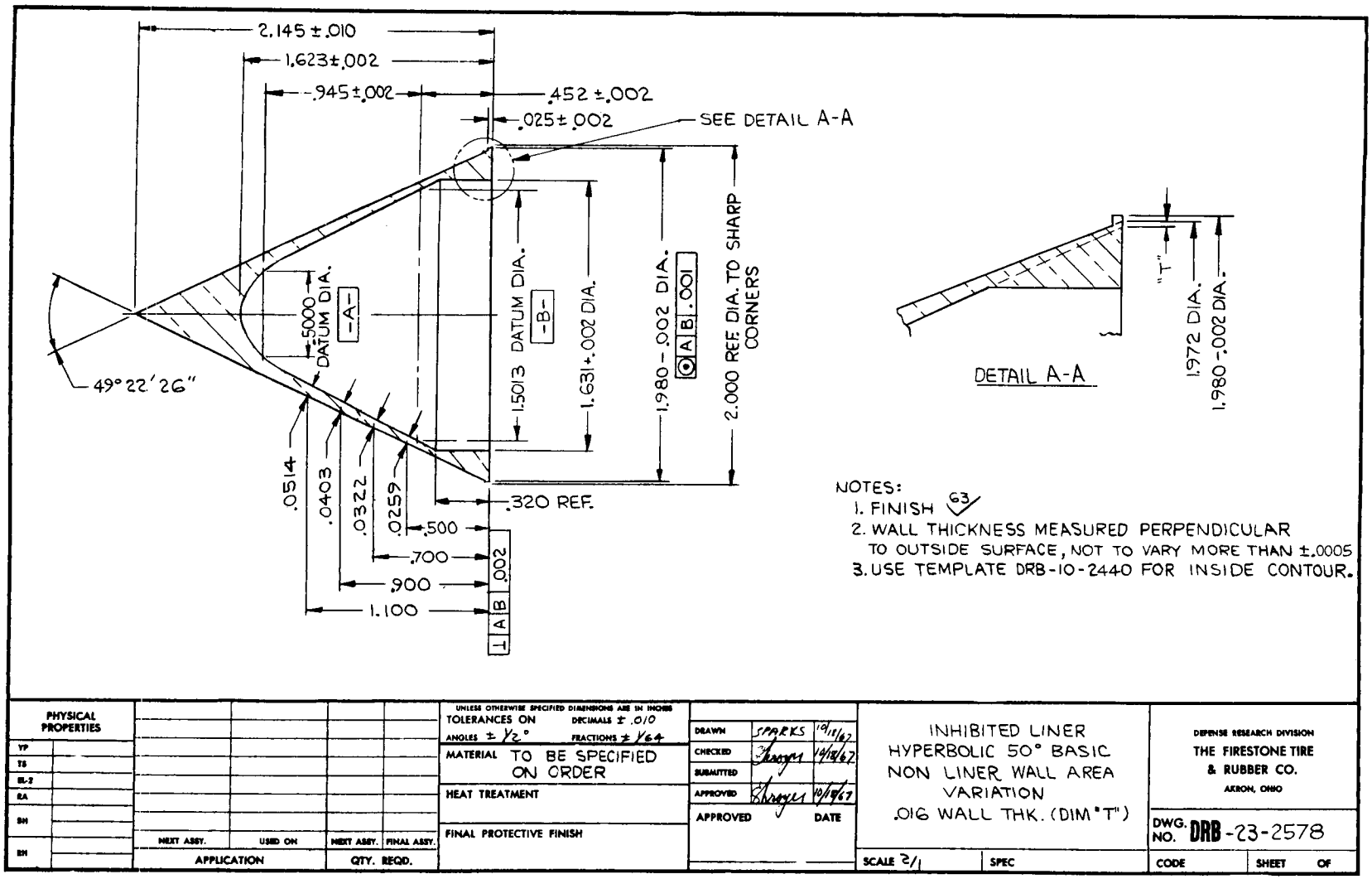

Fig. 43. 50° liner with cylindrical internal skirt type inhibitor.

50° NICKEL 270 HYPERBOLIC LINER
43° POLYURETHANE WAVE SHAPER
50° BI-EXPLOSIVE LOADING FIXTURE

.020-in. Wall (DRB-23-2586)
Tapered Inhibitor
Explosive:
Inner: 75/25 octol
Outer: HMX
Steel Adaptor Plate
976-7
Travel: 35-in. (vacuum)
Velocity: 11.80 km/sec

.016-in. Wall (DRB-23-2579)
Tapered Inhibitor
Explosive:
Inner: 75/25 octol
Outer: HMX
Aluminum Adaptor Plate
976-6
Travel: 36-in. (vacuum)
Velocity: 12.33 km/sec

.020-in. Wall (DRB-23-2585)
Cylindrical Inhibitor
Explosive:
Inner: 60/40 comp. B
Outer: 75/25 octol
Steel Adaptor Plate
976-10
Travel: 34-in. (vacuum)
Velocity: 11.74 km/sec

.016-in. Wall (DRB-23-2578)
Cylindrical Inhibitor
Explosive:
Inner: 60/40 comp. B
Outer: 75/25 octol
Aluminum Adaptor Plate
976-9
Travel: 36-in. (vacuum)
Velocity: 11.85 km/sec

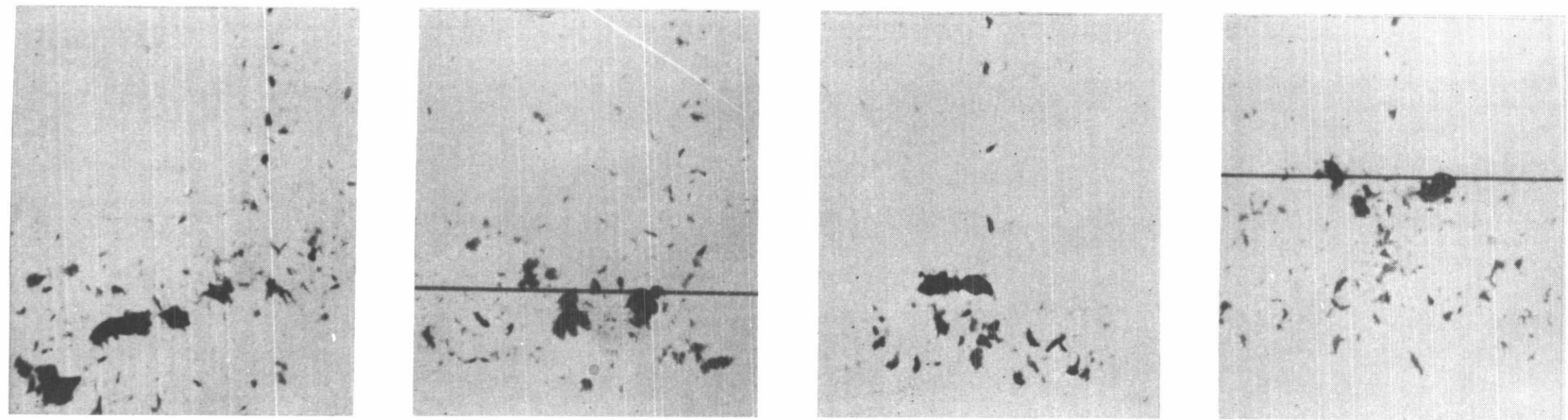

Fig. 44. Comparison of jets produced by skirted nickel hyperbolic liners.

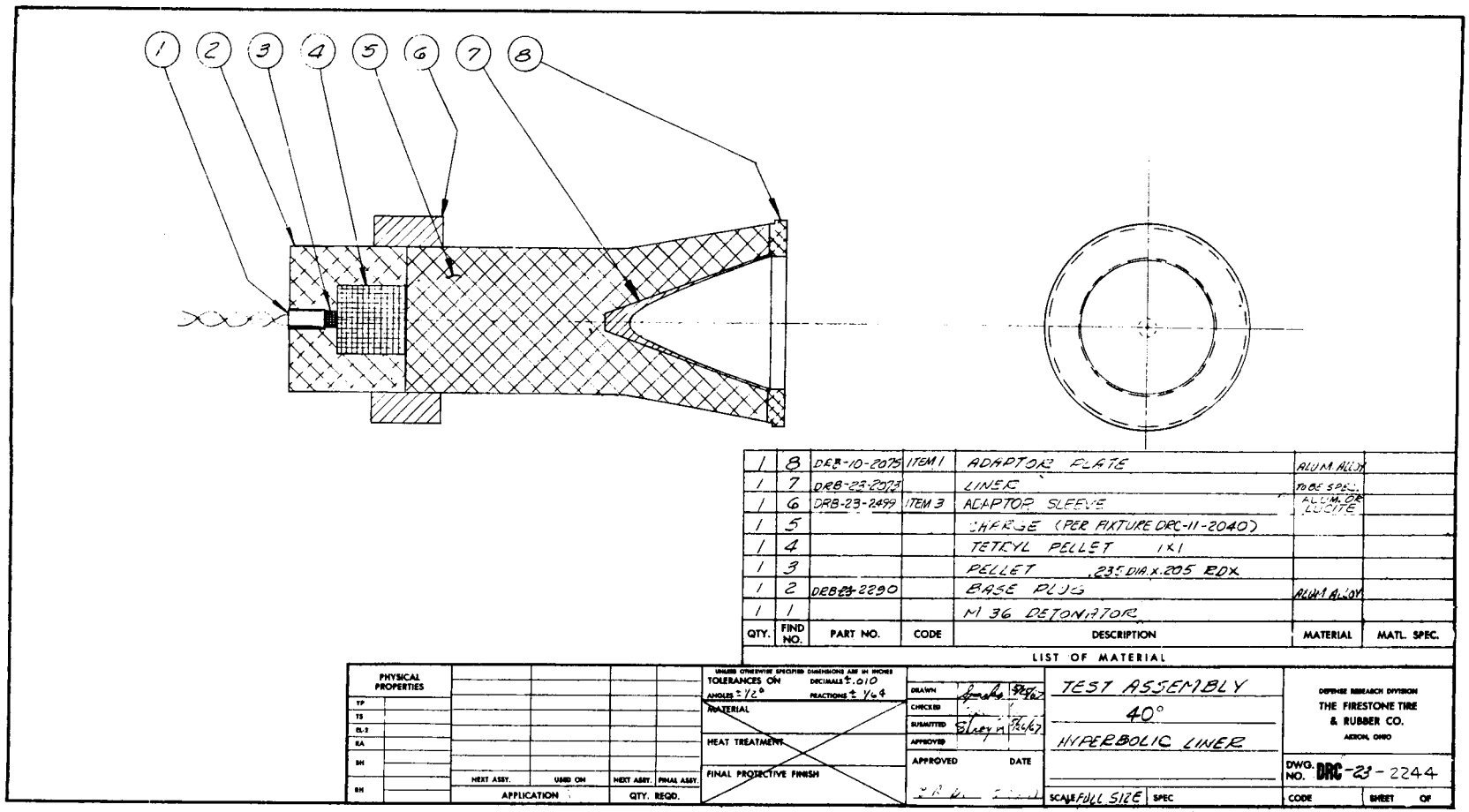

Fig. 45. Mono-explosive test assembly using 40° hyperbolic liner.

40°, .030-INCH WALL HYPERBOLIC LINER (DRB-23-2073-1)
EXPLOSIVE: 75/25 OCTOL

(1)these rounds were tested in the ϕ=12° charge configuration, all others used the ϕ=10°9' configuration.

approximate scale
(inches)

0 1 2 3

Fig. 46. Comparison of jets produced by 40°, .030-inch wall liners using various materials.

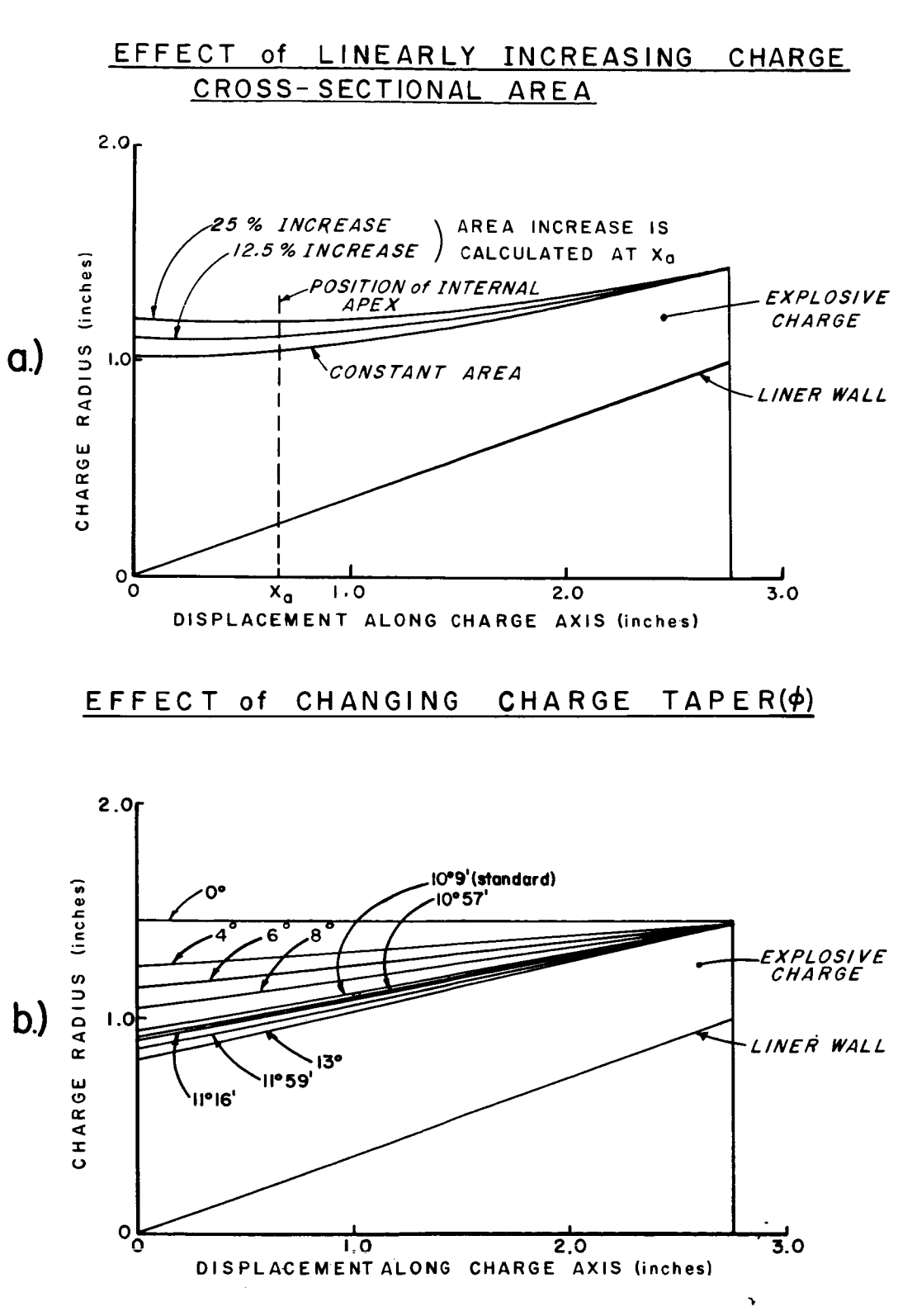

Fig. 47. Sketches of explosive external contour relative to liner outer wall.

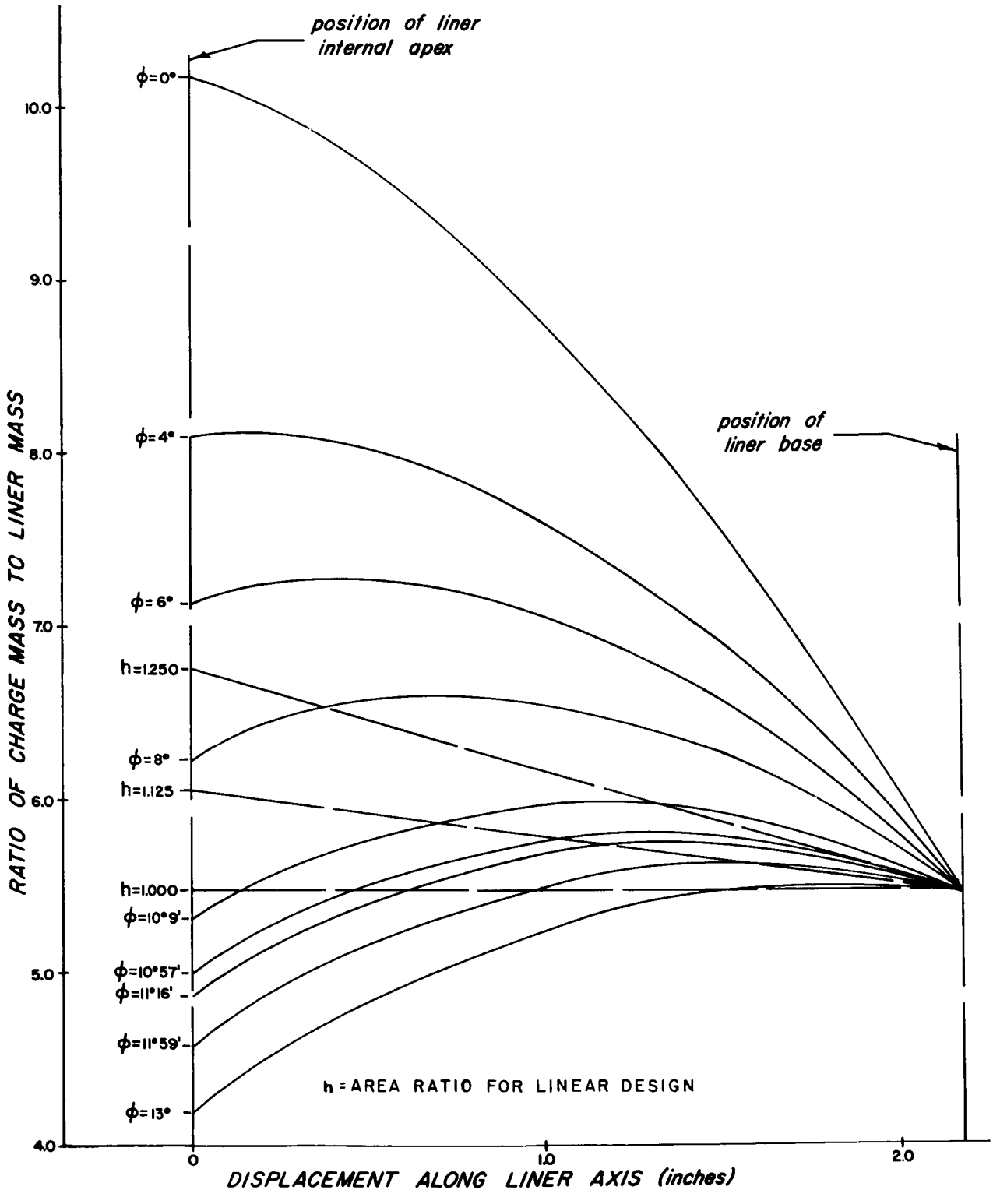

Fig. 48. C/M ratios for mono-explosive charge configurations tested.

40°, .020-INCH WALL NICKEL 200 HYPERBOLIC LINER (DRB-23-2171-1)
EXPLOSIVE: 65/35 OCTOL

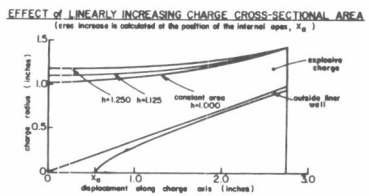

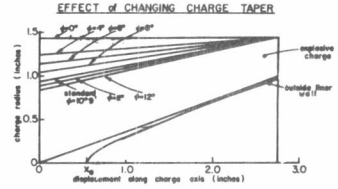

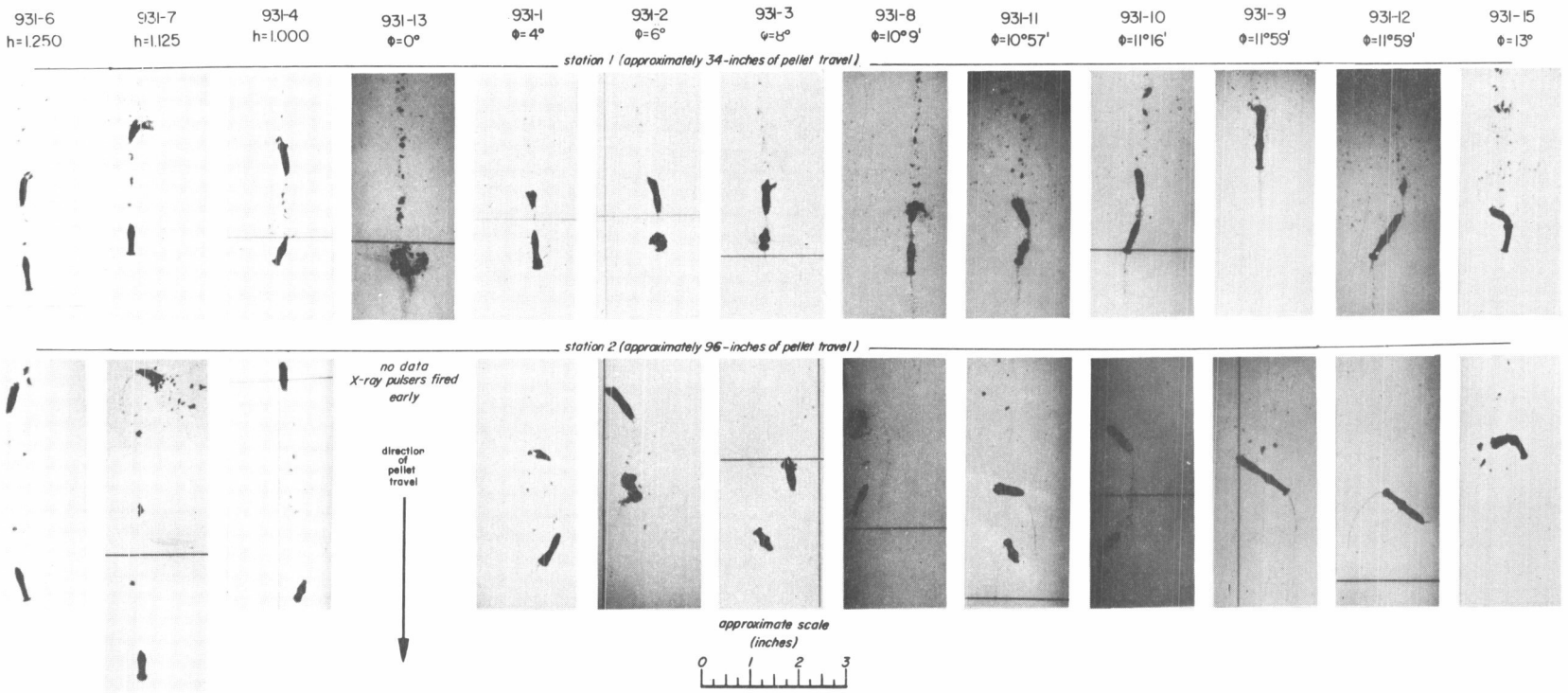

Fig. 49. Jets produced using various mono-explosive charge configurations.